Dipartimento di Ingegneria
Università del Sannio, Benevento

Dottorato di Ricerca in Ingegneria dell'Informazione
XXIV ciclo

High-Performance Measurement Systems for Characterizing and Monitoring Particle Accelerator Magnets

Candidato
Giancarlo Golluccio

Coordinatore
Ch.mo Prof. Luigi Glielmo

Relatore
Ch.mo Prof. Pasquale Arpaia
Co-relatore
Dr. Marco Buzio

Luglio 2012

To my Father

Contents

Sommario

Nel campo delle misure magnetiche per acceleratori di particelle, negli ultimi anni la ricerca è stata volta ad affrontare le attuali limitazioni in due settori principali: la caratterizzazione di magneti a piccola apertura e rapidamente pulsati, e il monitoraggio in tempo reale di campi magnetici molto disomogenei.
Allo stato dell'arte del primo settore, la misura a bobina rotante è il metodo di maggiori prestazioni metrologiche, ma presenta forti limitazioni per le dimensioni della bobina e la lentezza di misura.
Per il monitoraggio in tempo reale dei campi magnetici molto disomogenei, attualmente, forti limitazioni sono imposte dal trasduttore impiegato come riferimento assoluto, specialmente in condizione di impulsi rapidi di campo.
Il lavoro di ricerca di questa tesi si pone come obiettivo di colmare le suddette carenze dello stato dell'arte. In particolare, per la caratterizzazione dei magneti a piccola apertura e rapidamente pulsati, vengono proposte opportune soluzioni metodologiche per: i) la calibrazione di bobine di piccole dimensioni; ii) la misura di omogenita' di campo nei magneti di piccola dimensione e rapidamente pulsati; iii) e la misura di parametri geometrici di campo (quali direzione del campo e asse magnetico). Tali soluzioni sono state implementate al Centro Europeo per la Ricerca Nucleare (CERN) in una stazione di misura polivalente attualmente usata come sistema di riferimento per le misure degli oltre 100 magneti permanenti e rapidamente pulsati che verrano istallati nel nuovo acceleratore lineare.
Per il monitoraggio in tempo reale dei campi magnetici molto disomogenei, viene presentato un nuovo trasduttore basato su risonanza ferrimagnetica. A valle di un'attenta caratterizzazione metrologica, esso è alla base di un nuovo sistema di monitoraggio di campo magnetico per l'acceleratore Proton Syncrhotron facente parte della catena di iniezione del Large Hadron Collider al CERN.

Parole chiave: acceleratori di particelle, misure magnetiche, magneti resistivi, magneti permanenti, trasduttori di campo magnetico.

Resume

In the field of the magnetic measurements for particle accelerators, the research carried out during the last years has been devoted to face the current limitations in two main areas: the characterization of small-aperture and fast-ramped magnets, and the real-time monitoring of strongly inhomogeneous magnetic fields.

At the state of the art in the first area, the rotating coil measurement method provides the best metrological performance, but with strong limitations due to the coil dimension and the measurement speed, for small-aperture and fast-ramped magnets.

About the real-time monitoring of strongly inhomogeneous magnetic fields, severe limitations are mainly due to the transducer used as absolute reference, especially in fast-ramped conditions.

The work research of this Thesis focuses on filling up the aforementioned lacks of the state of the art. In particular, about the characterization of small-aperture and fast-ramped magnets, appropriate methodological solutions are proposed for: i) the calibration of small-dimension measurement coils; ii) the magnetic field homogeneity measurement for small-aperture and fast-ramped magnets; iii) and the measurement of field geometrical parameters, as direction and magnetic axis.

Such solutions have been implemented at the European Centre for Nuclear Research (CERN) in a polyvalent measurement station, currently used as reference system for the characterization of more than 100 permanent and fast-pulsed magnets to be installed in the new linear accelerator.

For real-time monitoring strongly inhomogeneous fields, a new transducer based on ferrimagnetic resonance is presented. After a thorough metrological characterization, the developed transducer is the kernel of a new magnetic field monitoring system for the Proton Synchrotron accelerator, a part of the injector chain in the Large Hadron Collider at CERN.

Keywords: particle accelerators, magnetic measurements, resistive magnets, permanent magnets, magnetic field transducers.

List of Publications

International Journals:

P. Arpaia, M. Buzio, G. Golluccio, L. Walckiers, "In situ calibration of rotating sensor coils for magnet testing", *Review of Scientific Instrument 83, 013306, 2012.*

P. Arpaia, M. Buzio, G. Golluccio, D. Oberson, "Metrological Performance of a Ferrimagnetic Resonance Marker for the Field Control of the CERN Proton Synchrotron", *IEEE Transactions on Superconductivity vol. PP, n 1, 2011.*

M. Buzio, G. Golluccio, A. Lombardi, F. Mateo, "Magnetic Qualification of Permanent Magnet Quadrupoles for CERN's Linac4", *IEEE Transactions on Superconductivity vol. PP, n: 1, 2011.*

International Conferences:

P. Arpaia, M. Buzio, G. Golluccio, "Measurement of eddy current transients in a fast cycled LINAC quadrupole magnet at CERN", XIX IMEKO World Congress Fundamental and Applied Metrology, Lisbon, September 2009.

P. Arpaia, M. Buzio, O. Dunkel, D. Giloteaux, G. Golluccio, A. Lombardi, "A Measurement System for Fast-Pulsed Magnets: a case study on Linac4 at CERN", International Instrumentation and Measurement Technology Conference, May 3-6, 2010, Austin, Texas

P. Arpaia, M.Buzio, G. Golluccio, F. Mateo: "In-situ calibration of rotating coil magnetic measurement systems: a case study on Linac4 magnets at CERN", IMEKO 2010 TC 4 and TC 19 Symposium & IWADC, September 8-10, 2010, Kosice, Slovakia

P. Arpaia, M. Buzio, G. Golluccio, G. Montenero, "Eddy Current Modeling and Measuring in Fast-Pulsed Resistive Magnets", International Instrumentation and Measurement Technology Conference, May 3-6, 2010, Austin, Texas.

M. Martino, G. Golluccio, R. Losito, A. Masi: "An analytical model of the effect of external DC magnetic fields on the AC voltages of an LVDT", International Instrumentation and Measurement Technology Conference, May 3-6, 2010, Austin, Texas.

M. Buzio, P. Galbraith, S.S. Gilardoni, D. Giloteaux, G. Golluccio, C. Petrone, L. Walckiers, "Development of Upgraded Magnetic Instrumentation for CERN's Real-time Reference Field Measurement Systems", First International Particle Accelerator Conference, IPAC'10, 23-28 May 2010, Kyoto, Japan.

P. Arpaia, M. Buzio, O. Dunkel, D. Giloteaux, G. Golluccio, A.M. Lombardi, F. Mateo Jimenez, S. Ramberger, "Magnetic Measurements of Permanent and Fast-pulsed Quadrupoles for the CERN LINAC4 Project", First International Particle Accelerator Conference, IPAC'10, 23-28 May 2010, Kyoto, Japan.

P. Arpaia, M. Buzio, Juan Perez, G. Golluccio, C. Petrone, L. Walckiers, “Magnetic field measurements on small magnets by vibrating wire systems”, International Instrumentation and Measurement Technology Conference, May 10-12, 2011, Binjiang, Hangzhou, China.

P. Arpaia, M. Buzio, F.Caspers, G. Golluccio, C. Petrone, “Metrological Characterization of a Ferrimagnetic Resonance Transducer for Real-Time Magnetic Field Markers in Particle Accelerators”, International Instrumentation and Measurement Technology Conference, May 10-12, 2011, Binjiang, Hangzhou, China

Introduction

Beams of high-energy particles are not only used for fundamental and applied research in sciences, but also in many technical and industrial fields. In particular, only about 1 % of the approximately 26.000 accelerators installed worldwide are devoted to basic research, while about 44 % are used for radiotherapy. The remaining 54 % are used for industrial applied research and biomedical application at low energy [1].

A particle accelerator exploits electromagnetic fields to propel charged particles to high speeds and to contain them in prefixed beams. Depending on the application, the beam particles, and the energy, different classes of accelerators are defined. The common factor is the need for a well-defined magnetic field to bend and focus the particle beam.

In the strong-focusing concept of the synchrotron accelerator design [2], instead of one huge magnet, hundreds of bending magnets, enclosing vacuum connecting pipes, are used. In synchrotron accelerators, the quality and the control of the magnetic field applied to the particles become more influent because the particle momentum increases during acceleration and the magnetic field B is to be turned up correspondingly, in order to maintain constant the orbit curvature. Specialized quadrupole magnets handle the beam focusing independently, while the acceleration itself is accomplished in separate RF sections.

For those reasons, the construction of magnets with highly precise tolerances and the subsequent verification of theirs manufacture by even more precise measurements are key factors for the construction of a reliable accelerator. On the other hand, the characteristics of the magnetic field have to be monitored during the operation of the accelerator, in order to give a feedback to the operators on the machine status and to control specific subsystems, as the RF accelerator cavities.

At CERN, the European Organization for Nuclear Research, the design and realization of the largest synchrotron in the world (Large Hadron Collider, LHC), has required a remarkable technological effort in many areas of engineering. In particular, the tests of the LHC superconducting magnets disclosed new horizons to magnetic measurements. In view of the future upgrades of the injector chain, to improve the luminosity of the LHC, a large effort have been done both for the *characterization of small-aperture magnets* and for *monitoring real-time strongly nonhomogeneous magnetic field with high precision*.

Main application of measurement systems for the *characterization of small-aperture magnets* is the focusing quadrupole of the new linear accelerator (Linac4) under development at CERN. The high-field gradients of the quadrupole magnets of linear accelerators prevent the use of normal conducting excitation coils. Fast-pulsed iron-dominated electromagnets are used in initial and last parts of the accelerator. The central part is equipped with permanent magnets, well suited for high-gradient small-aperture quadrupoles, e.g. the "Drift Tube Linac" of the new Linac4 [3]-[5]. For both the magnet types, multipole components affect both the emittance and the size of the beam.

Therefore, high-quality measurements are needed to verify the field quality tolerances defined by beam optics [5].

Another issue concerns the so-called 'magnet fiducialization' [6], relating the magnetic axis and the main field direction of a quadrupole to the external markers (fiducials) used to align the magnets in the accelerator. In this case, the position of the quadrupole axis with respect to an external frame is to be determined accurately. The "fiducialization" has generally two steps: a magnetic measurement to detect the axis position in a local reference frame, and the transfer of the axis coordinates to an external reference system attached to the magnet, materialised by a set of geometric references (the "fiducials"). For small-dimension magnets, this process becomes more difficult for two reasons: in this case, the magnetic measurement methods increase their uncertainty and standard mechanical measurements (e.g. a laser tracker) are limited by the magnet dimension.

Specifically for permanent quadrupoles, another issue is the measurement of the gradient strength, because, with respect to electromagnets, it cannot be easily adjusted [7]-[8]. Currently, the rotating coil system is the best solution to measure magnet multipoles, the magnet axis and field gradient at the same time in static conditions [9].

For small-aperture magnets, the small dimension of the external radius r of the rotating shaft limits the accuracy. The uncertainty on the coil sensitivity factors increases accordingly, while the signal-to-noise ratio decreases as r^3. Fabricating printed-circuit coils reduces these effects, but gives rise to a lower winding density, and thus to a reduced sensitivity.

For small-radius coils, the measurement accuracy depends essentially on the calibration [10], consisting in the evaluation of its geometrical parameters: length, width, and rotation radius [9]-[15]. The resulting area of a multilayer coil sensor can be assessed as a function of the inner and outer width [24]. Purely mechanical measurements are usually not adequate to evaluate the equivalent magnetic surface within the required uncertainty (namely $\pm$ 10 ppm), but can be useful to measure the coil length. Far better results are achieved by calibration in a nuclear magnetic resonance (NMR)-mapped reference dipole field [25], by definition yielding the equivalent surface, including all the non-ideal effects. The total area of the coil can be determined thus to a very high degree of accuracy, provided that the reference field is sufficiently stable and uniform [24].

The equivalent magnetic coil width can be measured as a function of the position along the coil by means of localized field sources. For example, the coil may be held fixed in a AC reference field [27], or it can be flipped or translated in a DC field [26]. A DC field made by permanent magnets is usually stable and easy to operate, however AC current driven fields provide higher sensitivities. In any case the field source must provide good field uniformity in a sufficiently wide region transversal to the coil, so as to relax the tolerance on transversal positioning [28].

In rotating coil-based fluxmeter another fundamental parameter is the rotation radius, i.e. the average distance of the coil with respect to the mechanical rotation axis. Any

uncertainty in the radius directly affects all measured harmonics, exponentially with the harmonic order.
The radius can be obtained in a reference quadrupolar field either by rotating the coil by a given angle or by measuring the field strength. The accuracy of the result obtained degrades for small coil diameters, which suffer from proportionally larger mechanical uncertainties [10].
Hall probes could also be used as field sensing elements to test multipole magnets homogeneity [11] but they are less accurate and provide only local measurements; in addition, a complete field mapping turns out to be cumbersome.
Systems based on wires (stretched, vibrating, or pulsed [12]-[13]) and rotating coils are the state of the art for testing properties of accelerators magnets, but with the non-trivial limitation of working only for static fields. For fast-pulsed magnets, the best solution is a static coil. In [14]-[15], stationary coil arrays have been proposed to measure the harmonic content of fast-changing multipole fields. The arrays are made by several printed-circuit coils, mounted on a cylindrical structure. This technique requires identical coils, very precisely positioned on the support, and turns out to be difficult for small-aperture magnets.
For *monitoring real-time strongly nonhomogeneous magnetic field with high precision,* a static coil measurement system is also used in accelerator magnets during the operation. Such a monitor system not only provides diagnostics, but several other systems, such as power supplies, RF cavities, and beam monitoring systems, may use the field as the input of feedback loops to correct the beam position and oscillations.
In slowly cycled superconducting magnets of LHC, models describing the dynamic response of the magnet based on magnetic measurements are accurate enough, because the effects due to eddy currents and iron hysteresis are not influent [16]. In case of fast-cycled resistive magnets real-time measurements of the field are usually carried out in a reference magnet powered in series with the accelerator magnets. A rotating coil fluxmeter could be in principle a valid choice for these measurements, especially because it could provide an absolute value of the field [17]. However, even state-of-the-art rotating coil systems can hardly provide a bandwidth larger than 10 Hz, typically three orders of magnitude lower than required for fast-cycled magnets. Therefore, it is natural to use a static coil fluxmeter, providing a voltage output proportional to the field rate *dB/dt,* with sensitivity increasing with the bandwidth.
An additional measurement is needed however to provide the integration constant. This is commonly carried out by a “field marker”, a device able to provide a digital trigger pulse as the field crosses a given threshold [18]. Different field measurement systems can be adopted as field markers [19]. In strong inhomogeneous magnet, as the combined function magnets, used at the same time to bend and to focus the particle beam, the peaking strip [29] is a good solution. A peaking strip is essentially a magnetically bi-stable wire of a high permeability material, immersed in a bias field and able to generate a large flux change when the external field becomes equal and opposite to the bias, causing

the magnetization to flip. A mechanical pre-stress is beneficial to create an almost rectangular B-H cycle.

Commercial solutions based on Hall-effect field sensors have also been used as a field marker [11]. Even if state-of-the-art transducers can have very high metrological performance, the need of sophisticated calibration and temperature drift compensation limits their use in a feedback system that must guarantee reliability and stability over a time span of decades.

Field sensors based on Nuclear Magnetic Resonance (NMR) are currently the metrological standard, providing the best absolute accuracy in a wide field range [20]. However, NMR sensors require a homogeneous magnetic field across the probe volume in order to obtain a response from all nuclei at the same frequency. That is not the case in presence of combined function magnets as the ones used in the Proton Synchrotron accelerator at CERN [21].

In this Thesis, methodological and technical solutions to overcome the limitations the abovementioned drawbacks in the characterization of small aperture and fast ramped magnets are presented. The limitation in characterizing small-aperture magnets are overcome by a polyvalent method exploiting: (i) in-situ coil calibration, for facing the limitation in the multipole measurement accuracy due to the small aperture of the magnet; (ii) rotating quadrupole magnets about their axis by exploiting their cylindrical machining accuracy, for facing the problem of the magnet axis fiducialization; (iii) and a step-by-step coil rotation technique, for measuring fast ramping fields over several excitation current cycles. This method provides a complete characterization of the gradient strength, field direction, axis, and multipole errors for both permanent and fast-pulsed quadrupoles.

For monitoring fast-ramped and strong inhomogeneous fields, in this Thesis, a novel solution for field marking based on Ferrimagnetic resonance (FMR) effect is proposed [22]. FMR is a type of electron spin resonance based on a slight imbalance of the energy emitted and absorbed by electrons flipping between opposite spin states under the influence of incident electromagnetic radiation. It has found widespread applications in microwave equipment such as tuneable oscillators and electronically tuneable filters [23].

In particular, in the first part of the Thesis, the different types of magnet used in synchrotron accelerators and all the measurement methods available in the literature to test the magnets in the different time life phases are described. In the second part, suitable methods and systems to achieve this task are proposed. The third part will show experiments to validate the above methods and system.

REFERENCES

[1] T. Federer, "Accelerator school travel university circuit", *Physics today, vol. 63, 2010*.

[2] P. Bryant, "The Principles of Circular Accelerators and Storage Rings", *Cambridge University Press, 1993*.

[3] K. Halback, 1980, "Design of permanent multipole magnets with oriented rare earth cobalt material", *nuclear instrument and method vol. 169*.

[4] L. Halbach, 1983, "Permanent Multipole Magnets with Adjustable Strength", *IEEE Transaction on Nuclear Science v. 30.*

[5] M. Vretenar, The Linac4 project at CERN, *Proceeding International Particle Accelerator Conference.(IPAC'11), 2011*.

[6] L. Bottura M. Buzio, S. Pauletta, N. Smirnov, "Measurement of magnetic axis in accelerator magnets: critical comparison of methods and instruments", *IMTC 2006 Instrumentation and Measurement Technology Conference, 2006.*

[7] S. Becker, "Characterization and tuning of ultrahigh gradient permanent magnet quadrupoles ", *Physical review, v. 12, 2009*.

[8] Vl. Skachkov, "Permanent Magnet Quadrupole for the 1-st Tank of Linac4", Proc. RuPac (Novosibirsk), 2006.

[9] L. Walckiers, "Fabrication and calibration of search coils", *CERN Accelerator school: specialized course on Magnets, CERN-2010-004, p. 357, 2009*.

[10] M. Buzio, " Fabrication and calibration of search Coils", *CERN Accelerator school: specialized course on Magnets, CERN-2010-004, p. 357, 2009*.

[11] C. Schott, R. S. Popovic, S. Alberti and M. Q. Tran*," H*igh accuracy magnetic field measurements with a Hall probe*", Rev. of Sci. Instr.*, Vol. 70, 2703, 1999.

[12] P. Arpaia, M. Buzio, J. J. G. Perez, G. Golluccio, C. Petrone, L. Walckiers, Magnetic field measurements on small magnets by vibrating wire systems, *IEEE Instrumentation and Measurement Technology Conference (I2MTC), 2011*.

[13] N. Smirnov, L. Bottura, M. Calvi, G. Deferne, J. DiMarco, N. Sammut, and S. Sanfilippo, Focusing Strength Measurements of the Main Quadrupoles for the LHC*, IEEE Transactions on Applied Superconductivity, vol. 16 no. 2, 2006.*

[14] P. Schnizer, H. R. Kiesewetter, T. Mack, T. Knapp, F. Klos, M. Manderla, S. Rauch, M. Schönecker, R. Werkmann, Status of the Mole for Measuring Fast-ramped, Superconducting Magnets, *16th International Magnetic Measurement Workshop (IMMW), 2009*.

[15] A. Jain, G. Ganetis, A. Ghosh, W. Louie, A. Marone, R. Thomas, P. Wanderer, Magnetic field measurement for fast-changing magnetic, *fields IEEE Transactions on applied superconductivity vol. 15, n. 2, 2005*.

[16] N. Sammut, L. Bottura, J. Micallef, "Mathematical formulation to predict the harmonics of the superconducting Large Hadron Collider magnets", *Phys. Rev. Special Topic Accelerators and Beams, vol. 9, 2006*.

[17] P. Bauer, M. Lamm, G. Lorenz, J. Nogiec, T. Peterson, R. Sood, W. Soyars, C. Sylvester, M. Tartaglia, G. Velev, "Cost Estimate For a Tevatron Reference Magnet System", *Fermilab internal note, FERMILAB - TD-02-042, 2006.*

[18] L. Symods, "Methods of Measuring Strong Magnetic Fields" *Reports on Progress in Physics, Vol. 18, 1955.*

[19] G. Franzini , "Final Design and Features of the B-Train System of CNAO", *Proc. of 1st Int. Particle Accelerator Conf. IPAC 2010, Kyoto 2010.*

[20] K. N. Henrichsen, "Magnetic field imaging" in *Encyclopedia of imaging science and technology*, V. J. P. Hornak, pp. 970-977, Wiley-VCH Verlag, New York, 2002.

[21] M. Buzio, Past and recent main PS magnet measurements and B-train, *workshop on CERN Power Synchrotron magnet field, Geneva, Switzerland, 2012.*

[22] M. Benedikt, F. Caspers, M.Lindroos "Application of Magnetic Markers for Precise Measurement of Magnetic Fields in Ramped Accelerators", *Particle Accelerators: 63 (1999).*

[23] P. Roschmann, "Compact YIG bandpass Filter with Finite-Pole frequencies for Applications in Microwave Integrated Circuit", *IEEE Trans. on Microwave Theory and Techniques, 1973.*

[24] S. Tumanski,"induction coil sensor-a review" *Measurement Science and Technologies, Vol. 18-3, R31,* 2007.

[25] K. Weiand, "Magnetometer calibration setup controlled by nuclear magnetic resonance" *IEEE Transactions on Instrumentation and Measurement, vol. 48-2, p. 668 ,1999.*

[26] R. Grössinger, M. Taraba, A. Wimmer, J. Dudding, R. Cornelius, R. Knell, R. Bissel, B. Enzberg-Mahlke, W. Fernengel, J.C. Toussaint, D. Edwards, "Calibration of an industrial pulsed field magnetometer", *IEEE Transactions on Magnetics, Vol. 38, p.2982, 2002.*

[27] E. Pulz," A Calibration facility for search coil magnetometers", *Measurement Science and Technologies, Vol. 13, p. N49, 2002.*

[28] E. T. Everson, P. Pribyl, C. G. Constantin, A. Zylstra, D. Schaeffer, N. L. Kugland, and C. Niemann, "Design, construction, and calibration of a three-axis, high-frequency magnetic probe (B-dot probe) as a diagnostic of exploding plasmas", *Review of Scientific Instrument,Vol. 80, 113505, 2009.*

[29] J. M. Kelly, "Magnetic Field Measurements with Peaking Strips", *Review of Scientific Instrument*, Vol. 22, pp. 256-258, 1957

PART I - STATE OF THE ART

Chapter 1

The magnetic field in particle accelerators

1.1 Overview

A particle accelerator is a machine that uses electromagnetic fields to accelerate charged particles and to contain them in well-defined beams. The class of accelerator depends on the application, the kind of beam, and the required energy. The common factor among the different classes of accelerators is the Lorentz equation. An electric field is needed for the acceleration and a magnetic field for guiding the particles on a given trajectory. High-quality magnetic measurements are necessary intensively from the early stages of the magnet prototyping to validate the design in terms of field homogeneity, and also during the series production (series verification mechanical assembly errors), installation (magnet alignment and fiducialization) and operation (monitoring of the field in the accelerator during the operations.

In this Chapter, after a brief review of the different accelerator types, a concise description of the magnetic field in the accelerator and the magnets for generating such a field (more details are given in Appendix A) is provided. In particular, the Chapter is focused on the qualification of an accelerator magnet and its magnetic field, by highlighting the important parameters to be measured with the related precision during the lifetime.

1.2 Particle accelerator basics

A particle of charge q moving through an electromagnetic field is submitted to the Lorentz's force expressed by:

$$\vec{F} = q\left(\vec{E} + \vec{v} \wedge \vec{B}\right) \tag{1.1}$$

where $\vec{F}$ is the electromagnetic force exerted by the electric field $\vec{E}$ and the induction field $\vec{B}$ on the particle with velocity $\vec{v}$.

According to the equation element is varying, the different kinds of accelerators can be classified. They can be divided in two basic classes:

- electrostatic accelerators, generating static electric fields, e.g. the cathode ray tube in an old television set;
- oscillating field accelerators, at the basis of all the modern accelerator concepts. Due to the high-voltage ceiling imposed by electrical discharge, in order to accelerate particles to higher energies, techniques involving more than one lower, but oscillating, high-voltage sources are used. The electrodes can either be arranged to accelerate particles in a line or

circle, depending on whether the particles are subject to a magnetic field during acceleration, causing their trajectories to arc.

In a linear accelerator (linac), particles are accelerated on a straight trajectory. They are often used to provide an initial low-energy kick to particles before they are injected into circular accelerators. To control the particle beam during the transportation, most linacs have quadrupole magnets in the drift tube. A drift tube is an array of charged plates that alternates their polarity. The particles pass through a hole in the plate, thus the polarity is switched so that the plate now repels them to accelerate towards the next plate.

In circular accelerators, the particles move along a circular trajectory until when they reach the required energy. Circular accelerators, with respect to linacs allows continuous acceleration because the particle can pass repeatedly inside the same cavity and for the same energy level the circular accelerator are smaller compared to linacs.

The simplest circular accelerator (the first cyclotron from Laurence had the dimension of a coin) has the fields $\vec{B}$ and $\vec{E}$ constants but the beam energy increases by changing the radius [3].

In synchrotrons, the magnetic field must vary proportionally to the particle momentum ρ_0 (Fig. 1.1) by keeping the radius fixed. Such accelerators can be divided in two families, the weak focusing synchrotron and strong focusing synchrotron.

In weak focusing as ρ_0 gets bigger (the beam energy increases) the field gradient to keep the particles focused in the vertical direction, for stability in the horizontal direction, should get smaller [3]. By getting the gradient smaller, the beam increases its size; this leads to inconveniently large-apertures with magnet combined function magnets with high precision poles profiles, which implies high fabrication and running costs.

Strong focusing or alternating-gradient focusing is the principle that the net effect on a particle beam passing through alternating field gradients is to make the beam converge. Since focusing simultaneously on the horizontal and vertical plane is impossible, two or more quadrupole magnets arranged alternately focus horizontally and vertically (the so called FODO structure [3]). The usual analogy is to refer to optical lenses. In this case, it is relatively easy to build layouts that are focusing overall (Figure 1.2).

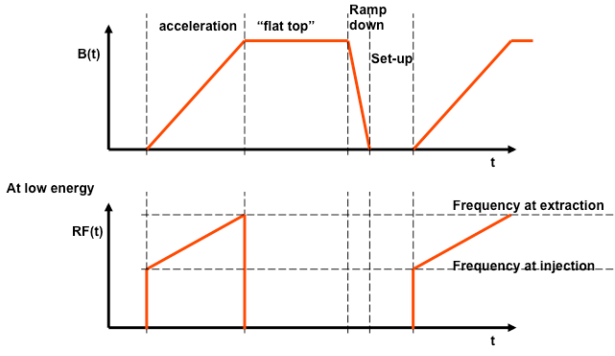

Figure 1.1: Magnetic cycle in synchrotron accelerators.

A particle travelling through a magnetic gradient in the vertical axis will be pushed in the centre in the horizontal plane according to the left-hand rule, but at the same time, it will be defocused in the vertical plane.
The strong focusing concept leads to relaxing the constraints on the field and on the distribution of the magnetic elements in the accelerator, by increasing the performance and making easier the machine operation.

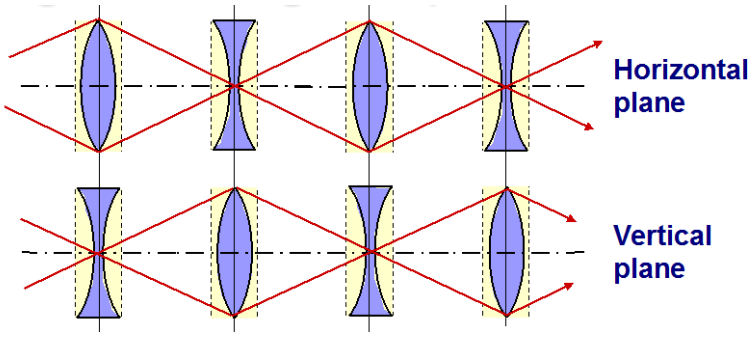

Figure 1.2: Layout of a particle passing through a Focusing/Defocusing structure.

Today, strong-focusing synchrotrons are an optimal solution for high-energy particle beams used in the research as the Large Hadron Collider (LHC) at European Centre for Nuclear Research (CERN). The LHC is only the last stage of the acceleration. Before to being injected into the LHC, the particles are prepared by a series of systems successively increasing their energy. The first system is the linear particle accelerator LINAC 2, generating 50-MeV protons feeding the Proton Synchrotron Booster. There, the protons are accelerated to 1.4 GeV and injected into the Proton Synchrotron, where they are accelerated to 26 GeV. Finally, the Super Proton Synchrotron is used to further increase their energy to 450 GeV before they are at last injected (over a period of 20 minutes) into the main ring of LHC. Here, the proton bunches are accumulated, accelerated (over a period of 20 minutes) to their nominal peak 7-TeV energy, and, finally make them collide at the four intersection points (ALICE, ATLAS, CMS, LHCb).

1.3 Magnets for accelerators

The most important elements in a synchrotron accelerator, together with the resonant cavities, are the magnets, providing the control of the beam in the circular or linear paths.
The magnetostatic fields are conventionally described in terms of multipoles [7], commonly derived from the solution of the differential form of Maxwell's equations:

$$\nabla \cdot \vec{B} = 0 \tag{1.3a}$$

$$\nabla \cdot \vec{D} = \rho \tag{1.3b}$$

$$\nabla \times \vec{H} = \vec{J} + \frac{\partial \vec{D}}{\partial t} \tag{1.3c}$$

$$\nabla \times \vec{E} = -\frac{\partial \vec{B}}{\partial t} \tag{1.3d}$$

where ρ and $\vec{J}$ are the electric charge and current densities (per volume unit), respectively, and $\vec{H}$, $\vec{D}$ are the magnetic intensity and the electric displacement, respectively, related to the electric field and magnetic flux density as:

$$\begin{aligned} \vec{B} &= \mu \vec{H} \\ \vec{D} &= \varepsilon \vec{E} \end{aligned} \tag{1.4}$$

The electric permittivity ε and magnetic permeability μ depend on the medium [7].

The magnetic field in a region of space free of charges and currents, as the aperture of a magnet, must satisfy the Maxwell equation:

$$\nabla \cdot \vec{B} = 0 \tag{1.5}$$

$$\nabla \times \vec{B} = 0 \tag{1.6}$$

Equation (1.6) is just (1.3a), and Eq. (16) follows from the Eq. (1.3c) equation given that $\vec{J} = \mathbf{0}$, $\vec{B} = \mu_0 \vec{H}$ and derivatives with respect to time vanish. In those conditions, a magnetic field $\vec{B} = (B_x, B_y, B_z)$ with B_z constant and B_x, B_y is given by:

$$B_y + iB_x = C_n (x + iy)^{n-1} \tag{1.7}$$

where i is the complex unit and C_n is a complex constant satisfying the equations (1.5) and (1.7). The field components B_x and B_y are real and are obtained from the imaginary and real part of the right end side of equation (1.7).

Fields of the form (1.7) are known as multipole fields. The index n (an integer) indicates the order of the multipole: $n = 1$ is a dipole field, $n = 2$ is a quadrupole field, $n = 3$ is a sextupole field, and so on. According to the principle of superposition, a more general magnetic field can be constructed by adding together a set of multipole fields:

$$B_y + iB_x = \sum_{n=1}^{+\infty} C_n (x + iy)^{n-1} \tag{1.8}$$

From this definition, an ideal multipole of order n has only the respective $C_n \neq 0$. The coefficients C_n describe the strength and the orientation of each multipole component in a two-dimensional magnetic field.

Rewriting the multipole expansion of the magnetic field in polar coordinates helps to understand some properties of multipole field. If in eq. (1.8) $x = r\cos(\theta)$ and $y = r\sin(\theta)$ are replaced, the result is:

$$B_y + iB_x = \sum_{n=1}^{+\infty} C_n r^{n-1} e^{i(n-1)\theta} \tag{1.9}$$

The strength of the field in a pure multipole of order n varies as r^{n-1} with distance from the magnetic axis and any rotation of the magnet around the z of a π/n angle changes the sign of the field.

In addition, if the coefficient C_n is rewritten by highlighting module and phase expression $C_n = |C_n| e^{in\phi_n}$, the phase ϕ_n gives the orientation of the multipole.

According to accelerator magnet convention, the multipole with $\phi_n = 0$ is called "normal" multipole or is a "skew" multipole with $\phi_n = \pi/2$. In Fig. 1.3, the magnet multipoles normally used in a synchrotron, with n up to 3, normal and skew, are shown.

In the SI units, the multipoles field are expressed in T/m^{n-1} (at a given reference radius R_{ref}). However, sometimes they are expressed dimensionless with respect to a reference field B_{ref} and a reference radius R_{ref}, that can be choose arbitrarily but need to be specified to interpret the C_n, in this case the eq. (1.9) becomes:

$$B_y + iB_x = B_{ref} \sum_{n=1}^{+\infty} (a_n + ib_n) \left(\frac{r}{R_{ref}} \right)^{n-1} e^{i(n-1)\theta} \tag{1.10}$$

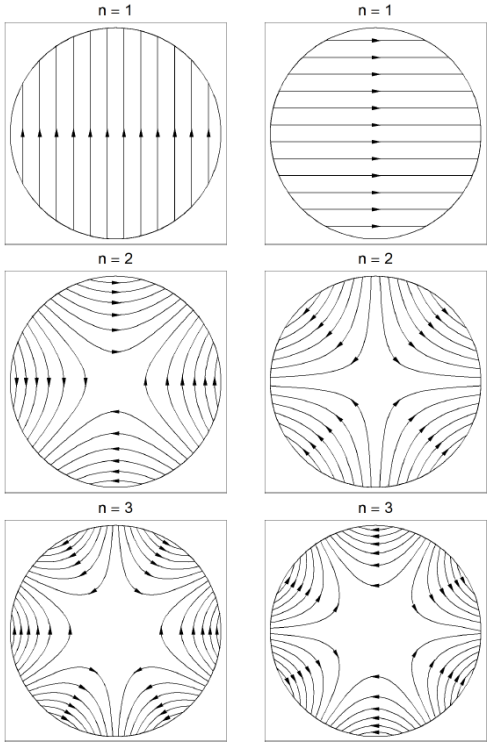

Figure 1.3: multipole fields. A dipole on the top, a quadrupole in the middle and a sextupole on the bottom (normal on the left column and skew on the right.

In a circular aperture, the multipole field in (1.10) can be created by opportunely distributing on a cylindrical pattern a sinusoidal current distribution (Appendix A.1). This approach underlies the so-called coil-dominated magnets, different from the iron-dominated magnets (Appendix. A.2), where the shape of the iron forming the magnet yoke gives multipoles. The third solution to produce a strong multipole field is to opportunely distribute elements of permanent magnets of rare earth material on a cylinder surface (Appendix A.3).

1.4 Magnet characterization in accelerator development

The flow diagram in Fig. 1.4 shows the typical life cycle of a magnet from the design and construction to the installation and operation and to its final disposal or destruction [6]. At the beginning of each project the requirements, constraints, and boundaries have to be defined. From this set of parameters a first analytic design should be derived followed by a basic numerical design. The basic performance parameters, which are typically provided by the accelerator physicists:

- Beam parameters: type of beam (mass and charge state), energy range and deflection angle.
- Magnetic field: integrated field (or integrated gradient in case of quadrupoles); alternatively the local field (gradient) and magnetic length can be defined.

Aperture: physical (mechanical) aperture and useful magnetic aperture (‘good field region’).

- Operation mode: continuous operation, pulsed-to pulse modulation, fast-pulsed, definition of the magnetic cycle and ramp rates for electromagnets.
- Field quality: requirements on field homogeneity (uniformity), the allowed harmonic content, requirements on stability and reproducibility, maximum settling time (time constant) for transient effects generated by eddy currents. A simple but effective method to judge the field quality of a magnet is to plot the homogeneity of the field or the gradient along the boundary of the defined good field region. As shown in Fig. 1.4 the magnetic measurements play an important role all along the fabrication process of the magnet. They, in the early lifetime of the magnet, enter in the iteration loop of design and validation of the prototype. At the end of the iteration process, and the verification of the final prototype, the production of the series measurement can start. At this point the magnetic measurement process is the only way to validate the production and to take the final decision if the magnet is ready to be installed in the machine or if there are some

corrections to apply to the fabrication process. However the magnetic measurement process does not end with the magnet fabrication, but it play also a role in the installation and the operation of the magnet in the accelerator. In the early step of the installation is important to know where exactly is located the magnetic field with respect to the mechanical reference of the magnet, this is what is called “fiducialization”. Once the magnet is installed in the accelerator and the accelerator is working sometimes in necessary to monitor the magnet behaviours during the operation to provide a feedback to other instrumentation installed in the accelerator complex that need for a real time measurement of the magnetic field in the accelerator.

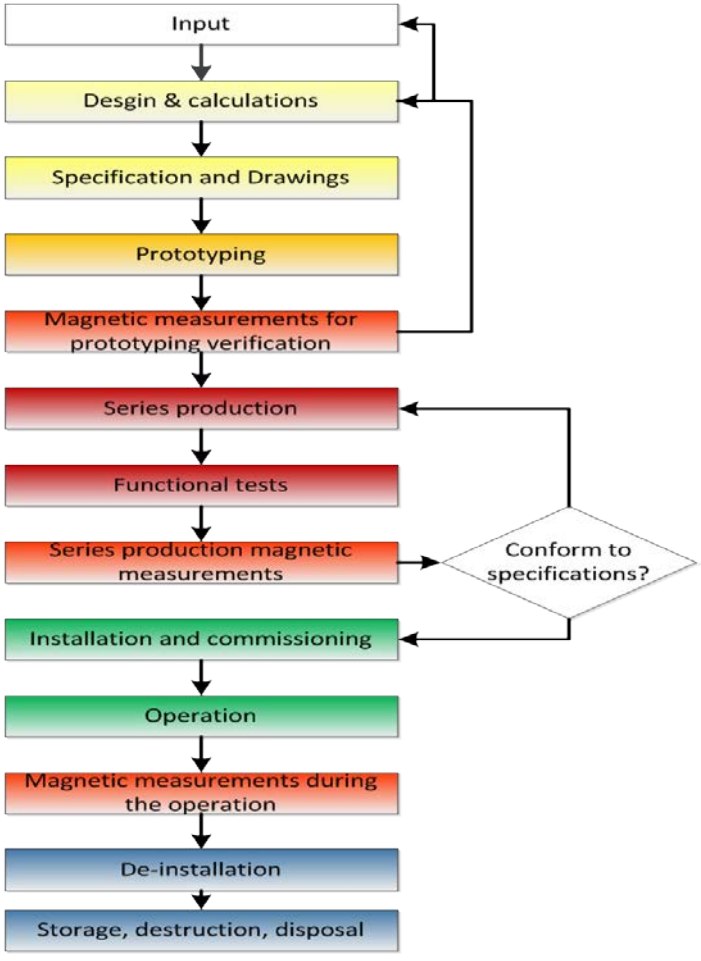

Figure 1.4: Magnet life cycle.

1.4.1 Alignment

Particles in the accelerator travel undisturbed on their design trajectory only when the magnetic axes of all beam steering components form a smooth continuous line in space. Establishing these positioning conditions is the goal of the alignment process. The setting of reference targets is a key task in this process [8]. These targets represent physically what otherwise cannot be accessed or referenced. In the task sequence of the alignment process, reference targets are used to represent the surveying coordinate systems (i.e. the surface net and the tunnel net), the geometric or electrical axes of diagnostic instruments, and the magnetic axes of the beam steering components [10]. The specifications of accuracy, for alignment, are related to beam optics—i.e. to the magnetic elements of the accelerator. Transverse errors in positioning are seen as imperfections of the guiding field: the particles no longer meet the theoretical magnetic field or gradient, and this creates a local perturbation of the motion, which is especially critical in focusing elements. Depending on the magnitude, location and distribution of these alignment errors, the resultant orbit may undergo deviations and oscillations of varying amplitude. Tilt errors induce vertical distortions of the trajectory, and related tolerances must be also specified for this critical parameter. The relative positioning of quadrupoles is therefore of major importance along particle beam lines, and this is the reason why the main criterion for precision is a relative and local one, leading to the best "smoothness" along the trajectory [9].

1.4.1.1 Magnet's fiducialization

The measurement of the magnetic axis is generally a two steps process, often referred to as "fiducialization", involving a) the detection of the field null in a local reference system by means of some kind of magnetic sensor, and b) the transfer of the axis coordinates to an external reference system rigidly attached to the magnet, materialised by a set of geometric references or fiducials (see a schematic representation in Fig. 1.5 [2], referred to the case of harmonic coil measurements). The fiducials are typically some kind of optical target, e.g. Taylor- Hobson spheres with prism or retro-reflectors for laser tracker measurements, or simple marks in case theodolites are used. Fiducials must be accessible for measurements both during the tests and after installation in the machine, which may represent a penalizing constraint. This is especially the case for superconducting magnets, where fiducials must be placed on the cryostat that fully encloses the magnet. Most accelerator laboratories develop their own alignment measurement systems, which are normally a mixture of commercial and custom-built components, highly tuned to their specific requirements. These will include in general: (i) a magnetic sensor with its conditioning electronics and acquisition system;(ii) a mechanical system used to scan the target field volume, carrying the sensor plus some suitable geometrical references and one or more angular references (e.g. optical encoder, tilt sensor);(iii) a computer-controlled

positioning system;(iiii) a 2D or 3D position measurement system able to relate the references on the probe to a set of fiducials on the magnet, possibly via a network of additional fixed external points. The measurement can be directly provided, all or in part, by the probe positioning system. The end result consists of the combination of the magnetic and position measurements.

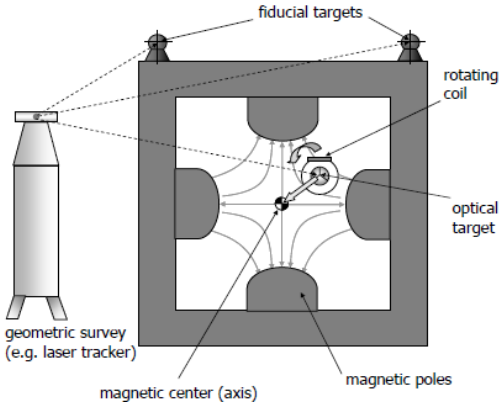

Figure 1.5: Magnetic axis measurement in a quadrupole magnet with harmonic coil method. Axis position is obtained in a frame centred on the coil's rotation axis, and then is transferred to magnet fiducials via geometric survey.

1.4.2 Field homogeneity

From the accelerator point of view, integrated field effects over the magnet ring govern the beam optics. The main field quality requirements are a suitable dipole-field integral, small dipole-field angle variations [16] and small high-order multipole coefficients (to minimize beam resonances and instabilities). In the case of high-order multipole coefficients, it is customary to specify tables of mean values and standard deviations over the entire magnet population [14]. The tables of mean values are referred to as systematic multipole specifications while that of standard deviations are referred to as random multipole specifications [15]. The specified values are all expressed at the reference radius, R_{ref}. In general for storage rings, the dipole and quadrupole field integrals must be controlled with a relative precision of the order of 10^{-3}. The variations in dipole field angles must be kept within a few mrad and the tolerance on quadrupole alignment is of the order of 0.1 mm. Systematic and random multipole specifications are normally useful up to the 4^{th} – 5^{th} order, but harmonics up to the 15^{th} order may are used to check the quality of the magnet design and production.

1.4.2.1 Magnetic field quality

The field quality of accelerator magnets is quantified by the amount of multipole error for a given geometry. The multipole errors are divided among "allowed" (by the symmetry) or systematic multipole errors and random multipole errors. Symmetry conditions allow the existence of certain errors while forbidding others. Thus, the identification of certain errors can be ascribed to fabrication and/or assembly errors and are considered random while others can be ascribed to the limitations of the ability to optimize and perfect a pole design. Both kind of multipole errors maybe affected by saturation and eddy current. An ideal N-pole magnet should have only the *N* component in the series expansion of equation 1.10. In general, a real magnet is characterized by a spectrum of harmonics including error terms due to the pole design, fabrication and/or assembly errors [20]. Fields are conventionally characterized by the complex function:

$$F = C_N z^N + \sum_{n \neq N} C_n z^n \tag{1.11}$$

$$F_n\left(\theta + \frac{\pi}{N}\right) = -F_n(\theta) \tag{1.12}$$

the symmetric condition applied to the 1.12 requires that:

$$\cos\left(n\theta + \frac{\pi}{N}\right) + i\sin\left(n\theta + \frac{\pi}{N}\right) = -\cos n\theta - \sin n\theta \tag{1.13}$$

The condition (1.13) can be satisfied only if

$$\sin\left(\frac{n\pi}{N}\right) = 0 \Rightarrow \frac{n}{N} = 1,2,3,4...$$

$$\cos\left(\frac{n\pi}{N}\right) = -1 \Rightarrow \frac{n}{N} = 1,3,5,7... \tag{1.14}$$

the more restrictive is that n/N are all odd integer, meaning that the harmonics allowed by the geometry are:

$$n_{allowed} = N(2m+1) \tag{1.15}$$

where *m* is a positive integer. As an example the allowed harmonics for a dipole are *n* = 3, 5, 7… while for a quadrupole *n* = 6,10,14… Those systematic effects can be reduced by a proper design of the magnet's poles. The non-allowed harmonics, the field errors (for a dipole n=2, 4, 8… and a quadrupole n=3,4,5,7..), are random and generally due to assembly imperfections. The summation of those different errors on in the good field region, defines the field homogeneity. The magnetic measurements during the

prototyping process are mainly dedicated to the design validation, while the measurements on the series magnets are needed to verify the goodness of the production.

1.5 Magnets monitoring during accelerator operations

As described in Fig. 1.4 magnetic measurements may be necessary even during the accelerator operation as monitor for the accelerator status (machine operators) but first of all as feedback for control system of other instruments as the RF cavities and the power supply using a current regulation as function of the magnetic field. Precise knowledge in real-time of the magnetic field in the main bending magnets in synchrotrons as a function of time is important for transversal beam control. In addition, certain measurement applications depend critically on such information for the correct evaluation of acquired data, such is the case of the RF cavities control. The demand on precision and resolution varies with application and machine [13]. In a superconducting machine like LHC the off-line approach was the only practical choice. The current semi empirical model ("FiDeL" [19]) has an adequate performance thanks to the vast database of test results, including all magnetic elements, which has been statistically analysed to extract model parameters. An accurate mathematical simulation is seemingly more difficult to obtain for accelerators based on resistive magnets and adopt the real-time measurement approach. Several major uncertainty sources apply in these cases, namely: temperature drifts, hysteresis behaviour in the iron, eddy current effects, material ageing etc. Other relevant factors are extent and precision of the measurement database and real-time number crunching power, both of which were hardly available in the past [10]. In other words, the magnetic model approach has, depending on its complexity, a number of poorly determined parameters, and his performance is worsening for accelerator with normal conducting magnet. In such case the best solution is to have a proper real-time measurement of the field, based in principle on the digitalization of a signal originating from a pick-up coil in a reference magnet.

1.5.1 Real-time monitoring of magnetic field

The requirements of such systems are quite strict in terms of precision since few tenth of mT can induce high instabilities in the particle beam radial position [11]. The most important requirement for such measurement application is the long-term reliability. As an example the five so called "B-Train" train system installed in the injector chain of the LHC at CERN have been in operation for several decades. Therefore, despite their successful track record, concerns over their long-term reliability are legitimate. In certain cases, performance improvements such as an increase of resolution by factor 2 from 10 to

5 μT are necessary to meet future demands. The B-train or the B-clock [17], or more generally magnetic field monitor systems, are usually a measurement system combining a stationary coil, measuring the dynamic field combined with a field sensor measuring stationary fields. The accuracy of such system mainly depends on the accuracy of the field sensor or also called ‘field marker’, giving the absolute reference for the integrated field. Different field measurement systems can be adopted as field markers [18]. In Chapter 2 will be detailed this real time system and in particular the different field marker technologies, custom or commercially available.

[1] T. Federer, Accelerator school travel university circuit, Physics today, vol. 63, 2010.
[2] L. Bottura M. Buzio, S. Pauletta, N. Smirnov, Measurement of magnetic axis in accelerator magnets: critical comparison of methods and instruments, IMTC 2006 – Instrumentation and Measurement Technology Conference, 2006.
[3] P. Bryant, The Principles of Circular Accelerators and Storage Rings, Cambridge University Press, 1993.
[4] M. Conte, W. W. MacKay., An Introduction to the Physics of Particle Accelerators", World Scientific, 2008.
[5] M.S. Livingston, Particle accelerators: A brief history, Harvard University Press Cambridge, 1969.
[6] T. Zickler, 2009, Basic design and engineering of normal-conducting, iron-dominated Electromagnets, CERN Accelerator School CAS 2009: Specialised Course on Magnets, 2009.
[7] A. Wolski, Maxwell equations for magnets, CERN Accelerator School CAS 2009: Specialised Course on Magnets, Bruges, 2009.
[8] A. Lestrade, Dimensional metrology and positioning operations: basics for a spatial layout analysis of measurement systems, CERN Accelerator School CAS 2009: Specialised Course on Magnets, 2009.
[9] M. Mayoud, Implementation and maintenance of the alignment of accelerators, CERN Accelerator School CAS 1995: Measurement and alignment of accelerator detectors and magnets, 1995.
[10] R. Ruland, Implementation and maintenance of the alignment of accelerators, CERN Accelerator School CAS 1995: Measurement and alignment of accelerator detectors and magnets, 1995.
[11] M. Buzio, P. Galbraith, G. Golluccio, D. Giloteaux, S. Gilardoni, C. Petrone, L. Walckiers, Development of Upgraded Magnetic Instrumentation for CERN Real-Time Reference Field Measurement Systems, 1st International Particle Accelerator Conference (IPAC'10), 2010.
[12] M. Buzio, Past and recent main PS magnet measurements and B-train, workshop on CERN Power Synchrotron magnet field, Geneva, Switzerland, 2012.
[13] F. Caspers, W. Heinze, J. Lewis, M. Lindroos, T. Salvermoser, An Alternative to Classical Real-time Magnetic Field Measurements using a Magnet Model, International Conference on Accelerator and Large Experimental Physics Control Systems (ICALEPCS '97), 1997.
[14] T. Garavaglia, K. Kauffmann and R. Stiening, Application of the SSCRTK numerical simulation program to the evaluation of the SSC magnet aperture. In M. MacAshan (ed.), Supercollider 2, New York: Plenum Press, 1990.
[15] A. Devred, Review of Superconducting Storage-Ring Dipole and Quadrupole

Magnets, CERN Accelerator School CAS 1998: Specialised Course on Magnets, 1998.
[16] D.A. Edwards et al., An Introduction to the Physics of High Energy Particle Accelerators, New York: John Wiley & Sons, 1993.
[17] T. Kasuga, B-clock System for the KEK Main Ring, IEEE transaction on Nuclear Science, vol. NS-24, N0. 3, 1977.
[18] J. M. Kelly, Magnetic Field Measurements with Peaking Strips, Rev. of Sci. Instr., Vol. 22, 1957.
[19] N. Sammut, L. Bottura, J. Micallef, The LHC Magnetic Model, Proceedings of 2005 Particle Accelerator Conference, 2005.
[20] J. Tanabe, Iron Dominated Electromagnets Design, Fabrication, Assembly and Measurements, World Scientific Publishing, 2005.

Chapter 2

Magnetic measurements methods

2.1 Overview

In section 1.1 the requirements in terms of accuracy for the different quantity to be measured during the different steps of magnet lifecycle has been described. In this chapter will be detailed the different measurement methods to qualify the magnet prototype, production and operation. It is curious to note that most measurement methods have remained virtually unchanged for a very long period, but the equipment has been subject to continual development. In the following, only the more commonly used methods will be discussed. These methods are complementary and a wide variety of the equipment is readily available from industry. For the many other existing measurement methods, a more complete discussion can be found in two classical bibliographical reviews [17]-[28]. The choice of measurement method depends on several factors. The field strength, homogeneity, variation in time, and the required accuracy all need to be considered. The number of magnets to be measured can also determine the method and equipment to be deployed. In [17] the author shows the accuracy that can be obtained in an absolute measurement as a function of the field level, using commercially available equipment. An order of magnitude may be gained by improving the methods in the laboratory. Here will be described the selected methods used for the different tasks of an accelerator magnet characterization and monitoring, focusing mainly on the measurement methods for the magnet fiducialization, magnetic field homogeneity and on the methods used for the real time field monitoring, with particular interest on the high accuracy field sensor used as marker.

2.2 Method for magnet fiducialization

The fiducialization process is usually performed on the magnet prototypes to validate the mechanical and field design, but it also needed on the series production before the installation in the machine. As described in chapter 1 it is a two steps process involving: (i) a magnetic measurement for finding the magnet axis and angle and (ii) a transfer process of this measurement to an external reference frame. In this section will be analysed the most common methods used for the first step, the magnetic measurement. The harmonic coils (rotating coils) are the classical method for such kind of measurements but is also the most versatile and useful to measure the field homogeneity, for this reason here will be just mentioned. In few words, the field harmonic coefficients are obtained from the Fourier analysis of the signal picked up by a rotating rectangular coil. The offset of the axis of the N-th order component (i.e. the main field) w.r.t. the rotation axis is computed from the measured amplitude of the component of order N-1, which is assumed to be generated by the so-called feed-down effect [18]. While generally

the magnet is excited in DC and the flux is integrated as the coil rotates, it is possible to enhance RT sensitivity exciting in AC and picking up the signal with fixed coils at different discrete azimuthal positions [7]. Here will be detailed the other two mostly common used methods for the quadrupole axis fiducialization: the stretched wire and the vibrating wire.

2.2.1 Single stretched wire

The SSW (Single Stretched Wire) [27] method consists of a high tensile conducting wire moved inside the magnet aperture by precision displacement tables. CuBe wires 0.1 mm thick are commonly used. The stages at both sides are assumed to move by precisely the same amount. The return wire is kept fixed, as much as possible in a field-free region. The flux lines crossed during this displacement, $\psi(x_1, x_2)$, and measured by a voltage integrator give the field integrated over the displacement, $d = x_2 - x_1$, and over the SSW length, L_w. When measuring a perfect dipole ($B_y = constant$, $B_x = 0$) the integrator gives:

$$\psi(x_1, x_2) = \int_0^L \int_{x_1}^{x_2} B_y(x, l) \cdot dx \cdot dl = d \cdot \int B \cdot dl \tag{2.1}$$

The measurement accuracy of the dipole strength is linked to the calibration of the integrator gain (10^{-4}-10^{-5}) and to the precision of the mechanical displacement. Commercially available stages reach accuracy better than 10^{-4} equal to 1 μm/10 mm. This method was crosschecked 30 years ago against NMR mapping and gave agreement within few 10^{-5}.

It is the simplest and most accurate method of finding the field direction of a dipole: accuracies of 0.1 mrad are commonly reached [30]. The single stretched wire technique is relevant to finding the axis, main field direction, and longitudinal position of a quadrupole magnet [13]. Further details about the method are given in Appendix B.1.

2.2.2 Vibrating wire

Mechanical oscillations of the stretched wire can be induced by the Lorentz force created by AC current flowing into the wire going through the static field of the measured magnet. This technique, proposed by A. Temnykh [29], has sub-micrometre sensitivity to sense a quadrupole axis. It can be used to measure separately the axis of several magnets aligned on a girder and has been extended to find sextupole axes. In practice, the AC current is usually tuned to the natural oscillation frequency of the wire or one of its harmonics, for reason of sensitivity in measuring the magnet axis. This is not true if the wire is used to measure the field homogeneity as has been proposed in [1] and [2] due to instability of amplitude oscillations at the natural frequency oscillation. The wire motion in the vertical, respectively horizontal, plane is caused by the Lorentz forces between the wire current and the horizontal, respectively vertical, magnetic field. Therefore two wire vibration detectors are mounted orthogonal to each other. A procedure to centre one

quadrupole is straightforward. The wire oscillation detectors can be located in a longitudinal position where the amplitude is large for the vibration harmonic considered. Since the Lorentz force is zero if the wire is aligned with the quadrupole axis, the magnet or the wire can be moved until vanishing oscillations are seen in both planes.

2.3 Methods for measuring magnetic field homogeneity

In the past, electromagnets were designed by using analytical calculations or by measuring representative voltage maps in electrolytic tanks and resistive sheets. Magnetic measurements on the final magnets and even on intermediate magnet models were imperative at that time. Today, it has become possible to calculate the strength and quality of magnetic fields with impressive accuracy. However, the best and most direct way to verify that the expected field quality has been reached is magnetic measurements on the finished magnet. It is also the most efficient way of verifying the quality of series produced [17]. At the early stage of the magnet life-time, the field homogeneity (i.e. the quality of the field in terms of multipole component) is the most important parameter and modifications can be made to the magnet design in order to meet the requirements. The most important method for such kind of measurement is without any doubt the fluxmeter method. It is based on the induction law. Nowadays the electronic and high precision mechanics development has made the rotating (or fixed) coil fluxmeter the best solution to measure the field inhomogeneity. More practical is the application for such kind of measurements of hall effect sensors [24].

2.3.1 Rotating coils

In a rotating coil measurement system, the flux Φ intercepted by the coil rotating in a static magnetic field can be expressed as a discrete series in N angular positions θ_k [30], equally spaced over the interval [0, 2π]. The field harmonic content is proportional to the DFT of the flux samples:

$$\Psi_n = \frac{2}{N}\sum_{k=1}^{N}\Phi_k e^{-2\pi i n\frac{k}{N}} \quad . \tag{2.2}$$

From these complex values of the DFT, the harmonic coefficients of the magnetic field multipoles (eq. 1.10) are derived:

$$C_n = B_n + iA_n = \frac{R_{ref}^{n-1}}{\kappa_n}\Psi_n \quad , \tag{2.3}$$

where:

- R_{ref} is a reference radius, namely the radius of the circumference bounding the good field region for the beam, i.e. the region where the multipole errors of the

field should remain inside the defined tolerances. In magnet test practice, usually it corresponds to the measurement radius [30];

- and κ_n are the complex geometric factors related to the coil windings position in the frame *x-y* with origin on the coil shaft rotation axis (Fig. 3.4):

$$\kappa_n = \frac{N_t L}{n}\left[\left(R_0 + i\frac{W_{eff}}{2}\right)^n - \left(R_0 - i\frac{W_{eff}}{2}\right)^n\right]e^{in\varphi_0} \tag{2.4}$$

where R_0 is the equivalent rotation radius of the coil, L is the length of the coil, W_{eff} is the equivalent width, and φ0 is the angle at the rotation start.

The results of a rotating coil measurement are usually reported with respect to the main field component. In the case of a quadrupole magnet, the real B_n and imaginary parts A_n of the C_n coefficients are normalized to C_2, expressed as 10^{-4} (units [30]) at the reference radius R_{ref}:

$$\underbrace{b_n + ia_n}_{c_n} = 10^4 \frac{B_n + iA_n}{\|C_2\|} \tag{2.5}$$

The harmonic coil method was developed with early analog integrators forcing the measuring coil to rotate stepwise between consecutive angular positions [11]. Fast angular encoders and purpose-developed voltage integrators with zero dead time between the angular positions are the basis of today's systems acquiring several hundred points per turn with a rotation rate as high as 10 turns per second. It is the best method for measuring higher order multipoles within a well-established theoretical frame, in particular for superconducting and quadrupole magnets having circular apertures. Progress in data acquisition equipment and data analysis tools alleviates the complexity of the formalism applied to the amount of data to treat, so that fully automated instruments and data analysis processes have been developed for measurements of series of magnets with high confidence in the final results.

The power of the harmonic coil method is its ability to measure any type of 2D magnetic field. It can be demonstrated [12] that a rotating coil measures the 2D field integrated over its length as long as the field component parallel to the rotation axis is zero on the two coil ends as defined in eq. 2.3.

The reference radius R_{ref} is an important concept for accelerator magnets having apertures much smaller than one metre. R_{ref} corresponds to: (i) the useful aperture for the beam, (ii) 2/3 of the yoke aperture in resistive magnets, (iii) the radius where the multipoles relative to the main field, the c_n in Eq. (2.5), have the same order of magnitude in a real magnet. It is important to carefully choose this reference radius at the beginning of a project because it will be the common term between beam optic physicists, magnet designers, measurement and data analysis teams.

The harmonic coil measures with high accuracy as well the direction of the main field component with respect to the measuring coil direction. It gives as well the axis of a

quadrupole or sextupole magnet with respect to the rotation axis of the measuring coil. This property is also useful to as first step of the fiducialization process described in chapter 1. The rotating coil gives the field description, in the reference frame *x'-y'* Fig. 2.1) at φ_0=0, usually given by the reference angle of the encoder.

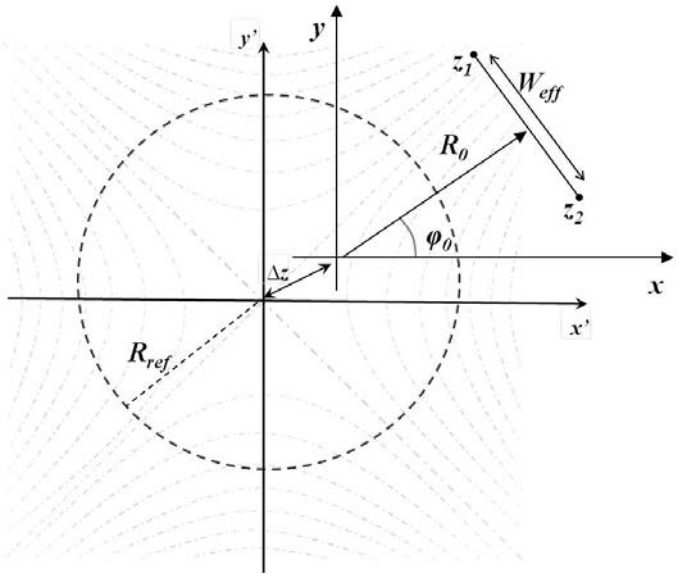

Figure 2.1: Geometry of a generic coil rotating in a quadrupolar field: magnetic *x'-y'* and coil *x-y* frames.

The main field direction corresponds to a zero main skew term (A_1 = 0 for a dipole magnet A_2 for a quadrupole). This field direction does not correspond (usually) to the mechanical symmetry plane of the magnet. For this reason, both, the coil and the magnet has to be aligned to the gravity. The angle of the main harmonic is the field direction of the magnet and can be calculated as follow:

$$\theta_f = \arctan\left(\frac{A_N}{NB_N}\right) \tag{2.6}$$

Where *N* is the order of the magnet. To obtain a univoque definition of the main field direction the arctan must be limited to the interval [-π/2 ... π /2].

The coil rotation axis (the origin of the frame *x'-y'*) could not be centred in the magnetic frame *x-y,* so the harmonics seen by the coil should be corrected by a factor given by the distance *Δz* between the two frames. This is the so-called 'feed-down' correction. The n^{th} multipole in the magnet frame (the subscript *m* here indicate the magnet frame) is related to the multipole in the coil frame (subscript *c*) by the following relation [8]:

$$C_{m,n} = \sum_{k=n}^{+\infty} \frac{(k-1)!}{(n-1)!(k-n)!} C_{m,n} \left(\frac{\Delta z}{R_{REF}}\right)^{k-n} \tag{2.7}$$

It must be stressed, however, that displacing the reference frame corresponds to describing the field outside the measurement circle, thus extrapolating the measurements outside their validity range. This feed-down correction loses validity for large values of $\Delta z/R_{ref}$. In chapter 4 will be shown how a first approximation of eq. 2.7 can be used to calculate the axis of a quadrupole and how this information is used in the fiducialization process.

In [30] is shown that high precision in measuring multipoles requires high quality encoders and high quality of the coil geometry and rotation mechanics. In addition, since the interested is focused on the harmonics error the best solution is suppress in a way the contribution of the main field component. By using another coil with the same magnetic surface and connecting it in opposition at the integrator input the resulting κ_1 is zero, so the dipole harmonic is directly rejected from the measurement. This assembly of coils is called "bucking coils" in literature [11]. The coil bucking also helps to remove systematic errors on the coil rotation having particular influence in measuring small magnet as will be shown in the following chapters.

2.3.2 Stationary coils

Most accelerator magnets (especially iron dominated magnets) have to be measured in fast current ramping conditions. A square coil is an easy tool to use in fixed position in a field pulsed from 0 to nominal value. Modern integrators with large bandwidth and time resolution connected to such a coil can give the full $B_1(t)$ curve and measure saturation effects of the iron yoke. Hysteresis and eddy current effects can be separated by measurements at different ramp rates. One precaution deals with the remanent field of the magnet being measured, i.e., the field at zero current value. Three ways can be used to solve it:

- have a bipolar power supply to perform symmetric sweeps from negative to positive maximum current;
- demagnetize the magnet first, with either a bipolar supply or a supply with an inverter;
- measure the remanent field with a flip coil or Hall plates for instance, low accuracy is sufficient in most of the cases.

Here the problem is that with one coil in one position is only possible to measure the main field component, more complex geometry or measurements procedure shell be adopted to measure the multipole errors in dynamic field conditions. In [23] is proposed a complex coil array that can measure any multipole magnet, or magnet component, in pulsed mode, i.e., with static coil array. Identical coils are located around a cylinder frame with the symmetry to be measured (Fig. 2.2).

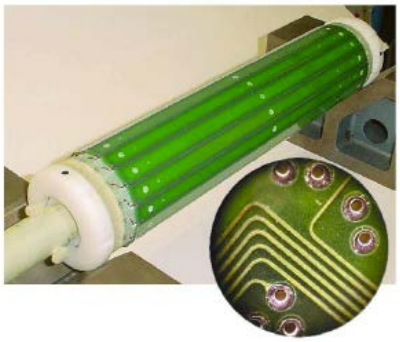

Figure 2.2: Measuring shaft with 16 individual coils made with printed circuit technology. A large number of harmonics can be measured in pulsed mode by using various connection schemes

The number of coils is equal to the multipole order to be measured: three coils for a sextupole, etc. Fig. 3.5 details an array of coils able to measure up to 16 harmonics by different connection schemes to put in series the individual 32 coils. Small discrepancies between the individual coils can be eliminated by turning the coil frame at different angular positions. The arrays are made by several printed-circuit coils, mounted on a cylindrical structure, e.g. 32 coils to measure up the 16th harmonic. This technique requires identical coils, very precisely positioned on the support, and turns out to be difficult for narrow-aperture magnets. One should not forget that a coil scheme sensitive to a multipole of order n is as well sensitive to order $n\ (2m + 1)$. Reference [19] describes the full theory of this technique. . In [21] and [26] stationary coil arrays have been proposed to measure the harmonic content of fast-changing multipole fields.

2.3.3 Hall probes

An arrangement of m Hall plates, equally spaced on the circumference of a ring and radially oriented, allows all the field components with an order lower than m to be suppressed. The measured signal for the field component of order m can be maximized if all the Hall plates are placed in the poles of the $2m$-pole field. (Fig. 2.3a and 2.3b) shows an arrangement of 3 Hall plates in a dipolar and a sextupolar field. Further details about this method are given in Appendix B.3.

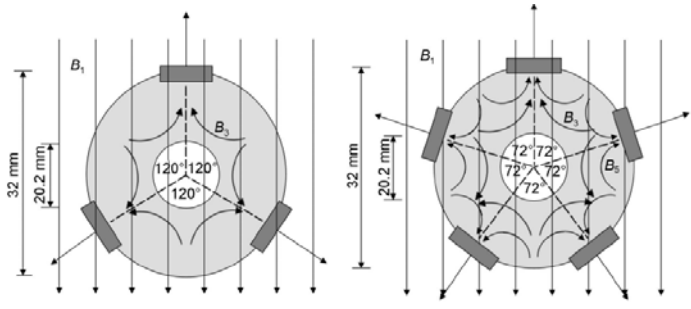

Figure 2.3: Hall probe arrangement for (a) a sextupole measurement with 3 and a (b) decapole with 5 Hall plates. The probes are used to measure multipoles 3 and 5 in a dipole field B_1.

2.4 Methods for magnets monitoring

In section 2.2.2 the measurement method with a static coil has been shown as the easiest solution to measure magnets in fast current ramping conditions. This measurement method can be adopted to measure the field quality as it was shown, but is also the base component to realize a more complex measurement system useful to measure the magnet behaviours during the machine operations. Such measurement is mainly used as feedback for the magnet power supplies having a control system based on the field. In section 1.5 the requirements of the measurement systems for monitoring the field inside the accelerator during the operation have been shown. As principle, there are two different approaches to monitor the field for ramped machines. One is based on mathematical models of the magnet as function of the magnet. As described in section 1.5, one of such model is Fidel, the field model of the LHC. Fidel, nowadays, has shown that the LHC superconducting magnets are quite reproducible form cycle to cycle, because the model is able to predict the magnetic field dynamics effect quite properly. In [10] is proposed a similar model also for the injector chain of the LHC, in particular for the Proton Synchrotron Booster (PSB). The model has shown a good reproducibility of the field as function of the excitation current, and at the moment is used as support in case of fault of the real-time measurement system. The other approach is the real time measurement with a fixed coil opportunely calibrated at low field with a more precise field measurement system as could be an Nuclear Magnetic Resonance (NMR) probe. In the following, will be detailed the two approaches with their advantages and limitations.

2.4.1 Time-domain magnetic modelling

A time domain magnetic model predicts the response of the magnets installed in the accelerator once a given current cycle is applied. The most representative of such model is Fidel (Field description of the LHC). It is a set of equations whose coefficients are obtained from the syntheses of the information available from magnetic field measurements (both room temperature and 1.9 or 4.2 K) on the LHC superconducting dipoles. The aim is to provide the integral transfer function (integral field vs. current) in a form suitable for inversion (current vs. integral field) for each circuit in the LHC. In addition, for the main ring magnets FiDeL will provide a prediction of the field errors to be used to set the corrector circuits [15].

As aforementioned, a mathematical model has been implemented also to describe the field in the LHC injector's dipole, in particular for the PSB. The theoretical magnet model of the Booster dipole, takes as input the vector array with the curve $L\ \partial I/\partial t$ (L is the magnet inductance), that is the same input send to the magnet power converter, and gives

as output the field as function of the time with 10^{-4} precision. This information is distributed on software channels to provide the magnetic field directly to the application programs and to create a synthetic B-Train [10].

2.4.2 Real-time magnetic field measurements

In most of the cases, especially for accelerator composed by iron dominated magnets (see Appendix A) a mathematical model is not enough to describe the magnetic field bending/focusing the particle beam, mostly due to the difficulty on predict the magnet powering history. So the best solution is to measure directly the field in the accelerator. The magnets in the accelerator ring are connected in series to the same power supply usually, or thanks to the high reproducibility of the current (better than 5 ppm in most of the accelerator power supply), it can be assumed that all the magnets have the same input current. The idea is to put a spare magnet in series to the ones installed in the accelerator and take this magnet (the reference magnet) as representative of the entire population and install in this magnet all the instrumentation to monitor the magnetic field in the machine. A rotating coil fluxmeter could be in principle a valid choice for these measurements, especially because it could provide an absolute value of the field [4]. However, even state-of-the-art rotating coil systems can hardly provide a bandwidth larger than 10 Hz, which is typically three orders of magnitude lower than what is required for fast-cycled magnets. Hence, it is natural to use a static coil fluxmeter, providing a voltage output proportional to the field rate *dB/dt,* with sensitivity increasing with the bandwidth. An additional measurement is needed however to provide the integration constant. This is commonly carried out by a "field marker", i.e. a device able to provide a digital trigger pulse as the field crosses a given threshold [28]. The field data are then distributed to the different subsystems, typically as two parallel incremental and decremental digital pulse trains ("B-trains"). By simply counting the pulses, each user can reconstruct the magnetic field as a function of the time [14]. In Fig. 2.4, the principle of a monitor system is shown. The field marker starts the digital train. The pulse frequency is proportional to the $|\dot{B}|$ sensed by a fixed coil with an equivalent surface A_{coil} during the ramp-up and ramp-down of the magnet. The coil voltage is proportional to the field gradient ($\dot{B}$), thus the field measured is:

$$B(t) = B_{\text{marker}}(t_1) + \int_{t_1}^{t} \dot{B} dt \tag{2.8}$$

where $B_{marker}(t_1)$ is the field measured by the marker at about 5 mT (below the injection flat bottom).

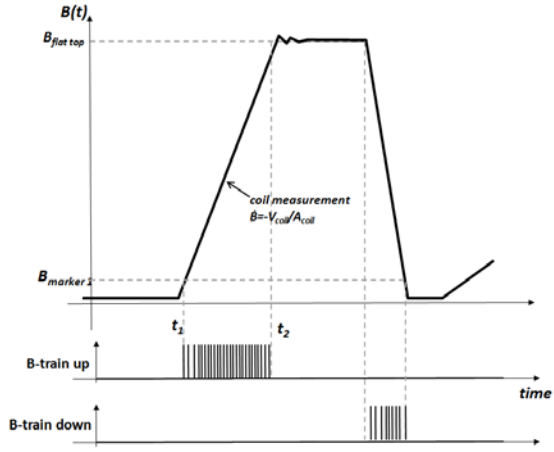

Figure 2.4: Principle of a monitor system.

A monitor system is actually used in the Proton Synchrotron (PS) injector of the LHC [9] to monitor the field generated by combined function magnets (see Appendix A) providing the focusing/defocusing and steering field to the beam. For such system a peaking strip (see section 2.4.2.1 for the details about the different types of field markers) is used as field marker. In Fig. 2.5, the present real-time measurement system of the PS is sketched. Several coils placed in different positions of the reference magnet aperture provide the $\dot{B}$ signal after a suitable amplification.

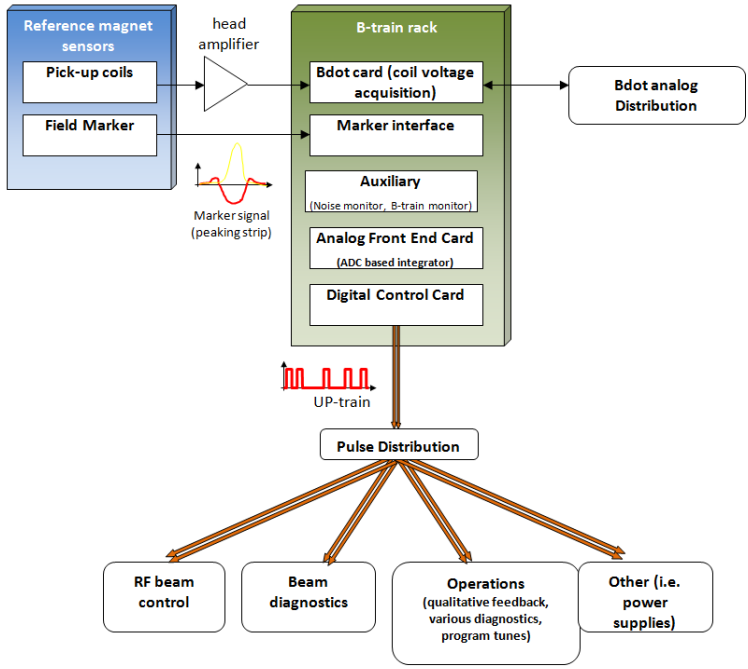

Figure 2.5: Overview of the monitor system of PS

The generated digital train pulse has a resolution of 10 μT: at each field increment of 10 μT, a pulse is released to the different users through a digital control card. Future requirements in terms of beam quality for the LHC have a direct impact on the performance, first of the PS in general, and, more specifically, on the field measurement [3].

2.4.2.1 Field markers

In the monitor measurement systems the accuracy of the overall measurement is dominated by the uncertainty of the field marker, because the coil used to measure the dynamic field can be dimensioned to have always a good signal to noise ratio according to the field ramp rate. Among the possible choices for the field marker [28], in many practical cases the peaking strip is the most appropriate [20]. In ref. [20] performance and limitations of this transducer are described. The achievable accuracy is mainly dominated by the width of the pulse. Kelly calculated the uncertainty of such a method fixing the limit to $\pm 2\ 10^{-6}$ T for a dB/dt of 1 T. The limitation of this transducer is mainly due to heating constraints on the biasing coil, making it unsuitable for operation above a few tens of millitesla.

Field markers based on Nuclear Magnetic Resonance Field sensors (NMR) are currently the "golden" metrological standard, providing the best absolute accuracy in a wide field range [17]. The physical principle of NMR probes is the excitation of the precession movement of the proton spin in a hydrogen nucleus [16]. The precession frequency is related to the external magnetic field by the gyro-magnetic ratio which is 42.576396 MHz/T for protons in water at 25°C [25]. In general NMR probes require a homogeneous bias magnetic field across the active volume in order to obtain a response from all spins at the same frequency. When this condition is not met, the response is "smeared out" over a considerably wider frequency range, causing a strong attenuation of the observed signal. This excludes the application of NMR probes in inhomogeneous fields as occur for example in quadrupole magnets. As mentioned above, the precession frequency of the protons in the active material depends only on the total magnetic field at the probe location. In general, this total field is given by the superposition of the external field (to be measured) plus a contribution from an auxiliary modulation coil nearby [22]. Also in dynamic conditions, the NMR is limited by maximum relative ramp rates of about 0.05 T/s as has been shown in [5].

If there is a need to take measurements in inhomogeneous fields by means of a spin resonance device, then one may consider the use of FerriMagnetic Resonance (FMR) probes. FMR is a type of electron spin resonance based on a slight imbalance of the energy emitted and absorbed by electrons flipping between opposite spin states under the influence of incident electromagnetic radiation. Due to their small probe sizes (diam. down to 0.3 mm) and comparatively low Q-values (~1000), considerable gradients can be tolerated. A useful FMR response has even been obtained in a typical accelerator

quadrupole magnet [6]. Details about the sensor and a transducer based on such technologies are given in chapter 5.

[1] P. Arpaia, M. Buzio, J. J. G. Perez, G. Golluccio, C. Petrone, L. Walckiers, Magnetic field measurements on small magnets by vibrating wire systems, IEEE Instrumentation and Measurement Technology Conference (I2MTC), 2011.

[2] P Arpaia, M Buzio, J Garcia Perez, C Petrone, S Russenschuck and L Walckiers, Measuring field multipoles in accelerator magnets with small-apertures by an oscillating wire moved on a circular trajectory, Journal of Instrumentation (JINST), vol. 7, May 2012.

[3] P. Arpaia, M. Buzio; F. Caspers, G. Golluccio, C. Petrone, Static metrological characterization of a ferrimagnetic resonance transducer for real-time magnetic field markers in particle accelerators, Instrumentation and Measurement Technology Conference (I2MTC), 2011.

[4] P. Bauer , M. Lamm, G. Lorenz, J. Nogiec, T. Peterson, R. Sood,W. Soyars, C. Sylvester, M. Tartaglia, G. Velev, Cost Estimate For a Tevatron Reference Magnet System, Fermilab internal note, FERMILAB - TD-02-042, 2002.

[5] A. Beaumont, Magnetic field markers of the B-Train for the Proton Synchrotron accelerator, rapport de stage ST50, 2008,

[6] M. Benedikt , F. Caspers, M. Lindroos, Application of Magnetic Markers for Precise Measurement of Magnetic Fields in Ramped Accelerators, Particle Accelerators: 63, 1999.

[7] L. Bottura M. Buzio, S. Pauletta, N. Smirnov, Measurement of magnetic axis in accelerator magnets: critical comparison of methods and instruments, IMTC 2006 Instrumentation and Measurement Technology Conference, Sorrento, 2006.

[8] L. Bottura, Standard Analysis Procedures for Field Quality Measurement of the LHC Magnets - Part I: Harmonics, CERN internal note LHC-MTA-IN-97-007, 2001.

[9] M. Buzio, P. Galbraith, G. Golluccio, D. Giloteaux, S. Gilardoni, C. Petrone, L. Walckiers, Development of Upgraded Magnetic Instrumentation for CERN Real-Time Reference Field Measurement Systems, Proceedings of International Particle Accelerator Conference (IPAC), 2010.

[10] F. Caspers, W. Heinze, J. Lewis, M. Lindroos, T. Salvermoser, An Alternative to Classical Real-time Magnetic Field Measurements using a Magnet Model, International Conference on Accelerator and Large Experimental Physics Control Systems (ICALEPCS '97), 1997.

[11] J. Cobb, D. Horelick, 1972, Proc. 3rd Int. Conf. on Magnet Technology, 1972.

[12] W. G. Davies, The theory of the measurement of magnetic multipole fields with rotating coil magnetometers, Nucl. Instrum. Methods, A311, 1992.

[13] J. DiMarco, H. Glass, M.J. Lamm, P. Schlabach, C. Sylvester, J.C. Tompkins, Field alignment of quadrupole magnets for the LHC interaction regions, IEEE Trans. Appl. Supercond., vol. 10-1, 2000.

[14] P.D. Eversheim,P. von Rossen,B. Schüller, F. Hinterberger, A fast Precise Magnetic

Field Control, Nuclear Instruments and Methods, Vol. 160, 1979.
[15] FiDeL, homepage, fidel.web.cern.ch/fidel/.
[16] F. Hartmann, Resonance Magnetometers, IEEE Transaction on Magnetics, MAG-8, 1972.
[17] K. N. Henrichsen, Magnetic Field Mapping, John Wiley & Sons, 2005.
[18] A. Jain, CERN Accelerator School: Measurement and Alignment of Accelerator and Detector Magnets, CERN 98-05, 1998.
[19] A. Jain, G. Ganetis, A. Ghosh, W. Louie, A. Marone, R. Thomas, P. Wanderer, Field quality measurements at high ramp rates in a prototype dipole for the Fair project, IEEE Trans. Appl. Supercond., vol 18-2, 2008.
[20] J. M. Kelly, Magnetic Field Measurements with Peaking Strips, Review of Scientific Instruments, Vol. 22, 1957.
[21] M. Kobayashi, Measurement of harmonic field contents of pulsed magnets using a stepping search coil Nuclear Instrument and Methods vol.103, 1972.
[22] Metrolab, NMR Teslameter PT2025: user manual, v. 2.0, 2003.
[23] G. H. Morgan Proc. 4th Int. Conf. on Magnet Technology, Upton, NY, USAEC CONF- 720908 Atomic Energy Commission, 1973.
[24] S.I. Redin, Nuclear Instruments and Methods in Physics Research A 473, 2001.
[25] NIST Journal, Vol. 95, Nb. 5, page 521, 1990.
[26] P. Schnizer, H. R. Kiesewetter, T. Mack, T. Knapp, F. Klos, M. Manderla, S. Rauch, M. Schönecker, R. Werkmann , A mole for Measuring Pulsed Supercondicting Magnets, IEEE transaction on applied superconductivity vol. 18, N.2. 2008.
[27] N. Smirnov, L. Bottura, M. Calvi, G. Deferne, J. DiMarco, N. Sammut, and S. Sanfilippo, Focusing strength measurements of the main quadrupoles for the LHC, IEEE Trans. Appl. Supercond., vol. 16-2, 2006.
[28] J. L. Symonds, Methods of Measuring Strong Magnetic Fields, Reports on Progress in Physics, Vol. 18, 1955.
[29] A. Temnykh, Vibrating wire field-mesuring technique, Nucl. Instrum. Methods Phys. Res., A 399 vol. 185, 1999.
[30] L. Walckiers, Magnetic Measurement with coils and wires, CERN Accelerator School: specialized course on magnets, 2009.

Chapter 3

Open Problems

3.1 Overview

The classical measurement methods for characterizing accelerator magnets in static and pulsed filed conditions are rotating and stationary coils, respectively. Nevertheless, such powerful methods have limitations arising from mechanics and electronics. The influence of mechanical imperfections or noise on the signal at the coil output becomes more and more important when the aperture of the magnet becomes smaller. Manufacturing coils and mechanics of few millimetre dimensions with a precision of 10^{-3} is a challenging process. In addition, for fast-pulsed electromagnets, the data acquisition system has to be fast and precise enough to not affect significantly the field quality evaluation owing to the dynamic effects of the magnets.

The precision of the real-time monitoring system of Section 2.4.2 depends mostly on the performance of the field sensor used as marker. The performance of high-precision field sensors as the NMR [1] is affected by: (i) the size of the probe in inhomogeneous magnetic fields, and (ii) the response to fast ramped fields. In accelerators with combined function magnets, both of these issues are relevant (Appendix A).

In this Chapter, the main problems arising from the test of small-aperture fast-pulsed magnets and the monitoring of strongly inhomogeneous combined-function magnets are detailed.

3.2 Characterization of small-aperture and fast-pulsed magnets

Mechanical or electronic imperfections mainly affect the measurement of the `higher order' multipoles, i.e., those with harmonic numbers higher than the magnet multipole order. There are three main error sources: (i) the voltage integrator offset coupled with irregular rotation rate of the coil, (ii) the error in the coil angle measurement due either to the angular encoder or to torsions of the coil shaft during rotation, and (iii) the instability or movement of the rotation axis of the coil shaft due to gravity, bearings quality, or vibrations.

Schemes of bucking coil have been developed [5] to remove the signal coming from the magnet main multipole, in order to increase the amplification factor at the input of the integrator. More notably, these compensation coil assemblies remove nonlinear coupling arising from the main harmonic and corrupting the high-order harmonic measurement. However, all the errors due to the mechanics and the electronics become more influent when the size of the coils becomes smaller. Manufacturing coils (windings supports, etc.) and rotation mechanics with 10^{-3} of precision become very difficult in the dimension of

few mm. PCB solutions can be adopted in such a case [3], but limited by the number of turns of the coil, giving rise to a significant influence of the offset and the electrical noise on the integration. An example of application of small-diameter coils for measuring field homogeneity is the permanent and electro magnets of the Linac4 accelerator at CERN [8]. For those small-aperture (e.g. range 20-40 mm) and short-length multipole magnets, the typical requirements for the measurement system are:

- to verify that magnet field strength is within accelerator designers tolerances, typically 0.5 %;
- to check that the higher multipole components up to 10^{th} order are less than 1 % of the main field;
- to verify the fiducialization, namely, that the quadrupole axis position and the roll angle (field direction) remain within the tolerance of ±0.1 mm and ±1 mrad with respect to mechanical markers on the external magnet surface (pins);
- to verify that the relative position of the mechanical markers on the magnet body remains in the defined tolerances for the entire batch of magnets installed in the accelerator;
- and, in addition, for pulsed quadrupole magnets, to define the field repeatability (history dependence and power supply stability) and to measure the eddy current effects.

The quality of the aforementioned measurements mainly depends on the coil sensitivity factors κ_n (3.11), thus on the shaft manufacturing tolerances. The measurement uncertainty depends on the coil mechanical quality, namely on the length, width, and rotation radius. In very-short and small-aperture magnets, tested with a coil of length higher than the longitudinal field distribution, the coil irregularities worsen the uncertainty of C_n. In other words, if the width and radius vary along the coil, the magnetic measurement depends on the average parameters weighted by the field. The averaged parameters, such as those obtained by calibrating the coil in a reference magnet longer than the coil, may lead to errors in the per cent range. For this reason, an accurate knowledge of the coil parameters along the effective magnetic length of the magnet is mandatory.

In the particular case of a linear accelerator, where the transversal focusing of the beam is achieved by quadrupoles mounted in the drift tubes [7]-[8], the knowledge of the geometrical position of the magnet quadrupole axis and the field direction with respect to the external frame, is crucial for the tubes assembling. In the fiducialization, the alignment of the magnets is obtained by referring the measured magnetic axis to an external mechanical target.

For standard use in accelerators, the dimensions allow the installation of optical targets on the magnet hit by a laser tracker [5]. The small dimension of the Linac4's quadrupoles and their further welding into the drift tube elements require another solution. Their external cylinders are machined within 10 micrometre and holes for reference pins are used to define a mechanical frame. Therefore, offsets between magnetic axis and these

references have only to be measured and limitations of optical systems, in the order of 30 to 100 μm, are overcome.
A further issue concerns the dependence of the multipole field components of a magnet (normal or superconducting) [6] on the field ramp rate. In dynamic conditions, the rotating coil method requires a coil rotation faster than the field changes. This solution is excluded for fields ramping in 200-300 μs. The natural solution to measure such a kind of fast-changing field is to integrate the flux from a stationary coil. If the measurement is repeated in different angular positions, their multipoles can be reconstructed. This approach is based on the reproducibility of the field from cycle to cycle: the magnetic fluxes are measured with a shaft positioned at a different angle for each cycle. The multipoles are deduced in a similar way as the classical rotating shaft method. The second approach is the one showed in Section 2.3.2 [4]. This method allows the multipole to be measured during one ramp, but a complex coil shaft manufacturing is needed and the maximum number of measurable multipoles is limited by the number of coils. In addition, each coil needs for an individual calibration to obtain a correct compensation of the main multipole terms.

3.3 Accurate monitoring of inhomogeneous field magnets

Performance of an accelerator field monitor system is limited mainly by the accuracy and the reliability of the field marker. Accuracy is limited by two parameters: (i) the size of the probe in not homogeneous magnetic fields, and (ii) the response to fast ramped fields. In accelerators with combined function magnets, as in the Proton Synchrotron (PS) magnets, both of these issues are relevant, with the additional problem that the same magnet is used to provide the focusing (F) and defocusing (D) effect, simultaneously. These twofold effects reduce the sensitivity to mechanical misalignment between the F and D and also lead to optimal location of corrector lenses (sextupoles and octupoles). Each magnetic unit is equipped with a coil providing the nominal field. It is wound around the top (south) and the bottom (north) poles. An additional coil with an “eight loop” (Fig. 3.1) is used to change the beam tuning (i.e. the gradient component in the two halves). This is installed around the pole profile, both on the north and the south pole and, as the name indicates, it has the shape of an 8 with the two poles D and F in one of the two eight-loops, respectively. The consequence is that the current goes in opposite direction in the loops around the two poles, and thus has an opposite change of the global field strength in the two half-units. It can thereby increase the gradient in one of the half units, while decreasing it in the other simultaneously.

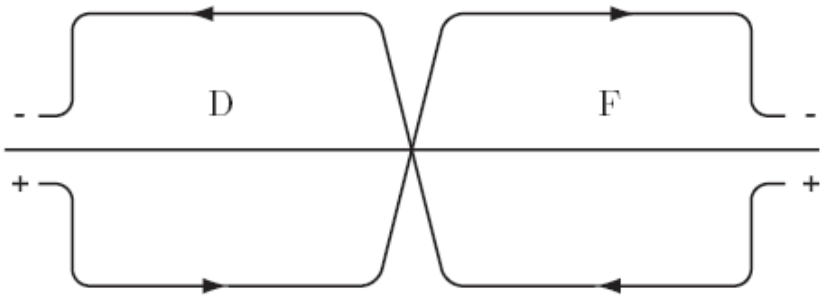

Figure 3.1: shape of 8 current coil circuit of PS combined function magnets.

This magnet has also other independent current circuits, on both the D and F sides of the magnet to adjust the tune (quadrupole field) and chromaticity (sextupole field) during the operation. All those current circuits (Fig. 3.2) contribute to the field quality [1]. For this reason, in the PS accelerator are installed two monitoring systems, one in the F and the other in the D half.

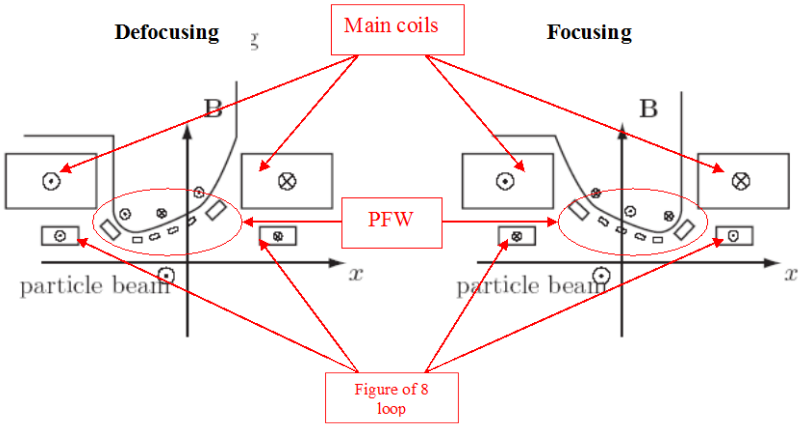

Figure 3.2: Cross section of the PS magnet with the different excitation coils.

In a recent measurement campaign, the cycling history of the magnet was shown to influence the beam radial position. In particular, Figs 3.3 and 3.4 show the results of the test campaign, aimed at understanding the source of an apparent discrepancy of a few Gauss between beam control parameters and the field monitor measurements, leading to cycling-dependent radial position errors. In particular, for the first time, the field in the F and D halves of the reference magnet has been tracked, showing how powering the coil between cycles (Fig. 3.4) imbalances the remanent field, possibly explaining the discrepancy observed in the subsequent cycle [2].

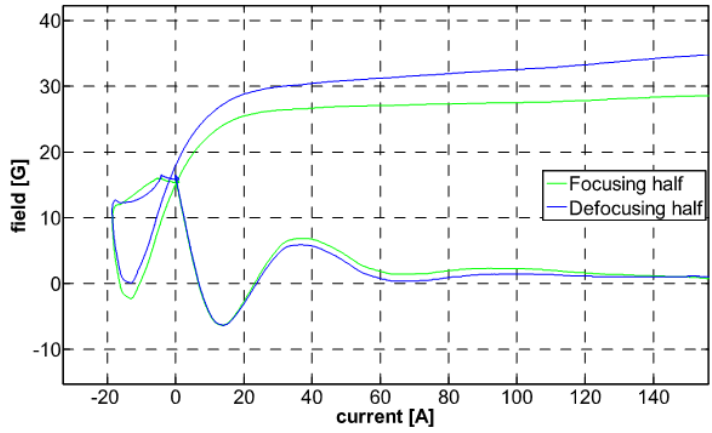

Figure 3.3: Zoom of the hysteresis loops in a typical case (linear part of the magnet transfer function B=2.5 10^{-4}T/A subtracted).

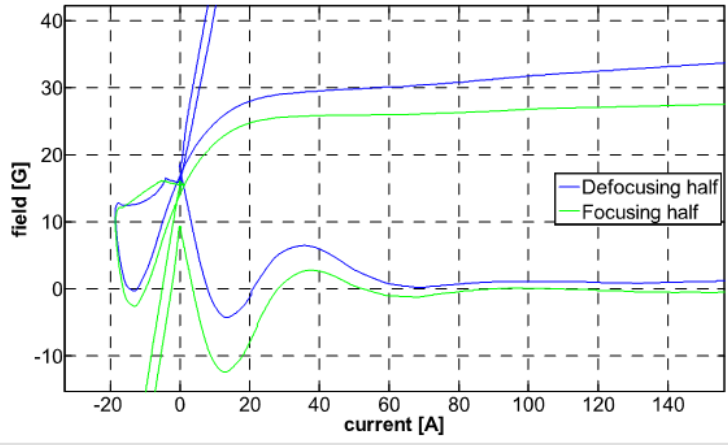

Figure 3.4: Hysteresis loop for a cycle exhibiting radial position displacement, just after an isolated figure 8 coil powering cycle.

Another result concerns the large fluctuation due to the history-dependent residual field (Fig. 3.5). They make more difficult a precise measurement when the field marker triggers at low field (4.98 mT, e.g. for the peaking strip). A higher trigger level (around 60 mT or higher) can improve the field stability and control. With the actual configuration of the B-train, using only one field marker as reference, the assumption to have a correct feedback information to the power supply and to the RF cavities control systems, is that the $B_D(t_0)=B_F(t_0)$=4.98 mT (with t_0 field marker trigger instant). When this assumption is not satisfied, the beam becomes instable.

The measurement campaign has addressed the field maker as the weak point for the improvement of the B-train having the challenging requirements to achieve $\pm$5 µT of

precision on the digital train pulse. In addition, the field marker has to be able to work in a range from 60 to 500 mT and to preserve long-term stability (at most $\pm$50 µT /year). Therefore, a scientific collaboration with the University of Sannio has been started aimed at developing a high performance field marker based on FMR for the B-train upgrade.

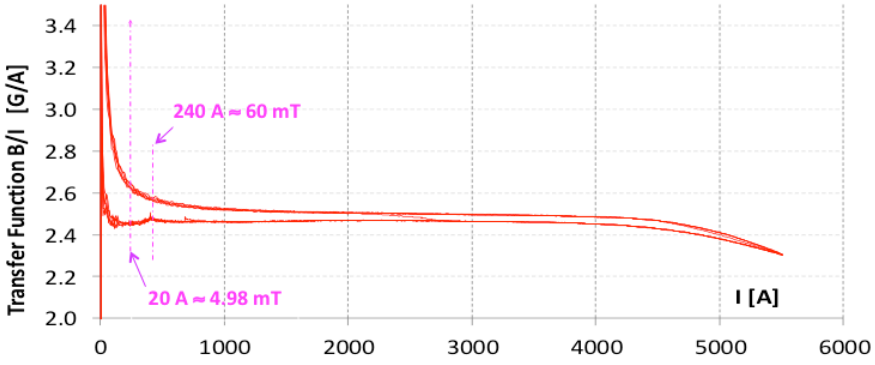

Figure 3.5: effect of the low-field fluctuations in the PS magnet.

[1] A. Beaumont, Magnetic field markers of the B-Train for the Proton Synchrotron accelerator, rapport de stage ST50, 2008,

[2] M. Buzio, P. Galbraith, G. Golluccio, D. Giloteaux, S. Gilardoni, C. Petrone, L. Walckiers, Development of Upgraded Magnetic Instrumentation for CERN Real-Time Reference Field Measurement Systems, Proceedings of International Particle Accelerator Conference (IPAC), 2010.

[3] Y. Iwashita, Modification and measurement of the adjustable permanent magnet quadrupole for the final focus in a linear collider, Particle Accelerator Conference, PAC2007, 2007.

[4] A. Jain, G. Ganetis, A. Ghosh, W. Louie, A. Marone, R. Thomas, P. Wanderer., Field quality measurements at high ramp rates in a prototype dipole for the Fair project, IEEE Trans. Appl. Supercond., vol 18-2, 2008.

[5] R. M. Main, Measurement and correction of the PEP interaction region quadrupole magnets, IEEE Transaction on Nuclear Science, vol. NS-26, N. 3, 1979.

[6] P. Schnizer, H. R. Kiesewetter, T. Mack, T. Knapp, F. Klos, M. Manderla, S. Rauch, M. Schönecker, R. Werkmann ¸ A mole for Measuring Pulsed Superconducting Magnets, IEEE transaction on applied superconductivity vol. 18, N.2. 2008.

[7] V. Skachkov, Permanent Magnet Quadrupole for the 1-st Tank of Linac4, Proceedings of Russian Particle Accelerator Conference (RuPac), 2006.

[8] M. Vretenar, Construction Status of Linac4, Proceedings of Particle accelerator Conference (PAC09), 2009.

PART II - PROPOSAL

Chapter 4

Measurement method for small-aperture and fast-ramped magnets characterization

4.1 Overview

The measurement of the magnetic field is often the final verification of the complex design and fabrication process of accelerator magnets. In several cases, when seeking high accuracy, the measurement technique and its realization can result in a considerable effort [6]. In this Chapter, the method and the system proposed to characterize the magnetic properties of accelerator magnets are shown. In particular, the methods and the systems to characterize permanent and fast-pulsed iron-dominated small-aperture magnets are described. The traditional harmonic coil measurement is enhanced specifically for small-aperture magnets by: (i) in-situ calibration, for facing coil machining inaccuracy, (ii) flipping the magnet around its axis, for correcting systematic effects, and (iii) measuring fluxes by stationary coils at different angular positions for current cycles shorter than 1 s to measure fast-pulsed multipole magnets. The system allows a quadrupole magnet for particle accelerators to be characterized completely, by assessing multipole field components, magnetic axis position and field direction [19]. In the following, the basic ideas of the proposed method and the architecture of the corresponding measurement system are detailed.

4.2 A polyvalent harmonic coil measurement method

A polyvalent method has been developed to overcome the open problems described in the previous Chapter and to satisfy the requirements of new-generation accelerators magnets.
An example of those magnets is the small-aperture quadrupole magnets, pulsed or permanent, currently produced for Linac4 at CERN, accelerating the beam up to 150 MeV. The first part of Linac4, accelerating the proton beam up to 3 MeV, is composed by several magnets, with an aperture of 22 mm, providing a high gradient (about 20 T/m). They are excited by pulses of 1 ms, synchronized with the particle passage for the first part of the acceleration path in order to limit ohmic heating of the magnet coils. For such magnets, a precise knowledge of the field gradient and of the multipole errors in the actual operation conditions is essential for the control of the particle beams.
Currently, the rotating coil system is the best solution to measure magnet multipoles in static conditions [22], [13]. For small-aperture magnets, the small dimension of the external radius r of the rotating shaft limits the accuracy. The uncertainty on the coil sensitivity factors increases accordingly, while the signal-to-noise ratio decreases as r^3. Machining the coils as printed circuits reduces the errors on small coils, but gives rise to a lower winding density, and thus to a reduced sensitivity [7]. For small-radius coils, the measurement accuracy depends essentially on the calibration [3]. Hall probes could be used as field sensing elements to test multipole magnets homogeneity. However, they are less accurate in inhomogeneous fields and provide only local measurements; in addition, a complete field mapping turns out to be burdensome. A stretched-wire system [21] measures suitably the

integral field strength, as well as the magnet axis and field direction (roll angle), with typical accuracy of 0.2 %, but does not provide a measurement of the multipole content.
Systems based on wires (stretched, vibrating, or pulsed) [4]-[14] and rotating coils are the state of the art for testing properties of accelerators magnets, but with the non-trivial limitation of working only for static fields. For fast-pulsed magnets, the best solution is a static coil. In [10]-[20], stationary coil arrays have been proposed to measure the harmonic content of fast-changing multipole fields. The stepped-fixed coil method [16] could attain an adequate precision, with appropriate encoder positioning and optimized coil design.
In this Chapter, the abovementioned drawbacks are overcome by a polyvalent method, exploiting: (i) in-situ coil calibration, for facing the limitation in the multipole measurement accuracy due to the small aperture of the magnet; (ii) rotating quadrupole magnets about their axis by exploiting their cylindrical machining accuracy, for facing the problem of the magnet axis fiducialization; (iii) and a step-by-step coil rotation technique, for measuring fast ramping fields over several excitation current cycles. This method provides a complete characterization of the gradient strength, field direction, axis, and multipole errors for both permanent and fast-pulsed quadrupoles [1].

4.3 In-situ calibration for rotating coils measuring field homogeneity

In this Section, (i) the basic idea, and (ii) the method, and (iii) the procedure of the proposed in-situ calibration for rotating coil fluxmeters.

4.3.1 Basic idea

In measuring magnets with a longitudinal field distribution shorter than the coil length, only the specific coil portion involved in the measurement has to be considered. The in-situ calibration of the coil allows the machining constraints on the fluxmeter to be relaxed by reference measurements of magnetic field and mechanical displacement directly in the magnet type to be measured [3]. In this method, the reference field measurement is given by a Single-Stretched wire system [21], the best solution to measure the field gradient of small aperture magnets.

4.3.2 Method

In a quadrupolar field (Fig. 4.1), a displacement Δz between the magnet axis and the coil rotation axis gives rise to a dipole component in the measured field series expansion. If the dipole and quadrupole terms and the displacement are measured, the two calibration parameters, the equivalent radius R_{0m} and area A_{cm}, can be determined by analytical considerations.
The field coefficients C_n of the multipole expansion (eq. 2.5) measured by a rotating coil system are referred to the frame x-y (Fig. 4.1). In general, a translation and a rotation in the

complex plane are needed for referring the harmonic coefficients to the magnet frame *x'-y'* [Henrichsen, 2002]. The distance $\Delta z = \Delta x + i\Delta y$ is calculated at first order as

$$\Delta z = -R_{ref}\frac{C_1}{C_2} \quad . \tag{4.1}$$

In other words, a virtual dipole component C_1 is generated by a translation of the coil with respect to the magnet frame. In principle, if the magnet is moved transversally by a given distance Δx and the quadrupole component C_2 is known,

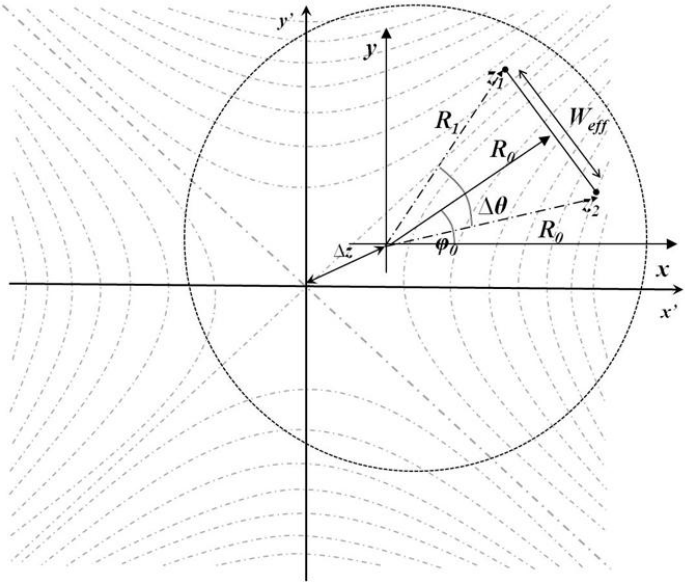

Figure.4.1: Coil frame x-y, with origin in rotation axis, and magnet frame x'-y'**.**

the radius R_{0m} and the total coil area A_{cm} can be obtained directly, because the system of equations determined from eqs. 2.4 and 2.5 for n=2 is defined:

$$\begin{cases} \dfrac{\Psi_1}{\kappa_1} = -\dfrac{C_2\Delta x}{R_{ref}} \\ C_2 = \dfrac{\Psi_2}{\kappa_2} \end{cases} \quad . \tag{4.2}$$

By computing κ_1 and κ_2 from (2.5) and by substituting them in (4.2) R_{0m} and A_{cm} are derived:

$$\begin{cases} R_{0m}e^{i\varphi_0} = -\dfrac{\Psi_2\Delta x}{\Delta\Psi_1} \\ A_{cm}e^{i\alpha} = ie^{i\varphi_0}\dfrac{\Delta\Psi_1 R_{ref}}{C_2\Delta x} \end{cases} \quad . \tag{4.3}$$

This method depends on the unknown initial offset Δz_0 between the frames. This can be avoided by considering the difference between two harmonic measurements with a given offset, i.e. ΔC_1 instead of C_1:

$$\Delta C_1 = \frac{\Delta \Psi_1}{\kappa_1} = -C_2 \frac{\Delta x}{R_{ref}} \quad . \tag{4.4}$$

The value of C_2, corresponding to the integrated quadrupole gradient (Focusing Strength) *FStrength*, must be determined by an independent measurement:

$$G_c = \frac{C_2}{R_{ref}} \quad . \tag{4.5}$$

In practice, the best solution providing the lowest uncertainty is the Single Stretched Wire (SSW see Section 2.2.1) [23], and *FStrength* is defined as the gradient integrated over the quadrupole axis:

$$FStrength = G_c \cdot L_{eff} = \int_{-\infty}^{\infty} G(l)\, dl \quad , \tag{4.6}$$

where L_{eff} is the effective magnetic length and G_c is the gradient at the longitudinal centre of the magnet [24].

4.3.3 Procedure

In Fig. 4.2, the flow diagram of the calibration procedure is depicted. First, *FStrength* is measured. Then, by keeping the magnet in the same position, a first rotating coil measurement is carried out to evaluate the flux arising from the quadrupole and dipole components (Ψ_2 and Ψ_1, respectively) at the starting position x_0. Finally, a displacement is applied to the magnet (or the coil), the flux measurement is repeated, and $\Delta\Psi_1$ and Ψ_2 are used in (4.3) to compute A_{cm} and R_{0m}. This procedure is independent on the measuring shaft dimension and can be also extended to higher-order magnets easily.

4.3.4 Coil calibration issues and influence on the field strength measurements

At the state of the art, for the in-situ procedure, the most precise solution for the absolute measurement of *FStrength* is the Single Stretched Wire (see Section 2.2.1). As a matter of fact, in strongly inhomogeneous fields NMR is not suitable [26]. Hall probes reach high accuracy but give only a local measurement and, moreover, needs for temperature compensation and frequent calibrations. Therefore, the SSW is the most accurate method, although limited by the dimensions of the magnet and its aperture, as well as by high-order multipoles [21]. The multipole influence increases according to the distance from the magnet axis. In particular, by exploiting the expression of *Smirnov* [21] at the radius R_{ref}, this influence can be estimated and compensated. However, in case of large multipoles, a

more detailed analysis showed that the accuracy of the reference stretched wire measurement itself could be affected. For instance, if we call $FStrength_x$ and $FStrength_y$ (according to eq. 4.6) the results of measurements done while translating the wire, initially centered, by

$$\begin{cases} \dfrac{Fstrength_x}{Fstrength} = 1 + \dfrac{1}{2}\left(\dfrac{\Delta}{r_{ref}}\right)^2 \dfrac{b_4}{10^4} + \dfrac{1}{3}\left(\dfrac{\Delta}{r_{ref}}\right)^4 \dfrac{b_6}{10^4} + \dfrac{1}{4}\left(\dfrac{\Delta}{r_{ref}}\right)^6 \dfrac{b_8}{10^4} + .. \\ \dfrac{Fstrength_y}{Fstrength} = 1 - \dfrac{1}{2}\left(\dfrac{\Delta}{r_{ref}}\right)^2 \dfrac{b_4}{10^4} + \dfrac{1}{3}\left(\dfrac{\Delta}{r_{ref}}\right)^4 \dfrac{b_6}{10^4} - \dfrac{1}{4}\left(\dfrac{\Delta}{r_{ref}}\right)^6 \dfrac{b_8}{10^4} + ... \end{cases} \tag{4.7}$$

i.e. the measurement error is proportional to each multipole and tends to diverge as Δ is made larger, in order to maximize the measured signal level. Such errors are prevented by selecting a "good magnet", i.e. with all harmonics lower than 0.2 %, and, in addition, Δ has to be reduced to the lowest value compatible with a reasonably high signal level [27].

Another issue concerns the uncertainty of the in-situ calibration on the measurement of R_{0m} and A_{cm}. The relative measurement uncertainty on R_{0m} is obtained by propagation through (4.3):

$$u_{R_{0m}} = \frac{\sigma_{R_{0m}}}{R_{0m}} = \sqrt{\left(\frac{\Delta z}{\Delta \Psi_1}\right)^2 \frac{\sigma_{\Psi_2}^2}{\Psi_2^2} + \frac{\sigma_{\Delta z}^2}{\Delta z^2}} \tag{4.8}$$

The uncertainty on the flux arises mainly from the signal-to-noise ratio of the acquisition system (few tens of ppm for low-order harmonics [28]). The uncertainty on Δz in the millimeter range reaches a few micrometers by using commercially-available mechanical systems based on linear encoders. Thus, u_{Rom} is dominated by the displacement uncertainty. The relative uncertainty on A_{cm} is derived as:

$$u_{A_{cm}} = \frac{\sigma_{A_{cm}}}{A_{cm}} = \sqrt{\frac{\sigma_{\Delta z}^2}{\Delta z^2} + \frac{\sigma_{C_2}^2}{C_2^2} + \frac{\sigma_{\Psi 1}^2}{\Psi_1}} \tag{4.9}$$

The main contribution to the uncertainty on C_2 arises from the SSW measurement. As an example, for a quadrupole magnet with an aperture of 20 mm and a length of 45 mm, a typical value is ±100 ppm.

The uncertainty on κ_n is derived from (4.3):

$$u_{\kappa_n} = \frac{\sigma_{\kappa_n}}{\kappa_n} = n\left(\frac{\sigma_{R_0}}{R_0} + \frac{\sigma_{A_c}}{2A_c}\right) \tag{4.10}$$

The determination of u_{κ_n} is critical because it affects the measured field multipoles by providing an upper bound for their maximum orders. The multipole precision depends mainly on the two calibration parameters, because they include all the uncertainty sources owing to the in-situ calibration.

Another point was taken into account were the systematic effects on the in-situ calibration. By considering that the (4.1) is only a first-order approximation of a more general equation [6]:

$$C'_1 = \sum_{n=1}^{+\infty} C_n \left(\frac{\Delta z}{R_{ref}} \right)^{n-1} \quad , \tag{4.11}$$

where C'_1 is the dipole in the frame x-y (Fig. 4.3), and C_n is the n-th order field component in X-Y. Therefore, at the n-th order, the (4.3) begins:

$$A_{cm} = \left\| \frac{\Delta\Psi_1 R_{ref}}{C_2 \Delta z} \frac{1}{1 + \sum_{n=3}^{+\infty} \frac{C_n}{C_2} \left(\frac{\Delta z}{R_{ref}} \right)^{n-2}} \right\| \tag{4.12}$$

where C_n/C_2 is the n-th field error component. The multipoles are less than 1 % for the useful aperture of most accelerator magnets. In the worst case of a quadrupole magnet with 1 % of C_3/C_2 and a displacement of 1 mm over 8 mm radius, the systematic effect due to the multipole on the area calibration is less than 1 ‰ [3].
The calibration of R_{0m} does not depend on the higher multipoles, but only on the gradient. It is therefore not affected by systematic multipole errors.

4.4 Flipping method for magnet fiducialization and alignment

In the following Sections, (i) the basic idea, (ii) the method derivation from the feed-down equation (2.7) and (iii) the procedure for the fiducialization of small-aperture quadrupole having their external surface as mechanical reference for the alignment in the accelerator are described.

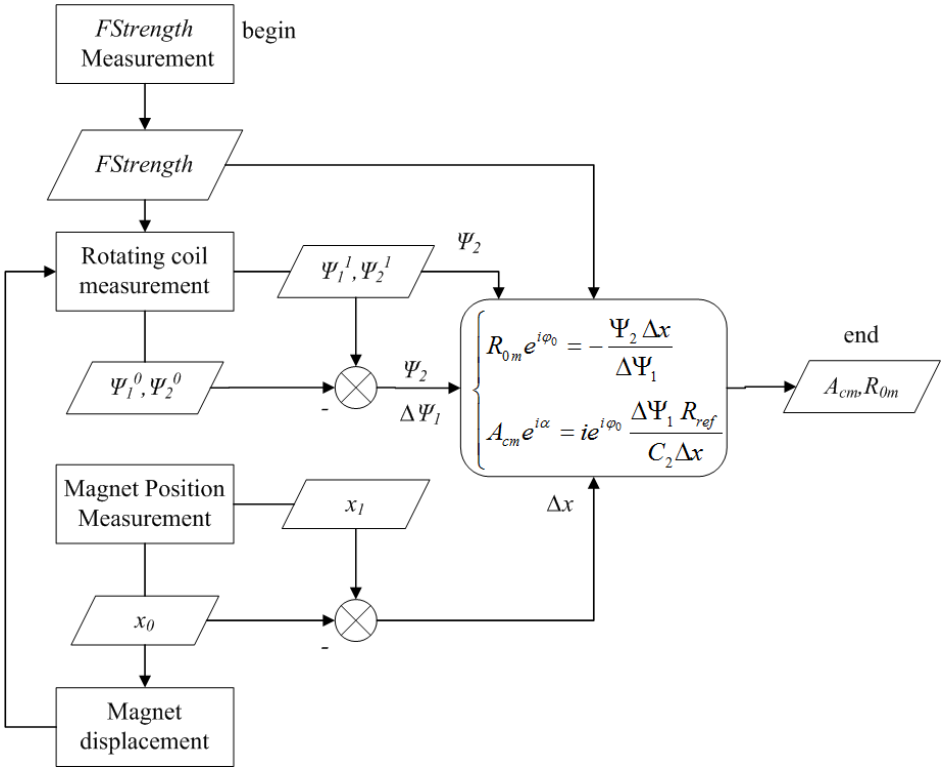

Figure 4.2: Flow diagram of the in-situ calibration

4.4.1 Basic idea

The flipping method is needed for correcting systematic errors when referring the magnetic axis with respect to the magnet frame. The results obtained from the harmonic analysis in (2.3), both for the step-by-step and continuous rotating method, contain information on the geometrical parameters as the field direction (roll angle) and the position of the magnetic axis [24]. This information must be related to the magnet mechanical references.

In the particular case of magnets to be installed in the drift tube of linac accelerators, the quadrupole geometry is defined by the precisely machined external cylinder and two reference pins on this cylindrical surface. Measuring the magnetic axis and field direction for different angular positions of the magnet under test removes systematic errors. The small weight, less than 3 kg, of these magnets allows easy handling for this operation.

4.4.2 Method

The measured distance Δz between the coil rotation x-y and the magnetic frame x'-y' is expressed in its real and complex components (4.1) at first-order approximation, assuming higher-order multipoles much lower than the main field component of n-th order (see eq. 2.7):

$$\begin{cases} \dfrac{\Delta x}{R_{ref}} \approx -\dfrac{1}{n+1}\dfrac{B_n}{B_{n+1}} \\ \dfrac{\Delta y}{R_{ref}} \approx -\dfrac{1}{n+1}\dfrac{A_n}{B_{n+1}} \end{cases}, \tag{4.13}$$

These equations are always valid independently from the magnet shape and are used to refer the magnetic field axis to the coil rotation axis. For the specific case of small magnets with a rectified yoke, the idea is to transfer mechanically the measurement of Δz to the external surface of the magnet. This is machined to be a reference surface for the installation of the magnet in the drift tube elements of the accelerator. For this reason, a rectified V-shaped support (Fig. 4.3) is needed to rotate the magnet around its mechanical axes to remove systematic effects with differential measurements. The mechanical frame of the magnet (*X*-*Y*) is defined by two orthogonal reference pins installed on the cylindrical case. Two pins are needed to install the quadrupole as a normal or a skew magnet. By flipping the magnet around the longitudinal axis of 180º (the *Z* direction in Fig. 4.4), it is possible to calculate the systematic offset (ΔX, ΔY) between the centre of the magnet and the rotating coil frames. The measurement of the magnetic axis in a given *p* angular position of the magnet (x_{mp}, y_{mp}), is the sum of two quantities: the offset (ΔX, ΔY) and the effective position (X_M, Y_M) of the magnetic axis in the frame *X*-*Y*. This last distance can be calculated by:

$$\begin{cases} \pm X_M = \Delta X + x_{mp} \\ \pm Y_M = \Delta Y + y_{mp} \end{cases} \tag{4.14}$$

By considering two set of measurements at 180° (Fig. 4.3) obtained by rotating the mechanical frame around the Z axis (here position 0 corresponds to the frame *X*-*Y* in Fig. 4.3 and in position 1 to the same frame rotated of 180°), the measured displacement in the (x_m,y_m) coil frame change sign, while the systematic offset (ΔX, ΔY) remains constant. Therefore, a set of 4 linear equations in 4 unknowns can be derived from (4.13) having solutions:

$$\begin{cases} X_M = \dfrac{x_{m0} - x_{m1}}{2} & \Delta X = -\dfrac{x_{m0} + x_{m1}}{2} \\ Y_M = \dfrac{y_{m0} - y_{m1}}{2} & \Delta Y = -\dfrac{y_{m0} + y_{m1}}{2} \end{cases} \tag{4.15}$$

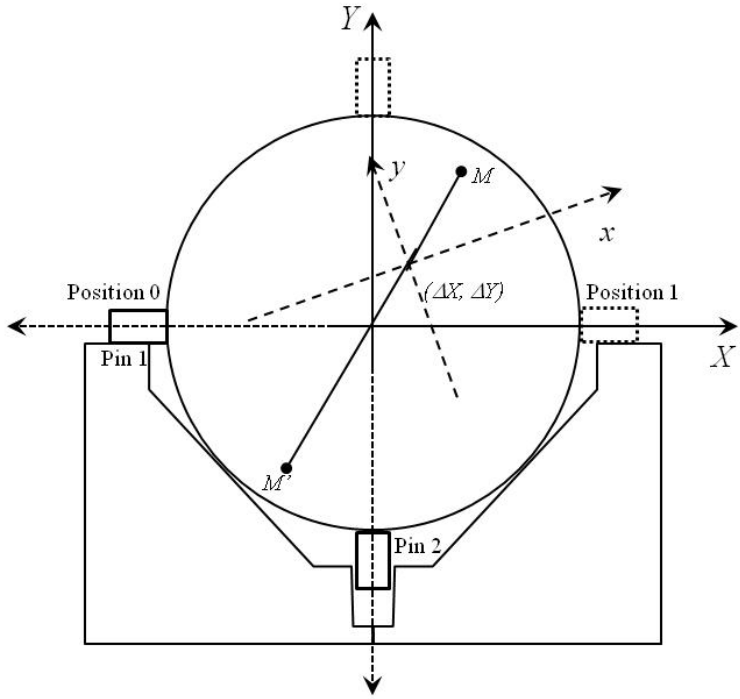

Figure 4.3: Scheme of the flipping principle measurement for axis measurements. The frame X-Y is the mechanical magnet frame defined by the precise cylindrical surface and 1 of the two pins 90° apart (Pin1 and Pin 2). The V-support allows the rotation of the mechanical frame from Position 0 to Position 1(dashed pins and frame). By rotating the magnet of 180º the position M of the magnet axis in the coil frame x-y changes sign while the systematic offset (ΔX, ΔY) between the coil frame and the mechanical frame remains constant.

Concerning the field direction, a rotating coil measurement gives information about the direction of the main field of a multipole magnet in the frame *x-y*. In particular, the direction of the field is given by the phase of the main harmonic with respect to the zero of the encoder used as angular reference.

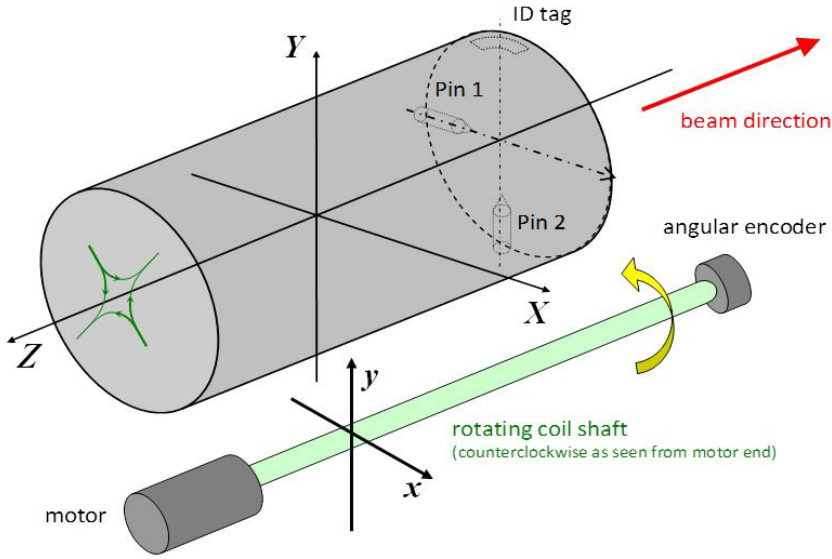

Figure 4.4: Axis references in the rotating coil measurement system. Pin 1 and Pin 2 are the mechanical reference of the magnet (fiducials).

This reference is affected by an offset ζ, namely the rotation angle between the (x-y) coil and the (X-Y) magnet case frames in Fig. 4.3. By defining the magnetic field direction φ and ψ respectively in the two frames (counter-clockwise from the y axis), the measured angle in position 0 will be:

$$\psi = \phi_{m0} + \zeta \tag{4.16}$$

The measured angle (i.e. skew term) of all harmonics changes sign when the magnet or the measurement system is rotated by 180 º around the Y axis (here called position 2) [15]:

$$-\psi = \phi_{m2} + \zeta \tag{4.17}$$

Also in this case a system of 2 linear equations returns ζ and ψ:

$$\begin{cases} \psi = \dfrac{\varphi_{m0} - \varphi_{m2}}{2} \\ \zeta = -\dfrac{\varphi_{m0} + \varphi_{m2}}{2} \end{cases} \tag{4.18}$$

The same approach can be applied to measure magnetically if the orthogonality between the two reference pins is inside the tolerance. The magnet is rotated in a way that Pin 2 (Fig. 4.3) is placed in the position of Pin 1, i.e. the frame X-Y is rotated of 90º. In this case, the orthogonality is given by:

$$\phi_{m0} - \phi_{m3} = \frac{\pi}{2} \tag{4.19}$$

4.4.3 Procedure

The procedure in the previous Section is based on the rotation of the mechanical magnet frame around the 3 axes in Fig 4.4. The first measurement is the reference measurement position 0 in table 4.1, the magnet is placed to produce a defocusing effect on a H- particle beam travelling in the –z direction of Fig. 4.4 according to the schematics of the magnet in Fig. 4.5.

The second measurement (position 1) is carried out with the magnet rotated of 180° around the z-axis. In this position, all the odd normal and skew multipole terms change sign:

$$\begin{aligned} B_n^1 &= (-1)^n B_n^0 \\ A_n^1 &= (-1)^n A_n^0 \end{aligned} \tag{4.20}$$

For this reason, also the dipole term changes sign and the axis offsets ΔX and ΔY can be calculated. A third measurement rotated at 180° around the Y-axis is mandatory to calculate the angular offset ξ, because in this case the odd skew and even normal harmonics change sign:

$$\begin{aligned} B_n^2 &= (-1)^n B_n^0 \\ A_n^2 &= (-1)^{n-1} A_n^0 \end{aligned} \tag{4.21}$$

Table 4.1: table resuming the different rotation of the magnet for the flipping method

Position	Side/Frontal view
0	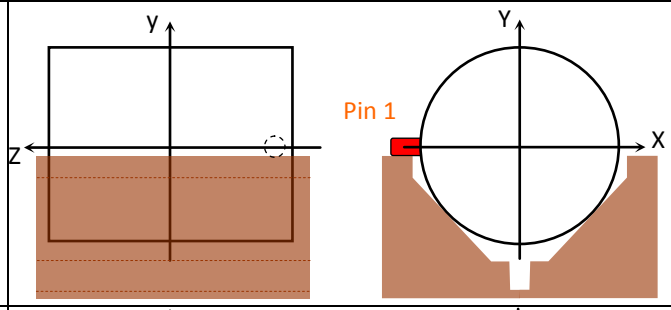
1	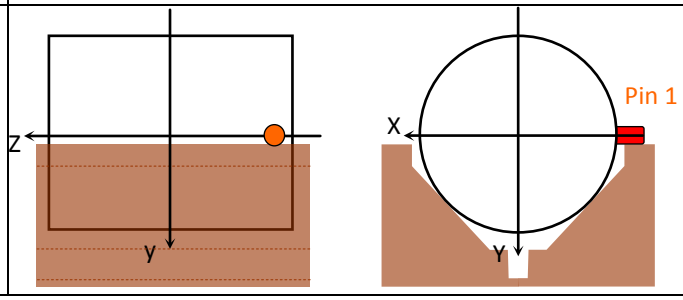

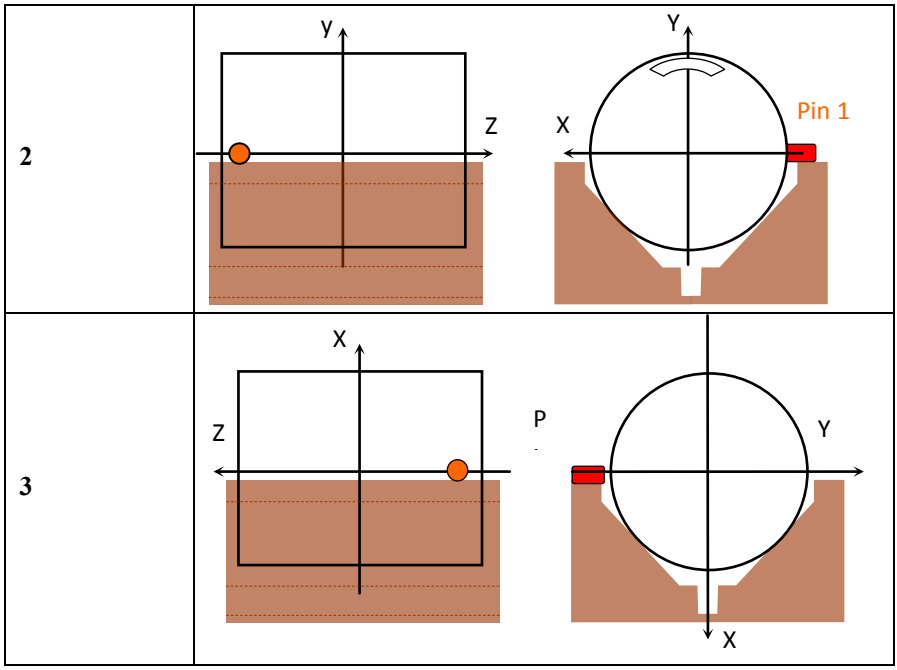

By rotating of 90° with respect to the reference measurement (in other words, by bringing the pin 2 to touch the same point of pin 1 in position 0), the odd normal and skew harmonics are swapped and the main field changes the sign:

$$B_n^3 = \cos(\frac{\pi}{2}(n-1))B_n^0$$
$$B_n^3 = \sin(\frac{\pi}{2}(n-1))B_n^0 \quad (4.22)$$

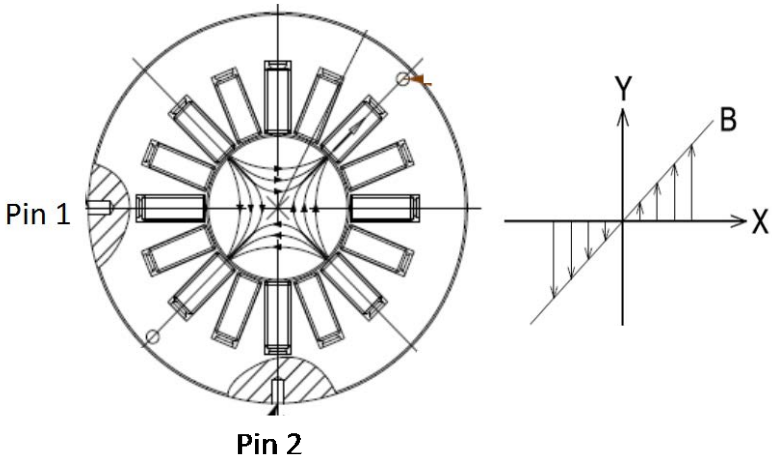

Figure 4.5: section of a permanent quadrupole magnet used in the drift tube. In this position of the magnet, a particle beam H^- travelling in the z-direction going in to the sheet will be defocused.

The same procedure can be applied to fiducialize the magnetic axis once the magnet has been installed in the drift tube of the linac tank [25]. For this measurement, a special support is needed to hold the tube and make possible the rotation (Fig. 4.4).

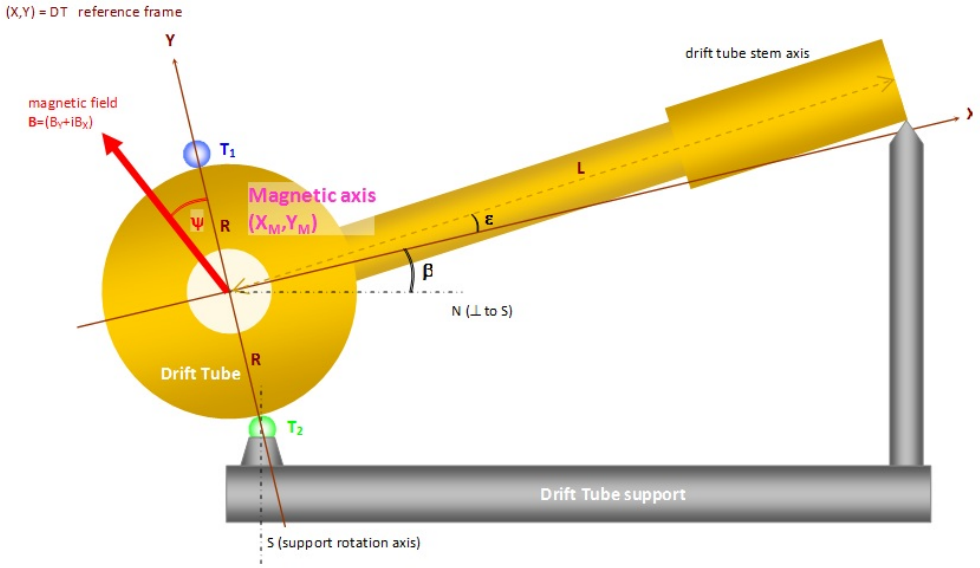

Figure 4.6: flipping method for a magnet installed in the linac drift tube (DT).

In Fig. 4.6 R is the external radius of the drift tube and the points T_1 and T_2 define the drift tube reference frame. L is the axis of the drift tube stem and the two angles β and ε are the support tilt and the stem perpedicularity error, respectively. The sum of those angles corresponds to the systematic offset ξ in eq. (4.18). In this case, the systematic offsets ΔX, ΔY and the magnetic axis position in the drift tube frame X_M, Y_M are given by:

$$\begin{cases} X_{cm} = \beta R + \dfrac{x_0 - x_2}{2} & \Delta X = 2\beta R - \dfrac{x_{0m} + x_{2m}}{2} \\ Y_{cm} = \dfrac{y_{0m} - y_{1m}}{2} & \Delta Y = -\dfrac{y_{1m} + y_{2m}}{2} \end{cases} \tag{4.23}$$

The angular offsets can be calculated according to the following matrix:

$$\begin{Bmatrix} \psi \\ \zeta \\ \varepsilon \\ \beta \end{Bmatrix} = \frac{1}{2} \begin{bmatrix} -1 & -1 & -1 & 1 \\ 1 & -1 & 1 & 1 \\ 0 & -1 & 0 & 1 \\ 0 & 0 & -1 & 1 \end{bmatrix} \begin{Bmatrix} -\varphi_{0m} \\ \varphi_{1m} - \pi \\ \varphi_{2m} \\ -\varphi_{3m} + \pi \end{Bmatrix} \tag{4.24}$$

4.5 Step-by-step method for harmonic measurements in fast-pulsed magnets

In the following Sections, the (i) basic idea for measuring small-aperture and fast-ramped electro quadrupole, (ii) the method based on stepping the coil by different angular positions, considering also how to measure the dynamic effect on iron-dominated electromagnets, and (iii) the procedure to attain a field quality measurement for magnets pulsed with current cycles less than 1 ms, are described.

4.5.1 Basic idea

In the case of a fast-ramped electromagnet, the same approach is applied by measuring the flux harmonic content through a step-by-step rotation. This allows the same shaft for permanent magnets to be used, as well as the same compensation scheme [16] to be adopted in order to reduce the main field components and to increase the sensitivity to higher-order field harmonics.

4.5.2 Method

In measuring fast-pulsed magnet with a stationary coil, it is important to understand the dynamic behaviour of the magnet under test. In the procedure for the step-by-step measurement method, described in the next Section, the integration of the coil signal (the stop trigger integration in Fig. 4.7) is stopped just after all the dynamic effects are ended. In other words the stop trigger has to be sent after a given delay that depends on the dynamic behaviour of the magnet mainly related to the eddy current in the iron yoke [17].

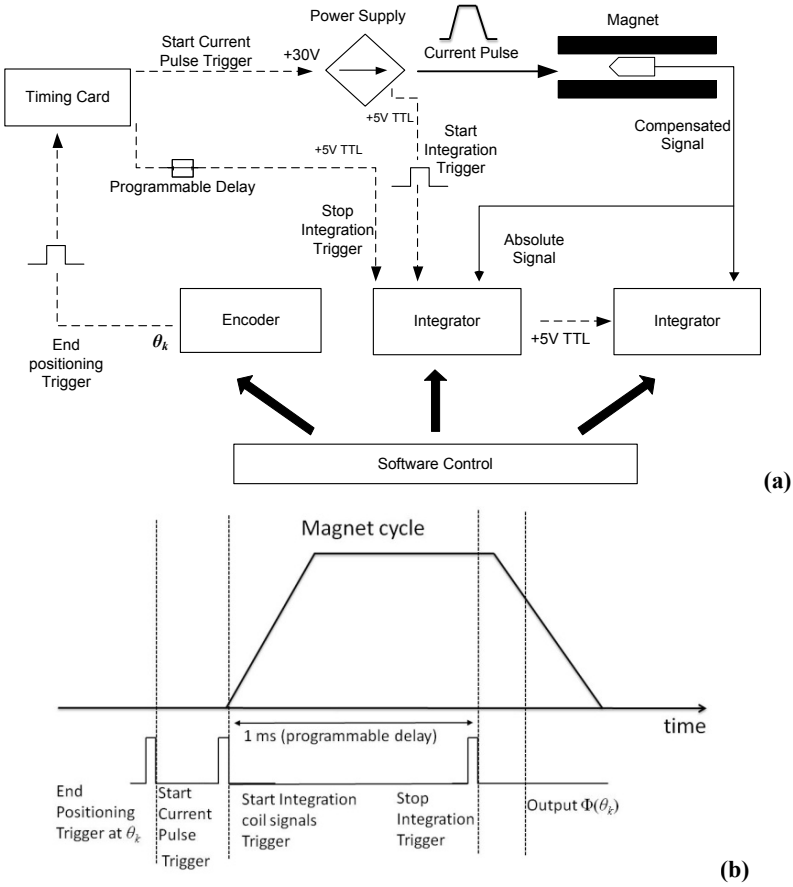

Figure 4.7: Step-by-step measurement: (a) block diagram, (b) magnet cycle repeated for 2n angular positions.

Such delay can be modelled and measured as described in [2]. The current flat top stability is determined essentially by the decay of the eddy currents induced during the ramp, as well as by other parasitic effects [Zickler 2009]. In general, the main effects of eddy currents are: (i) to screen flux changes, (ii) to delay the achievement of nominal DC field, (iii) to introduce high harmonic content perturbing the field [12]. An equivalent circuit model is necessary to fully understand the eddy currents effects, as well as to plan possible corrective actions [8]-[23]. Eddy current effects are hard to predict accurately because they depend on a number of uncertain parameters, such as the magnetic properties of the iron yoke, its temperature, the surface resistivity of the laminations [18], the mechanical tolerances leading to unwanted air gaps in the magnetic circuit, etc. As a consequence, an

experimental approach is necessary to validate both design calculations and manufacturing quality [T. Zickler 2009].

The eddy currents are generated by electric fields arising from variable magnetic fluxes [18]. They build up during the current pulse ramp-up and decay during the constant portion. In the proposed model, their effect is considered as a bypass current, flowing through a chain of R/L circuits connected in parallel to the main coil (Figure 4.8) [5].

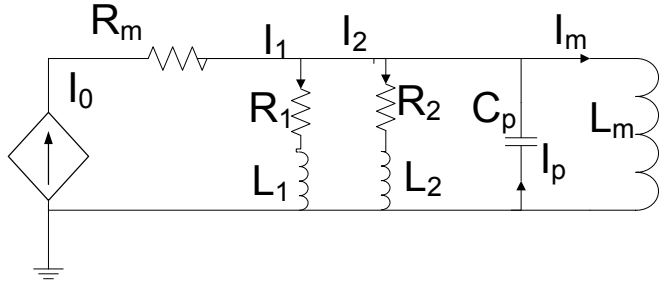

Figure 4.8: equivalent model circuit of eddy current effect

For a short magnet such as the fast-ramped magnet of the Linac (called for the linac4 Type III), the contribution of the fringe field may be dominant [8]- [11], thus two R/L chains are considered in order to take into account: (i) the eddy currents parallel to the main coils (i.e. across the laminations), which have a short time constant, and (ii) the eddy current circuit, in the plane of the end laminations (i.e. perpendicular to the magnet axis) due to the fringe field. The model also takes into account the parasitic capacitance of the magnet coil that could influence the main field at high frequency (about 1 MHz or above). The bypass eddy currents (I_1 and I_2) are negligible with respect to the main current, thus can be considered as mutually independent and the analysis can be simplified [8]. The current I_m flowing through the main coil of the magnet is given by:

$$I_m = I_0\left(1 - \frac{L_m}{L_1 + L_m}\exp\left(\frac{R_1}{L_m + L_1}\right) - \frac{L_m}{L_2 + L_m}\exp\left(\frac{R_2}{L_m + L_2}\right)\right) + I_p \tag{4.25}$$

where I_0 is the current source, L_m the main coil inductance, R_1, R_2, L_1, and L_2 are the equivalent resistance and inductance of the eddy current circuits, respectively. The current I_p flowing through the parasitic capacitor will introduce small ripples in the flux. Assuming the static field B to be simply proportional to the magnet current, the main field component can be described by:

$$B = B_0\left(1-\alpha\exp\left(-\frac{t}{\tau_1}\right)-\beta\exp\left(-\frac{t}{\tau_2}\right)\right)+B_{ac} \tag{4.26}$$

where B_0 is the main field at the end of the double exponential decay and B_{ac} is the high-frequency ripple introduced by I_p; α and β are the amplitudes of the exponential decays, and τ_1 and τ_2 are the time constants delaying the field response. The effect of this parasitic effect can be measured considering that the e.m.f. V_C induced in the coil has to be integrated in order to obtain the linked flux ϕ. Assuming that the quadrupole is excited starting from a demagnetized state at $t=t_0$, the flux ϕ seen by a search coil with N_t turns inserted in the magnet is calculated as:

$$\phi(t) = \frac{1}{N_t}\int_{t_0}^{t} V_C(t)dt \tag{4.27}$$

In the ideal (linear) case, this flux would be simply proportional to the excitation current via the mutual inductance L_{CM}, depending on the geometry and on the magnetic permeability of the iron core [9]:

$$\phi(t) = L_{CM}(t) \tag{4.28}$$

In actual conditions, a current difference ΔI can be defined as:

$$\Delta I = \frac{\phi(t)}{L_{CM}} - I(t) \tag{4.29}$$

The current difference (4.29) includes contributions from all non-ideal effects, builds up during the ramp and decays over the flattop. Assuming that the transient has completely died out at the end of the flat top, i.e. $\Delta I(t_S)=0$, one can derive:

$$\frac{1}{L_{CM}} = \frac{N_t I(t_s)}{\int_{t_0}^{t_s} V_C(t)dt} \tag{4.30}$$

By considering that the measured signals are affected by electrical noise, mains hum, power supply ripple and so on, the accuracy of the ratio (4.29) can be increased by averaging both the terms, the current excitation and the voltage coil integral over a short time interval t_S-$\Delta t \le t \le t_S$.

4.5.3 Procedure

In Fig. 4.7a, the measurement procedure is outlined. Once the coil has reached the angular point θ_k (Fig. 4.7b), the encoder sends a trigger to the power supply through the timing card. In turn, the power supply triggers the start of the integration of the signals from the absolute and the compensated coils and, with a fixed delay, generates a current pulse. The timing card ends the integration by providing a pulse delayed by a fixed duration (e.g. 1 ms), when all the dynamic effects estimated with the eq. 4.29 are supposed to become negligible. The flux sample Φ_k generated by the integrators at each k position is given by:

$$\Phi_k(\theta) = \int_{t_{start}}^{t_{stop}} N_t L \,\mathrm{Re}\left\{\sum_{n=1}^{+\infty} \frac{C_n(t)}{\kappa_n} e^{in\theta_k}\right\} dt \tag{4.31}$$

These samples are used directly in (4.1) and (4.2) to calculate C_n.
By dividing the turn in 2^n angular steps, the multipoles up to the $2^n/2$ order are achieved. The field reproducibility is guaranteed by using the same power supply foreseen for the accelerator, required to be stable within $\pm$100 ppm.

4.6 Polyvalent measurement system architecture

In this section the technical solutions adopted to implement the measurement bench integrating in a unique polyvalent method to fulfil all the above requirements are described. In Fig. 4.9, the architecture of the measurement system is shown. Three coils mounted on a cylindrical shaft are rotated in the magnet aperture by means of a dc stepper motor steered by a motor controller. A high-quality V-support provides a 1-μm accuracy in positioning the magnet axis. Mechanics is conceived to easily disconnect the motor head from the coil, in order to flip or replace the magnet, by maintaining the angular reference simultaneously. The zero angular reference of the encoder does not change by more than a few tenth of μrad when flipping the magnet end to end, because field axis direction and multipole measurements are directly related to this reference [24].

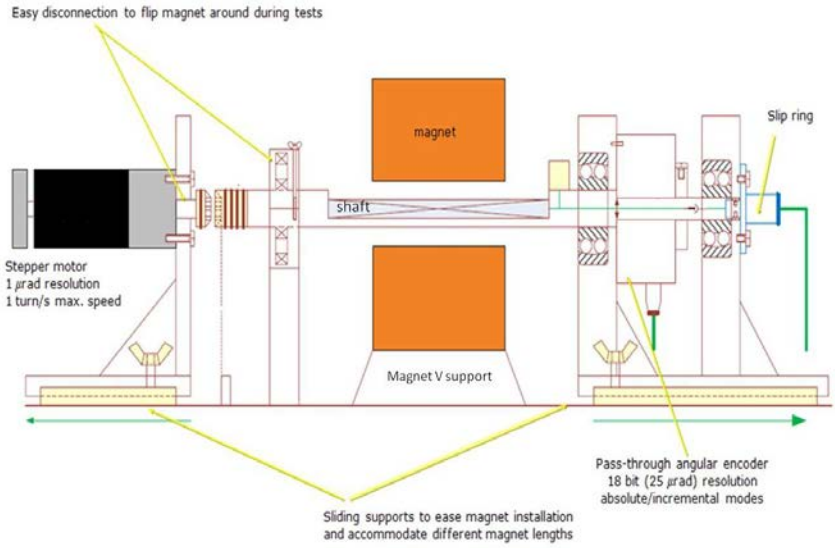

Figure 4.9: The architecture of the polyvalent measurement system.

The architecture showed in Fig, 4.9 has been implemented as shown in Fig. 4.10. In the final version has been added also the 2-D stage to implement the in-situ calibration. A 2D translation stage (a), mounted between the shaft ends (b), permits a controlled motion to the permanent quadrupole under test (c) in the cross-section plane of the coil, within ±2 μm of uncertainty. The same mechanics and electronics [2] are exploited to both calibrate and test the magnet, thus all the errors are taken into account by the coil sensitivity factors. The magnet displacement is limited to ±1 mm for the clearance between the coil and the magnet aperture. The origins of the magnet and coil frames are made to be coincident by minimizing iteratively the dipolar flux through the 2-D stage. This allows the calibration results to be crosschecked, because the position of the rotation axis after a given displacement is related to the ratio C_1 / C_2. A set of three bucking coils, opportunely positioned in a 20-mm shaft frame (Fig. 4.11), allows the contribution of the main harmonics (dipole and quadrupole terms) to be compensated in order to improve the sensitivity to higher-order multipoles, by attenuating systematic effects due to vibrations and sag [16]. In particular, the shaft in Fig. 4.11 has two tangential coils in series (1 and 2), compensating for the quadrupole, and a third coil, compensating for the dipole.

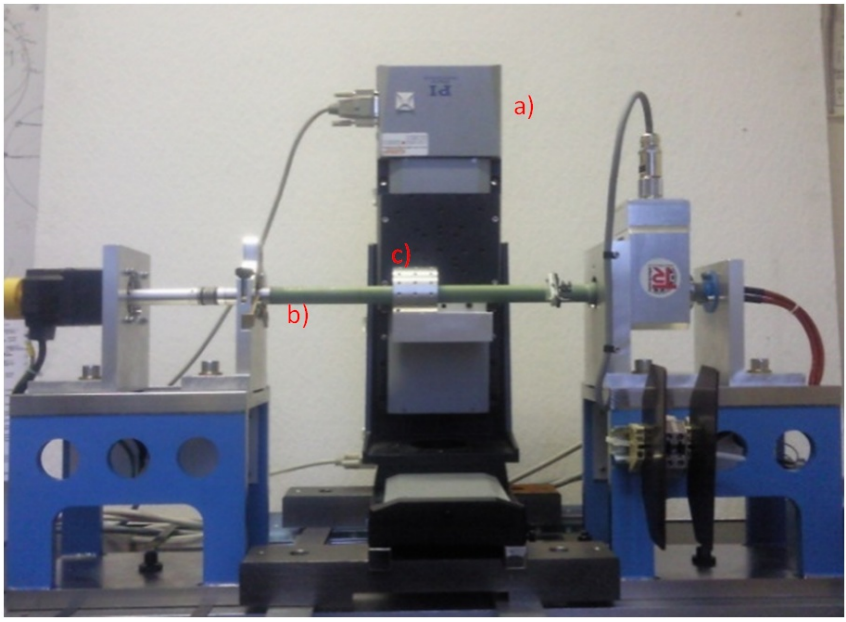

Fig. 4.10. Calibration set up: (a) 2D translation stage for magnet movements in the coil cross-section plane, (b) rotating shaft under test, and (c) permanent quadrupole.

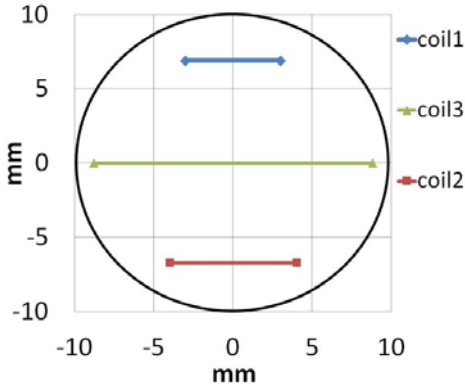

Figure 4.11: Geometry of the 20-mm coil shaft.

The coil 1 has 100 turns for 7 mm of width and 200 mm of length; coils 2 and 3 have the same length, 64 turns, and width of 8 and 17.6 mm, respectively. They are wound with flat multistrand wires of 0.08-mm diameter, resulting in a winding groove section of 0.8×0.8 mm^2 of the 100-turn coil winding groove, and 0.57×0.57 mm^2 of the 64-turns coils. These small dimensions allow a natural bucking ratio β of about 20. β is defined as the ratio between the voltages from the absolute (V_{abs}) and the compensated (V_{comp}) coils [16].
The bucking is improved by connecting resistors in parallel to the coils with a larger sensitivity to dipole and quadrupole components. In Fig. 4.12, the coil connection circuit is shown for the shaft in Fig. 4.11. The series of the two coils generating the voltages ε_1 and

ε_2, with resistance R_{c1} and R_{c2}, respectively, mainly sensitive to the quadrupole component, is connected in opposition series to the third coil (ε_3, R_{c3}). The voltages ε_1, ε_2, and ε_3 are directly proportional to the κ_n of the coils, thus the equations optimizing the bucking for the dipole and the quadrupole are derived:

$$\begin{cases} \left(\frac{R_{p1}}{R_{c1}+R_{p1}}\right)\kappa_1^{coil1} + \kappa_1^{coil2} - \left(\frac{R_{p3}}{R_{c3}+R_{p3}}\right)\kappa_1^{coil3} = 0 \\ \left(\frac{R_{p1}}{R_{c1}+R_{p1}}\right)\kappa_2^{coil1} + \kappa_2^{coil2} - \left(\frac{R_{p3}}{R_{c3}+R_{p3}}\right)\kappa_2^{coil3} = 0 \end{cases} \tag{4.33}$$

By resolving the equations with respect to R_{p1} and R_{p3} is possible to improve β.The angular encoder provides incremental and absolute outputs as angular reference for the acquisition in continuous and in stepped mode for permanent electro-magnets, respectively. The motor controller and the encoder interface are coupled both to position precisely the shaft and to generate trigger pulses as function of the rotation angle with high resolution. The encoder incremental output has two quadrature channels (90° out of phase) providing an angular reference with a resolution of 25 μrad. All the angular measurements can be referred to the gravity by means of an electrolytic inclinometer sampled by a 17-bit ADC integrated in the PXI control card interface.

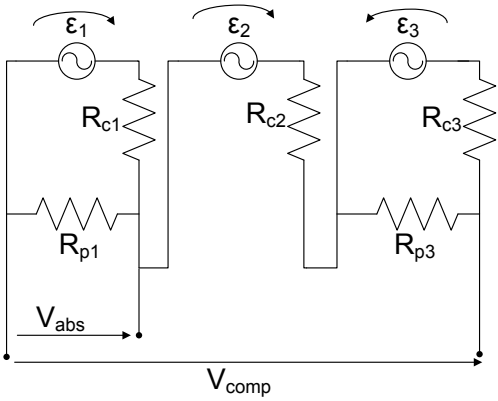

Figure 4.12: Bucking scheme for the coil compensation using a parallel resistor.

Two fast digital integrators [1] acquire a flux sample on the absolute and bucking coils between two encoder triggers. Those cards guarantee a typical signal-to-noise ratio of 105 dB in a bandwidth of 250 kHz, well suitable for both continuous and step-by-step measurements. For step-by-step mode, the acquisition must be also synchronized with the current pulse generator in order to release flux samples at each coil step. A dedicated timing card relates the triggers from the encoder and the magnet power supply. In Chapter 6 will be shown the performance of the system and of the method in terms of accuracy, validated on the prototypes and the series magnets of the Linac4 accelerator.

[1] P. Arpaia, M. Buzio, G. Golluccio, L. Walckiers, A polyvalent harmonic coil testing method for small-aperture magnets, *submitted to Rev. Sci, 2012*.

[2] P. Arpaia, M. Buzio, O. Dunkel, D. Giloteaux, G. Golluccio, A Measurement System for Fast-Pulsed Magnets: a case study on Linac4 at CERN, *Proc. IEEE International Instrumentation and Measurement Technology Conference, 2010*.

[3] P. Arpaia, M. Buzio, G. Golluccio, L. Walckiers, In situ calibration of rotating sensor coils for magnet testing, *Rev. Sci. Instrum. 83, 013306, 2012.*

[4] P. Arpaia, M. Buzio, J. J. G. Perez, G. Golluccio, C. Petrone, L. Walckiers, Magnetic field measurements on small magnets by vibrating wire systems, *IEEE Instrumentation and Measurement Technology Conference (I2MTC), 2011*.

[5] P. Arpaia, M. Buzio, G. Golluccio, G. Montenero, Eddy Current Measuring and Modelling in Fast-Pulsed Resistive Magnets: a Case Study on Linac4 at CERN, *Proc. IEEE International Instrumentation and Measurement Technology Conference, 2010*.

[6] P. Arpaia, A. Masi, G. Spiezia, Digital integrator for fast accurate measurement of magnetic flux by rotating coils, *IEEE Transactions on Instrumentation and Measurements, Vol. 56, No. 2, 2007.*

[7] L. Bottura, Magnetic Measurement of Alignment of Main LHC Dipoles and Associated Correctors, *IEEE transaction on applied superconductivity vol 12, N.1, 2002.*

[8] M. Buzio, G. Golluccio, A. Lombardi, F. Mateo, Magnetic Qualification of Permanent Magnet Quadrupoles for CERN's Linac4, *IEEE transaction on Superconductivity vol. PP issue: 1, 2011.*

[9] F.-J. Decker, S. Anderson, D. Kharakh, M. Sullivan, Permanent Magnet Skew Quadrupoles for the Low Emittance LER Lattice of PEP-II, *Proceeding of European Particle Accelerator Conference (EPAC), 2008.*

[10] S. Fang, W. Chou, Analysis and Measurements of Eddy Current Effects of A Beam Tube in a Pulsed Magnet, *Proceedings of European Particle Accelerator Conference (EPAC), Vol. 3, 1997.*

[11] Feeley, A Simple Dynamic Model for Eddy Currents in a Magnetic Actuator, *IEEE Transaction on Magnetics, vol. 32, n° 2, 1996.*

[12] M. Kobayashi, Measurement of harmonic field contents of pulsed magnets using a stepping search coil, *Nuclear Instrument and Methods vol.103, 1972.*

[13] K. Koseki, M. Tawada, H. Nakayama, H. Kobayasi, M. Shirakata, K. Okamura, Pulsed bending magnet of the J-PARC MR, *Proceedings of European Particle Accelerator Conference (EPAC), 2006.*

[14] S. Igarashi, Eddy Current effects on the J-Parc RCS sextupole Magnets, *IEEE Transactions on Applied Superconductivity, vol. 18, N. 2, 2008.*

[15] Y. Iwashita, T. Mihara, Permanent Magnet Quadrupole for Final Focus for Linear Collider, *Proceedings of Particle accelerator conference (PAC), 2003.*

[16] A. Jain, G. Ganetis, A. Ghosh, W. Louie, A. Marone, R. Thomas, P. Wanderer,

Magnetic field measurement for fast-changing magnetic fields *IEEE Transactions on applied superconductivity vol. 15, n. 2, 2005.*

[17] A. Jain , Rotating coils, CERN Accelerator school: specialized course on Magnets, *CERN Accelerator School CAS 2009: Specialised Course on Magnets, 2009.*

[18] R. M. Main, Measurement and correction of the PEP interaction region quadrupole magnets, *IEEE Transaction on Nuclear Science, vol. NS-26, 1979.*

[19] G. Moritz, Eddy currents in accelerator magnets, *CERN Accelerator school: specialized course on Magnets, CERN-2010-004, 2009.*

[20] M. Negrazus, D. George, V. Vrankovic, M. Werner, Eddy Current Reduction in a Fast-ramped Bending Magnet, *IEEE transactions on applied superconductivity, vol. 16, N. 2, 2004.*

[21] P. Schnizer, H. R. Kiesewetter, T. Mack, T. Knapp, F. Klos, M. Manderla, S. Rauch, M. Schönecker, R. Werkmann, *Status of the Mole for Measuring Fast-ramped, Superconducting Magnets, 16th International Magnetic Measurement Workshop (IMMW), 2009*.

[22] N. Smirnov, L. Bottura, M. Calvi, G. Deferne, J. DiMarco, N. Sammut, and S. Sanfilippo, Focusing Strength Measurements of the Main Quadrupoles for the LHC, *IEEE Transactions on Applied Superconductivity, vol. 16 no. 2, 2006.*

[23] M. Sullivan, Result from a Prototype Permanent Magnet Dipole-Quadrupole Hybrid for the PEP-II B-Factory, *Proceedings of Particle accelerator conference (PAC), 1997.*

[24] N. Tani, T. Adachi, H. Someya, Y. Watanabe, H. Sato, and J. Kishiro, Eddy Current Effect of Magnets for J-Parc 3–GeV Synchroton, *IEEE transactions on Applied Superconductivity, vol. 14, N. 2, 2004.*

[25] L. Walckiers, Magnetic measurement with coils and wires, *CERN Accelerator school: specialized course on Magnets, CERN-2010-004, 2009.*

[26] M. Vretenar, The Linac4 project at CERN, *Proceeding International Particle Accelerator Conference.(IPAC'11), 2011.*

[27] K. Weyand, Magnetometer Calibration Setup Controlled by Nuclear Magnetic Resonance, *IEEE Transactions on Instrumentation and Measurement, vol. 48-2, 1999.*

Chapter 5

System for monitoring inhomogeneous field based on ferrimagnetic resonance marker

5.1 Overview

In fast-cycling particle accelerators, monitoring the magnetic field used to bend and focus the particle beams is often relevant during the machine operations. Information about the field trend over the time is used by several systems, such as power supplies, RF cavities, and beam monitoring systems, as the input of feedback loops to correct the beam position and oscillations.

The corresponding measurement system is sometimes referred to as a "B-train system", from the fact that the field value is broadcast as a train of incremental digital pulses. Real-time measurements are usually carried out in a reference magnet powered in series with the accelerator magnets.

A Monitor system is based mainly on a combination of two sensors: usually, a coil, measuring the field as function of the time, and, a so-called "field marker", giving the absolute measure of the field at a given instant. The precision and the reliability of such a system depend mainly by the performance of the field marker.

In this Chapter, a novel development of a monitor system based on a FerriMagnetic (FMR) field marker, able to work in fast-ramped fields and (for his dimension) in high-inhomogeneous fields, is exposed. The transducer has to provide a precision of ± 50 μT in critical conditions of field variation (ramp rates higher than 2.3 T/s) and homogeneity (higher than 2 %/cm).

5.2 Architecture

A rotating coil fluxmeter could be in principle a valid choice for these measurements, especially because it could provide an absolute value of the field [3]. However, even state-of-the-art rotating coil systems can hardly provide a bandwidth larger than 10 Hz, i.e. typically three orders of magnitude lower than required for fast-cycled magnets. Hence, it is natural to use a static coil fluxmeter, providing a voltage output proportional to the field rate *dB/dt,* with sensitivity increasing according to the bandwidth. An additional measurement is needed however to provide the integration constant. This is commonly carried out by a "field marker", i.e. a device able to provide a digital trigger pulse as the field crosses a given threshold [11].

In the framework of the long-term consolidation of CERN injector chain, and keeping in mind the requirements of various planned future upgrades, the options to improve performance and reliability of the field markers currently in use have been investigated. CERN's Proton Synchrotron accelerator (PS), used to accelerate proton and ion beams up to 26 GeV in the injection chain of the LHC, exploits a monitor system for real-time measurements of the main magnetic field during operation [6]. The PS includes 100

combined function magnets (see Appendix A) providing a maximum field of 1.2 T and a gradient of 4.8 T/m, ramping up to 2.3 T/s. Current and future beam quality requirements for the LHC, especially in terms of limiting the emittance upstream in the injector chain, have a direct impact on the specifications of the marker.

The challenge for the new system currently under development is to achieve a precision of $\pm$50 μT with a resolution 5 μT on the measured value of the field, while maintaining the very-high long-term reliability. It has to be emphasized that, in order to control the integrated dipole field in a synchrotron, the absolute accuracy is relatively unimportant, since all magnets are powered in series and average closed orbit displacement of a few 10^{-3} can be trimmed easily. The most critical issue is the long-term stability of the field measurements, which in the PS must be of the order of 3×10^{-5} (relative to the peak field) for reliable machine operation.

For this reason, a new field marker able to work in the critical condition of a fast-ramped combined function magnet, based on commercially available filters using the FerriMagnetic Resonance (FMR) effect, has been developed [5].

A recent campaign of measurements has shown that the accuracy of the field measurement at 4.98 mT of the old monitor system can be poor. This is due to a combination of effects, including mainly hysteresis (as a function of excitation history) and temperature, leading in some cases to unacceptable radial oscillations of the beam (Fig. 5.1) [7]. An initial field imbalance induced by the current cycles in the two halves of the function magnets of the PS, due to not correct measurements of the old monitor system, induces a large displacement in the beam radial position of more than 10 mm, not at all tolerable for the machine operation. The red line in Fig. 5.1 is the current cycle with the imbalance causing for the displacement of the radial position of the beam (red spots). This effect is mainly due to the wrong detection of the actual monitor system at low field. The blue line is the reference measurement the current cycle without the initial imbalance having no effect on the beam position.

Magnetic stability would be greatly enhanced by increasing the field flat-bottom level, currently around zero, to a value between 60 and 100 mT, variable according to the kind of beam accelerated.

The principle of the new monitor system is shown in Fig. 5.2. The signal from a set of 5 coils (opportunely connected in series), able to measure at the same time the dipole, the quadrupole, and the sextupole components of the PS magnets, respectively, is integrated with an 18-bit integrator card. The reference measurement is given by a low field marker B_{mark}^{low} at a given instant.

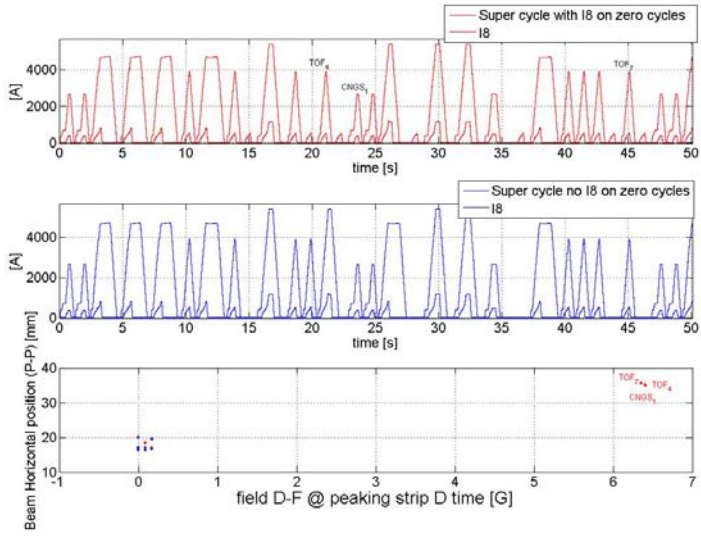

Figure.5.1: Instability of the horizontal beam position due to the low marking level of the old monitor system: (red) current in the Focusing part of the PS magnets, (blue) current in the Defocusing part of the PS magnet.

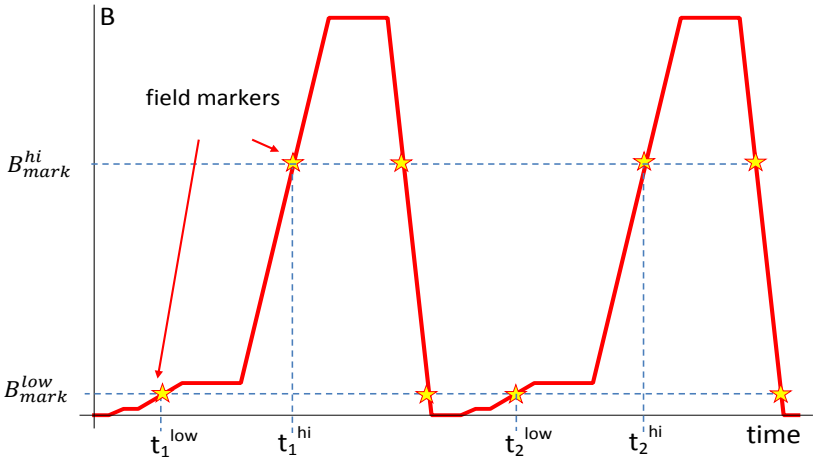

Figure.5.2: working principle of the new monitor system.

The threshold B_{mark}^{low} can be set, depending on the kind of beam to accelerate, between 60 and 100 mT. Another marker at higher field B_{mark}^{hi} is used for an adaptive auto-calibration of the integrator gain. The measurement output is the field computed as function of the time:

$$B(t) = B_{mark}^{low} + \int_0^t (1+\varepsilon)(\dot{B}(t) - \dot{B}_0)dt \qquad 5.1)$$

where $\dot{B}$ is the coil signal divided by the coil surface and ε is the integrator gain updated when a different marker level is reached:

$$\varepsilon = \frac{\int_{t_1}^{t_2} \dot{B} dt}{B_{mark}^{hi}(t_2) - B_{mark}^{low}(t_1)} - 1 \tag{5.2}$$

The integrator drift $\dot{B}_0$ is updated when the same marker level is reached.
In the specific case of the combined function magnet of the PS, the same magnet is divided in two halves providing the focusing and the defocusing effect to the beam (Fig. 5.3).

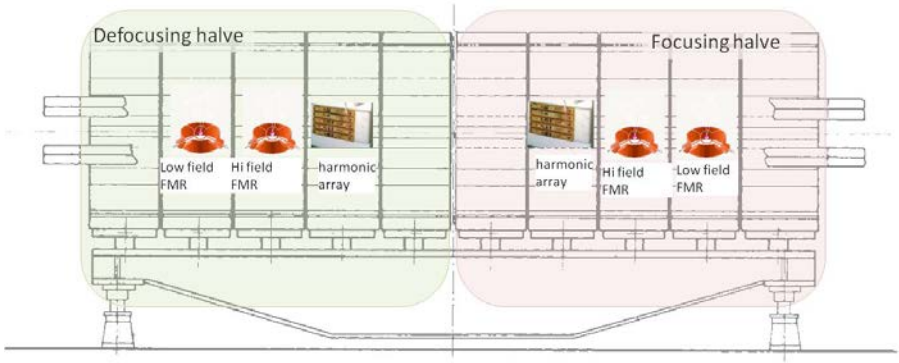

Figure.5.3: Proton Synchrotron Reference magnet

For this reason, two sets of sensors are installed in the reference magnet, needed to calculate the average field B_{av} weighted by a factor k taking into account the differences in field between the two halves:

$$B(t) = \frac{1}{2}(1-k)B_D + (1+k)B_F \tag{5.3}$$

In Fig, 5.4, an overview of the new monitor system system project based on and FMR field marker is shown. The sample of the coil signals sampled at 2 MS/s by the 18 bits analog to digital converter (ADC) card, are sent to the control PC to be processed. The integrated value is then corrected by the measurement of the FMR markers. The data of the field value at the instant t_i is calculated on line as follow from the voltage V acquired from the coil in the focusing of defocusing half of the magnet ($V_{D/F}$):

$$B_{D/F}(t) = B_{mark}^{low} + A\sum_{n=t_i-1}^{t_i}(1+\varepsilon_{D/F})V_{D/F}(t_n) \tag{5.4}$$

where B_{mark}^{low} is the reference value given by the FMR signal at low field for the focusing or defocusing half of the reference magnet. At each sample of field generated the correction of eq 5.2 is applied to remove eventual drift of the amplifiers of the ADC. The

samples from both side of the magnet is then used to calculated B_{av} according to eq. 5.3 that is then distributed to the different subsystems (power converter, RF cavities control system and machine operation control system) over a 32-bit serial line by means of a "white-rabbit" link [12].

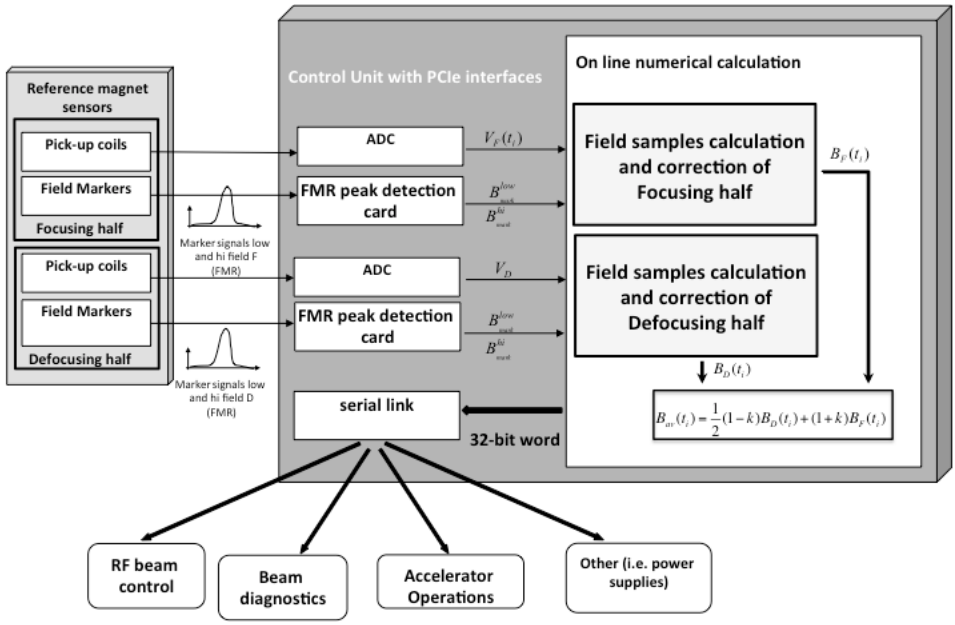

Figure.5.4: Overview of the monitor system based on FMR marker.

5.3 Ferrimagnetic field marker

FMR is a type of electron spin resonance based on a slight imbalance of the energy emitted and absorbed by electrons flipping between opposite spin states under the influence of incident electromagnetic radiation. It has found widespread applications in microwave equipment, such as tuneable oscillators and electronically tuneable filters [10]. The sensor developed is a modified version of commercially available filters Yittrium Iron Garnet (YIG).

In the following, the sensing element, the filter, and the developed transducer are detailed.

5.3.1 The sensor

The ferrimagnetic resonance occurs in certain ferrites, which are electrical insulators and thus well suited to high-frequency operation. In a simplified theory for FMR the modulus of the electron spin vector *s* of a free electron is given as:

$$|s| = \sqrt{s(s+1)h} \tag{5.5}$$

Where s =1/2 is the spin quantum number and h is the Plank constant. The magnetic moment of the electron is then found to be:

$$\vec{\mu}_s = -g_s \cdot \frac{e}{2m_0}\vec{s} \tag{5.6}$$

Where g_s=2.0023 is the Landé factor for a free electron [5]. A free electron in a static magnetic field can have two possible orientations of the s_z component of the spin vector (if z is parallel to the static field direction), parallel or antiparallel:

$$s_z = \pm\frac{1}{2}h \tag{5.7}$$

The energy difference between those two possible orientations (Fig. 5.5):

$$\Delta E = g_s \mu_B B_0 = h\nu \tag{5.8}$$

Where is the Bohr magneton μ_B = 9.2732e^{-24} [Am^2]. The frequency ν = 28.086 [GHz/T] of this transaction corresponds to the gyromagnetic ratio if the equation 5.7 is rewritten using the Larmor frequency.

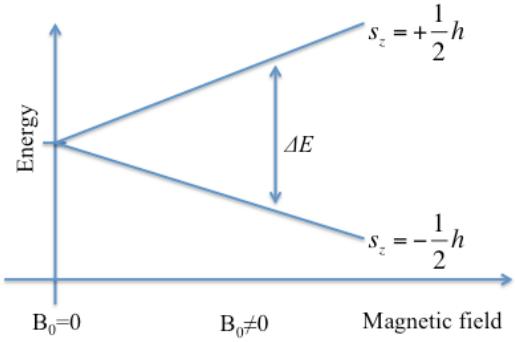

Figure 5.5: Energy of the electron spin vector as function of the magnetic field applied.

Unlike NMR, electron resonance phenomena are affected by a number of environmental and chemical factors, including prominently the temperature.

The mechanical layout of such a YIG filter is depicted in Fig. 5.6. RF energy transfer takes place between two orthogonal, semicircular loops of TEM transmission lines. This prevents unwanted coupling between the loops in case of the absence of the YIG resonance. The construction also permits the DC bias field B_0 to be orthogonal to the RF magnetic fields of both coupling loops [5].

The chosen unit, manufactured and customized to our specifications by OmniYig® Inc., Santa Clara, CA, is made by two semi-circular RF loops coupled via a ∅0.3 mm single-crystal YIG sphere [2].

In case of a YIG filter used as field marker, eddy currents generated on the mechanical support (Chapter 7) of the filter when B_0 is varying over the time, arise. This effect was

made negligible by requiring the manufacturer of building the case in plastic material, instead of aluminium.

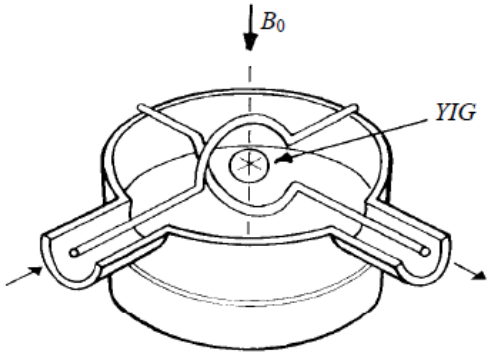

Figure.5.6: Layout of the YIG filter.

The quality of the field measurement depends strongly on the Q-factor of the YIG filter, which improves when losses are low or, equivalently, coupling is weak [5]. Single-crystal YIG filters can reach high Q values, close to 10^4, although their response to external field strongly depends on the temperature and, due to the anisotropy of the crystal, on its alignment in the resonator [4]. In the thesis application, a value of Q of about 1000 is reached.

Polycrystalline spheres, such as the one used so far at CERN, have better stability in the temperature range 25 to 55 °C, although with a Q lower by about an order of magnitude. In the thesis application, the temperature excursion is relatively low, about ±2°C, thus, a properly aligned single-crystal sphere was considered as the best solution. According to the above requirements, the manufacturer optimized the orientation of the sphere in order to achieve the best stability in the desired field range.

The ferrite must be magnetized beyond saturation to guarantee both a high Q-value and minimal hysteresis effects in the material itself [1]-[9]. Typical values for the saturation magnetization of YIG are between 30 and 100 mT. These values also define the lower limit of the measurement range.

5.3.2 The transducer

The above sensor needs for a conditioning circuit to pass from the RF domain to the working frequency range of the electronics used in the monitor system at CERN. At this aim, the transducer of a previous version in [5] was adapted according to the block diagram of Fig. 5.7. A signal synthesizer sends an RF wave to the YIG filter through an RF coaxial cable at a given frequency. The 5 dB attenuators at the YIG input and output ports reduce the multiple wave reflections due to impedance mismatch between the source output and YIG filter input, as well as between the amplifier and the filter output.

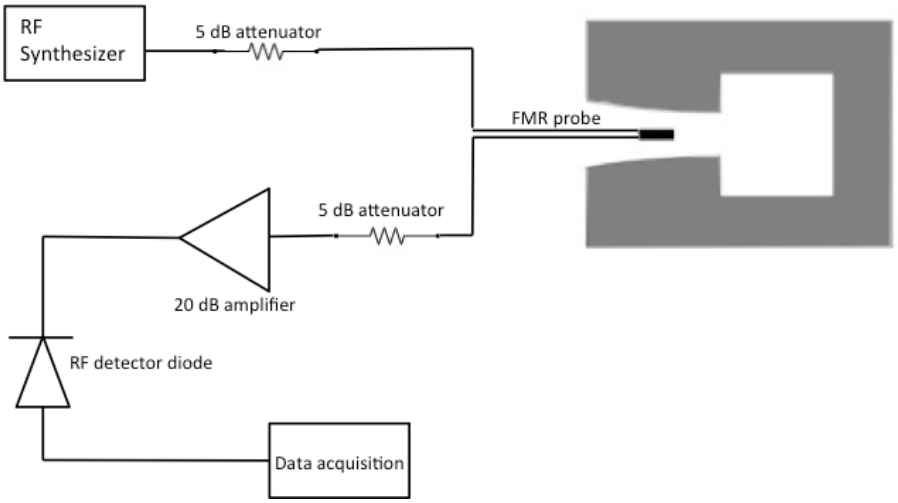

Figure.5.7: circuital scheme of the FMR transducer.

The signal must be amplified before to be rectified by an RF detector diode, providing a final output containing essentially the amplitude envelope. The power output of the RF synthesizer should not be so high to saturate the filter, neither too low to avoid the influence of the noise on the peak detection. The optimum solution was found at 0 dBm.
As for standard NMR equipment, the FMR transducer can work in two basic modes:
a) Marker mode, i.e. the input frequency is fixed and the field changes: the response shows a resonance peak when the field reaches the corresponding value (Fig. 5.8). The peak is then detected to generate a digital trigger pulse.
b) Teslameter mode, i.e. the field is fixed while the input frequency is swept across a given range, generating a resonance curve. This mode might be of interest for possible future applications.
The new sensor and the transducer were characterized in a dipole reference magnet and then tested directly in the PS reference magnet and calibrated with respect to the previous version of the monitor system at the moment used for controlling the power supply of the PS accelerator (see Chapter 7 for the results).

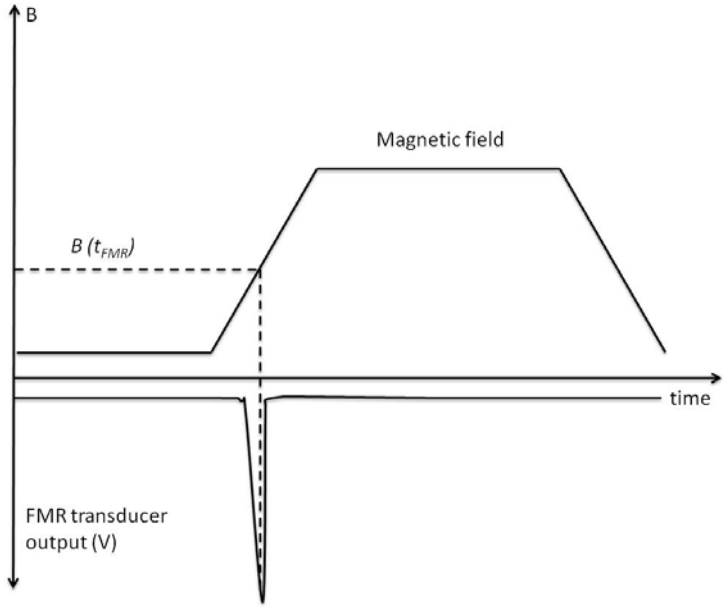

Fig. 5.8: signal from the FMR transducer.

REFERENCES

[1] P. Arpaia, M. Buzio; F. Caspers, G. Golluccio, C. Petrone, Static Metrological Characterization of a Ferrimagnetic Resonance Transducer for Real-Time Magnetic Field Markers in Particle Accelerators, *IEEE International Instrumentation and Measurement Technology Conference, 2011*.

[2] P. Arpaia, M. Buzio; F. Caspers, G. Golluccio, D. Oberson, Metrological Performance of a Ferrimagnetic Resonance Marker for the Field Control of the CERN Proton Synchrotron, *IEEE transaction on Superconductivity vol. PP issue: 1, 2011*.

[3] P. Bauer , M. Lamm, G. Lorenz, J. Nogiec, T. Peterson, R. Sood,W. Soyars, C. Sylvester, M. Tartaglia, G. Velev, Cost Estimate for a Tevatron Reference Magnet System, Fermilab internal note, *FERMILAB - TD-02-042, 2002*.

[4] F.K. Beckmann, H. Dotsch,P. Roschmann,W. Schilz, Remote Temperature Sensing in Organic Tissue by Ferrimagnetic Resonance Frequency Measurements, *11th European Microwave Conference, Amsterdam, 1981.*

[5] M. Benedikt , F. Caspers, M. Lindroos, Application of Magnetic Markers for Precise Measurement of Magnetic Fields in Ramped Accelerators, *Particle Accelerators*: 63, 1999.

[6] M. Buzio, P. Galbraith, G. Golluccio, D. Giloteaux, S. Gilardoni, C. Petrone, L. Walckiers, Development of Upgraded Magnetic Instrumentation for CERN Real-Time Reference Field Measurement Systems, *1st International Particle Accelerator Conference (IPAC'10), 2010.*

[7] M. Buzio, Past and recent main PS magnet measurements and B-train, *workshop on CERN Power Synchrotron magnet field, Geneva, Switzerland, 2012.*

[8] C. Carpenter, H. Kenneth; M. K. daSilva, Phaselocked yttrium iron garnet magnetometer for remote measurement of small field changes in a fluctuating background, *Review of scientific instrument Vol. 53, 1982*.

[9] F. Caspers, Offenlegungsschrift 2902572, *Deutsches Patentamt 31.5.1980 "Vorrichtung zur Messung und Stabilisierung von Magnetfeldern.*

[10] P. Roschmann, Compact YIG bandpass Filter with Finite-Pole frequencies for Applications in Microwave Integrated Circuit, *IEEE Transaction on Microwave Theory and Techniques, 1973*.

[11] J. L. Symods, Methods of Measuring Strong Magnetic Fields, *Reports on Progress in Physics, Vol. 18, 1955.*

[12] CERN, 2012, http://www.ohwr.org/projects/white-rabbit, *CERN open hardware project website, 2012.*

PART III – EXPERIMENTAL VALIDATION

Chapter 6

Measurement system for magnet characterization

6.1 Overview

The methods and the system developed in this thesis and illustrated in Chapter were validated on the field in order to verify their performance in actual conditions. In particular, they were used to qualify the production and the prototypes magnet for the new Linac4, currently in construction at CERN [14]. In this Chapter, the experimental results of the tests of the measurement quality and the systematic effects in measuring the field strength, direction and fiducialization on two different magnets with an aperture of 22 mm are reported.

6.2 Magnets under tests

The methods and system have been validated on the series and prototype quadrupoles for the new Linac4 accelerator under development at CERN [14]. This machine includes a large number of narrow-aperture quadrupole electromagnets (EMQ) in order to keep the beam focused along the acceleration path. These magnets must provide a high gradient (of the order of 20 T/m) in a very limited space, and are therefore powered with relatively high currents up to 200 A. The transversal focusing of the beam is achieved in the Drift Tube Linac (DTL) [14] by including several Permanent Magnet Quadrupoles (PMQ) allowing gradients and RF efficiency higher than the electromagnetic quadrupole ones, owing to their compactness. In the following the details of the two different types of focusing quadrupoles are reported.

6.2.1 Permanent Magnet Quadrupole (PMQ)

The first type of the magnet under test is a permanent quadrupole (called in the following PMQ), chosen as the best practical solution to provide the required high gradient within the small volume available inside the high-frequency accelerating structure. Additional advantages include simple fixed-optics operation and no heat losses [15],[5]. The prototypes used for the tests are based on Halbach design [9], with an integrated field gradient between 1 and 4 T/m·m for a length between 45 and 80 mm. The external cylindrical surface of these magnets was machined in order to be a reference for the installation in the Linac drift tube.

The PMQs will be welded inside the copper drift tubes, aligned through the outer cylindrical surface and radial pins. The PMQs are arranged in a Focusing/Defocusing (F/D) layout and must be tuned in pairs to the same integrated gradient $\int Gdl$, generally decreasing along the linear accelerator. The tuning is done by the manufacturer and is checked at CERN, through a common measurement reference, as a part of the acceptance tests of each magnet. Since the drift tubes are not adjustable in any way, corrective

interventions on assembled tanks would be very costly and must absolutely be avoided. For this reason, all magnets shall be re-tested once mounted in their respective drift tube, by paying particular attention to the field polarity, the centring of the magnetic axis the mechanical axis and any deterioration due to welding-induced heating.

The design of the PMQ is shown in Fig. 6.1a. The main parameters are listed in Table 6.1. The field is generated by 16 rectangular permanent magnet blocks, all magnetized to the same residual magnetization B_r along the appropriate direction, housed in slots cut at different radial positions to adjust coarsely the gradient. The blocks are held in place by a set of 32 radial silver-plated screws and the gradient can be fine-tuned over a 0.5 % by adding up to 25 μm of stainless steel shims at the inboard. (Optimization of the harmonics would be also possible with this design, but was not necessary.) The material selected is Sm_2Co_{17}, with high maximum $B_r \approx 1.2$ T and, most importantly, the best long-term stability against neutron-induced degradation and temperature effects, with a dB_r/dT about $-3 \cdot 10^{-4}$ K^{-1}. The housing is made by a special grade of austenitic steel 316 LN, originally developed for the LHC, with very-low magnetic permeability ($\mu_r \leq 1.003$). Stainless steel matches well copper in terms of thermal expansion and galvanic potential, and its low thermal conductivity protects the magnets against accidental overheating during welding.

A number of prototypes made by different manufacturers were tested at CERN. The main designs include:

a) Round magnet bars (Fig. 6.1b): the field is generated by two arrays including 27 transversally magnetized bars. Tuning the $\int Gdl$ is achieved by adding iron washers at the ends. The major drawback is poor field quality w.r.t. the final design, with low-order harmonic errors about twice as high.

b) High gradient (Fig. 6.1c): this is a classic Halbach array with 16 trapezoidal sectors, filling almost completely the volume available and hence providing almost double the gradient for the same magnetization. Apart from the higher gradient being unnecessary, with this design the $\int Gdl$ can be tuned only by changing the magnetization of the blocks or by enlarging mechanically the bore, both options being impractical.

c) Low gradient (Fig. 6.1a): this is the final design with 16 segregated blocks. The aluminum frame used initially was found to react electrochemically with the copper drift tube even in the presence of minute amounts of air moisture during the installation, leading to corrosion. A titanium frame was tested as a possible alternative, however its cost is four times higher than steel with no measurable advantage. Field harmonics of Al- and Ti-frame units, plotted in Fig. 6.2, do not differ significantly from those of steel-frame ones.

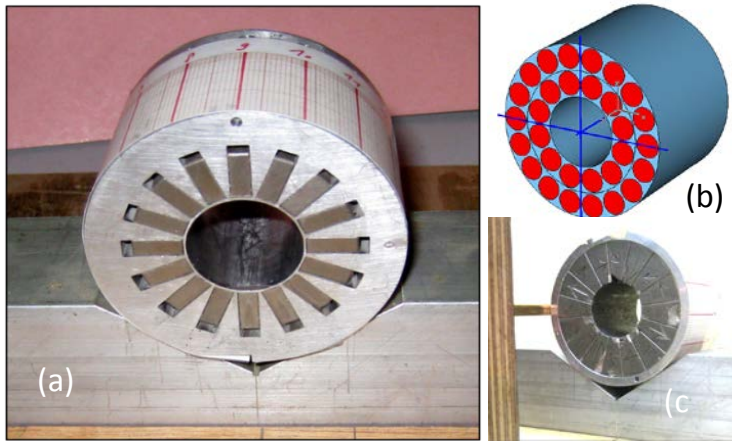

Figure.6.1: (a) 45mm long PMQ for Tank I; (b) schematics of 27-round bar prototype; (c) high-gradient prototype with standard Halbach blocks

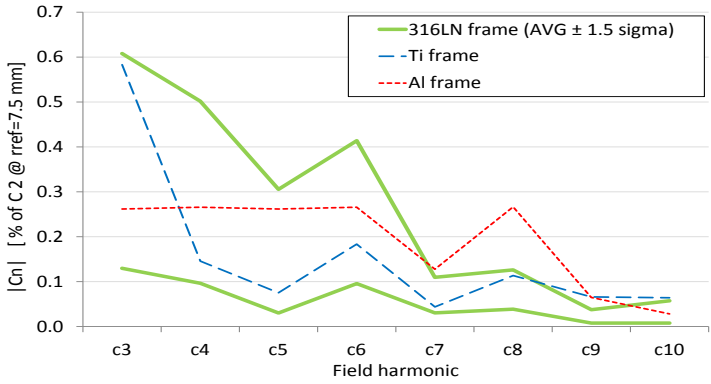

Figure.6.2: Norm of the field harmonics of all tested PMQs. The continuous lines represent the upper and lower bound of the 3σ spread of the series units.

Table 6.1: PMQ Parameters

Parameter	**Value**
Peak gradient [T/m]	23.6 – 56.4
Integrated gradient [Tm/m]	1.0-2.5
Length [mm]	45-80
Bore diameter [mm]	22
reference radius R_{ref} [mm]	7.5
Outer diameter [mm]	60

6.2.2 ElectroMagnet Quadrupole (EMQ)

The other magnets prototypes have been tested with the system are the fast-pulsed air-cooled quadrupole electromagnets (in the following EMQs). They are excited with relatively short current cycles (1 ms) and with a current ramp rate up to 600 kA/s. These magnets provide a field gradient, integrated over an effective magnetic length L_{eff} of 0.056 m, between 16 and 30 Tm/m.

The specific magnet under test are the so-called Type III quadrupoles (Fig. 6.3a), installed in the Chopper line of Linac4 [11]. This 60-mm long, 29-mm aperture magnet is powered by the current cycle of Figure 6.3b. The current ramp-up lasts 200 μs and is followed by a flat-top of 600 μs at a nominal current of 200 A, where the field is required to be stable within 10^{-3}. Table 6.2 resumes both the geometrical and the excitation parameters of the EMQ.

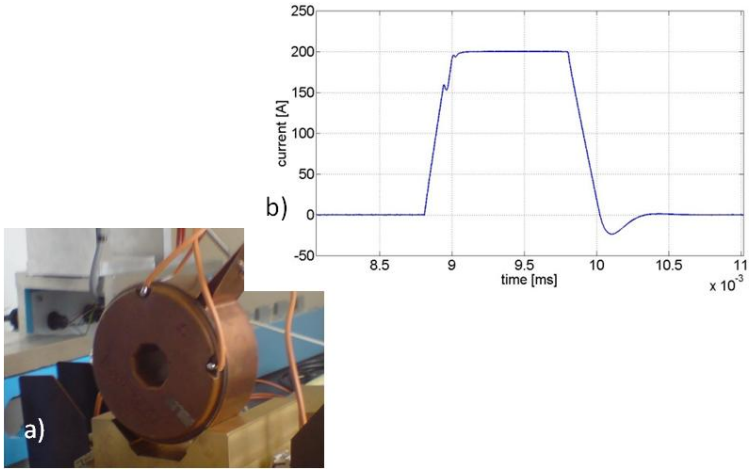

Figure 6.3: a) current excitation waveform for the laminated b) EMQ iron-core quadrupole magnet.

Table 6.2: EMQ Parameters

Parameter	**Value**
Length [mm]	55-150
Aperture Ø [mm]	20-80
Central gradient [T/m]	6-31
Maximum Current [A]	200
Rise time [ms]	0.2
reference radius R_{ref} [mm]	7.5

Flat-top duration [ms]	0.6

6.3 Quality of magnetic field strength

In general, measurement of magnets as small as the PMQs and EMQs is a challenging task. Considering e.g. a rotating coil inside a bore of radius r, the maximum number of coil turns wound with a conductor of given gauge is proportional to r^2; therefore, the signal corresponding to the harmonic of order n scales as r^{n+1}. In addition, the measured field coefficients C_n are inversely proportional to the geometrical coil sensitivity factors κ_n (see chapter 2), which in turn scale as r^n [16], thus the relative impact of radial mechanical tolerances and calibration errors δr is $\delta C_n/C_n = n\delta r/r$.

At the end, measurement uncertainties can be expected to be one to two orders of magnitude larger than in typical synchrotron magnets having $r \approx 50$-100 mm. Mechanical imperfections on small coil lead to longitudinal non-uniformity of width and radius higher 0.6%. When measuring a magnet shorter than the coil, such variations imply that the usual calibration of the average geometry is practically useless. The in-situ calibration removes this problem, but some issue arises when the procedure is applied as shown in Section 4.3.4.

The in-situ calibration was tested on the first prototypes of the PMQ Linac4 (but it remains valid for the EMQ, because they have the same length). Two coil shafts were manufactured to experiment the validity of different measuring coil concepts for testing small-aperture magnets.

At this aim, the coils were calibrated by the traditional [7] and the in-situ procedures, in order to obtain two sets of sensitivity coefficients κ_n^T and κ_n^m, respectively. The quadrupole magnet was further tested by means of the rotating coil and the single-stretched wire methods. The flux measured by the coil is processed by exploiting the κ_n^T and κ_n^m, resulting in the gradient measurements $FStrength^T$ and $FStrength^m$, respectively. These values were finally compared with the reference gradient $FStrength^{SSW}$ obtained by the single-stretched wire method. The method has been tested on 2 different types of rotating shafts (Fig. 6.4):

a) a first shaft, with two nested radial coils on the same plane (Fig. 6.4a), with equal equivalent area, for the sake of compensation.
b) a second shaft (Fig. 6.4b), with two tangential coils in series, compensating for the quadrupole, and a third one (coil3), compensating for the dipole.

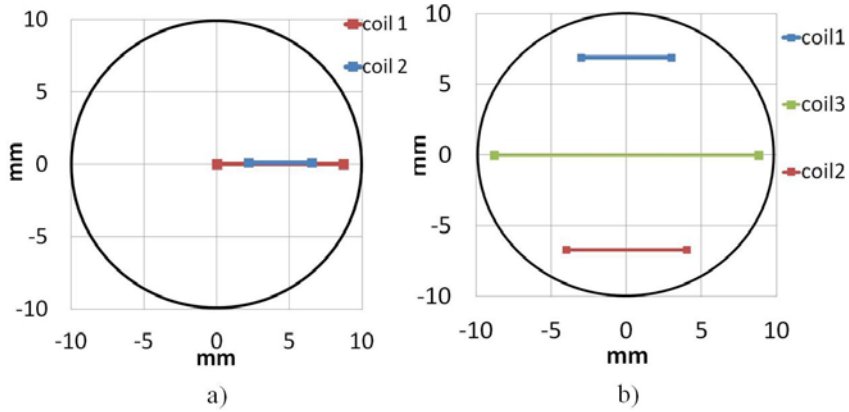

Figure 6.4: Coil design of the shaft with two radial coils (a) and the shaft with three tangential coils (b).

In the two rotating coil shafts, the small dimensions of the support (200 mm long, less than 10 mm wide, and 0.5 mm for the winding groove) make arduous the winding. Thus, a multi-strand wire, allowing a precise layering over multiple turns [4], was used. However, problems of low rigidity of the coil arise, because the wire has to be wound manually. As an example, for an 8-mm wide coil, the typical precision of the wire positioning is ±0.2 mm, resulting in ± 2 % of uncertainty on A_c. Furthermore, this non-uniformity affects the measurement quality when the magnetic field L_{eff} is shorter than the measuring coil L_c. The (2.4) is valid for coils with point-like windings. The finite dimension of the section produces a systematic error increasing according to the multipole to measure. Squared-shaped windings give the best approximation of the infinitesimal size assumption [16] and a multi-strand wire leads to very uniform geometries.

The two shafts were calibrated according to the in-situ and the traditional calibrations on a Linac4 quadrupole. Then, the calibrated coils were used to test several other Linac4 quadrupoles. The values obtained from both methods are directly compared to the magnet strength measured by the SSW.

In Table 6.3, the focus strength results obtained through the in-situ ($FStrength^m$) and the traditional ($FStrength^T$) procedures are compared with the stretched-wire ($FStrength^{SSW}$). The in-situ procedure reduces the average error to 0.1 % (two coils) and 0.03 % (three coils), with respect to the 5.5 % (two coils) and 0.5 % (three coils) of the traditional calibration. For the three-coil shaft, the traditional calibration performs better owing to the improved machining and design. The in-situ results met the requirements of ± 0.5 % from the Linac4 beam even if the type-B precision [10] of the rotating coil (± 0.3 %) is lower than the stretched wire (± 0.1 %).

Table 6.3: Results from the validation applied to several magnets of the Linac4 drift tube.

Magnet	Magnet length (mm)	$FStrength^{SSW}$ (Tm/m)	$\frac{FStrength^{*} - FStrength^{SSW}}{FStrength^{SSW}}$ (%)		$\frac{FStrength^{T} - FStrength^{SSW}}{FStrength^{SSW}}$ (%)	
			(3-coils)	(2-coils)	(3-coils)	(2-coils)
107	45	2.334	-0.1	-0.3	0.4	5.8
108	45	2.331	-0.2	-0.3	0.6	6.2
109	45	2.317	0.1	0.2	0.4	6.2
905	45	2.328	0.2	-0.3	0.6	5.4
R1	45	2.431	0.0	0.0	0.3	6.4
R2	45	2.449	0.1	0.2	0.5	4.6
1637691	80	6.861	-0.1	-0.3	0.4	4.7
1637690	80	6.833	0.1	0.1	0.3	5.1

The deviation of the traditional procedure was confirmed by applying the in-situ calibration in different longitudinal positions (Figs. 6.5 and 6.6) to show the difference between the nominal parameters A_c, R_0 and the local A_{cm}, R_{0m}. For the two-coil shaft (a), the coil 1 (Fig. 6.4) in the central part shows a high variation in the surface profile. Being nested, the coil 2 is more uniform. Nevertheless, the radius variation increases along the rotation axis: 5 % for coil 1, and 3 % for coil 2, on 200 mm. Therefore, the longitudinal measurement position is chosen far from the coil end, namely at 100 mm from the left coil edge, where the width is almost uniform. For the 3-coils shaft (Fig. 6.5b), the enhancement in coil quality is highlighted by a smaller difference among the values of A_c and R_0 averaged over the length, given by the traditional calibration, and the local results A_{cm} and R_{0m}. In Figs. 6.6a and 6.6b, the differences between the measured and nominal values of the coil equivalent radius are shown at different longitudinal positions. The coils of the two-coil shaft are affected by higher irregularities owing to the winding, the support machining, and the sag effects.

According to (6.2) and (6.3), the total uncertainty is equal to $\pm$ 0.3 % for the equivalent radius and $\pm$ 0.6 % for the area. About half of this uncertainty arises from the repeatability of the calibration, assessed by fixing the displacement Δz and by using the same permanent quadrupole (i.e. fixed *FStrength*). The effect of higher multipoles (6.6) is one order of magnitude lower than the repeatability. According to (6.4), the uncertainty on A_{cm} and R_{0m} affects also the higher-order harmonic coefficients proportionally to the multipole order. In Fig. 6.7, the percentage uncertainty on κ_n^m in a given longitudinal position, obtained by varying the displacement between -1.1 and 1.1 mm and the *FStrength* between 2.0 and 2.4 Tm/m, is shown for the three-coil shaft.

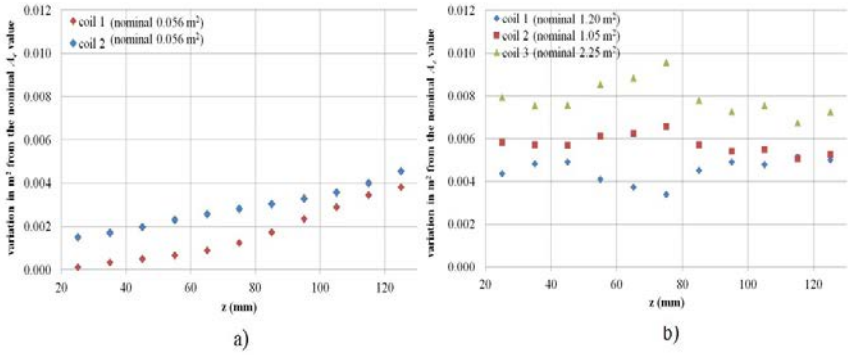

Figure.6.5: Difference in m^2 between the locally measured A_{cm} and nominal equivalent area A_c vs the longitudinal position along the coil for (a) the two-coil and (b) the three-coil shaft.

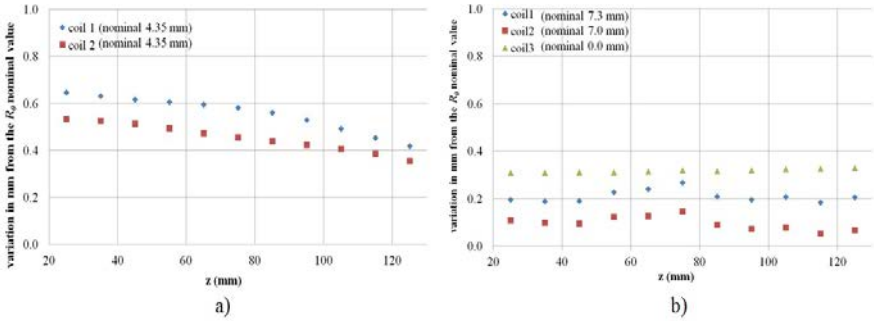

Figure 6.6: Difference in mm between the locally measured R_{0m} and nominal equivalent radius R_0 vs the longitudinal position along the coil for (a) the two-coil and (b) the three-coil shaft.

For coil 3, the uncertainty is linear, such as expected. Conversely, for the other two coils, the uncertainty on κ_6^m and κ_8^m increases by a factor 3. These two coils are tangential, therefore insensitive to multipole order having an angular period, or an integer number of periods, corresponding to the coil opening angle $\Delta\theta$ (Fig. 6.1):

$$\Delta\theta = 2\arctan\left(\frac{W_{eff}}{R_0}\right) \quad (6.1)$$

These two coils have an aperture close to the 12-pole and to the 16-pole, corresponding to 1.047 and 0.78 rad, respectively. The sensitivity to harmonics higher than the quadrupole is relevant only for coil 1, because the two other coils are only used to compensate the dipole and quadrupole terms. Coil 1 is optimized to measure the multipoles up to n=8 (16-pole), i.e. the field errors in a quadrupole magnet. In practice, calibrating the amplitude of high order multipoles (n>2) to better than 10 % turns out to be useless.

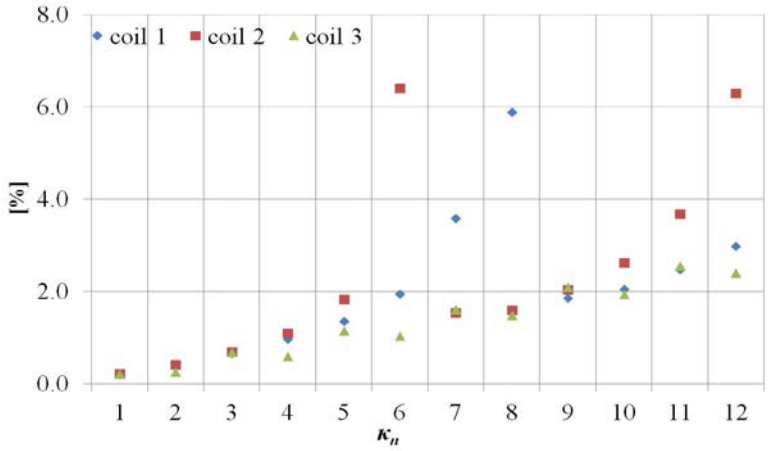

Figure 6.7: Uncertainty of the coil sensitivity factor for each n-pole (three coils shaft).

The influence of the SSW systematic error in (6.1) was proved by (i) in-situ calibrating the 3-coil shaft by a "bad" quadrupole with strong multipole components of 46, 32 and, 4 units for b_4, b_6 and b_8, respectively, (ii) by testing successively 21 magnets, (iii) in-situ calibrating the same 3-coil shaft by a "good" quadrupole, with low multipole errors of less than 14 units of b_4 and less for the higher orders. For the "bad" quadrupole, the deterministic error computed from (6.1) was equal to 0.67 %, and the measured value was 0.58 %, while, for the "good" quadrupole, the computed error was 0.14 %, and the measured error 0.03 %.

6.4 Quality of homogeneity measurements

The multipole field components, measured by means of the rotating coil, are affected by systematic effects due to mechanical errors, sag in the coil profile, and vibrations. For a small-radius shaft, the bucking coil solves the problem only partially: lateral movements during the coil rotation, e.g. due to irregular bearings, induce non-linear coupling with the quadrupolar field and generate erroneous multipoles of lower and higher orders. Furthermore, a deflection due to gravity of 10 μm on a reference radius of 10 mm will introduce an error of 0.1 % on the dipole and 0.03 % on the sextupole. This effect is measured to amount to 0.05 % (5 units) on the sextupole component (Fig. 6.8). This effect was assessed by measuring the harmonics as a function of the roll angle when rotating the mechanical frame. In Fig. 6.8, the systematic effect Δ_S of a displacement of the coils in a quadrupole field is shown to be a sinusoidal function of the frame roll angle. Therefore, by averaging the harmonics measured in two positions spaced by 180º, the Δ_S can be calculated and removed. After averaging, the main contribution to the measurement uncertainty u_R arises from noise-like mechanical vibrations.

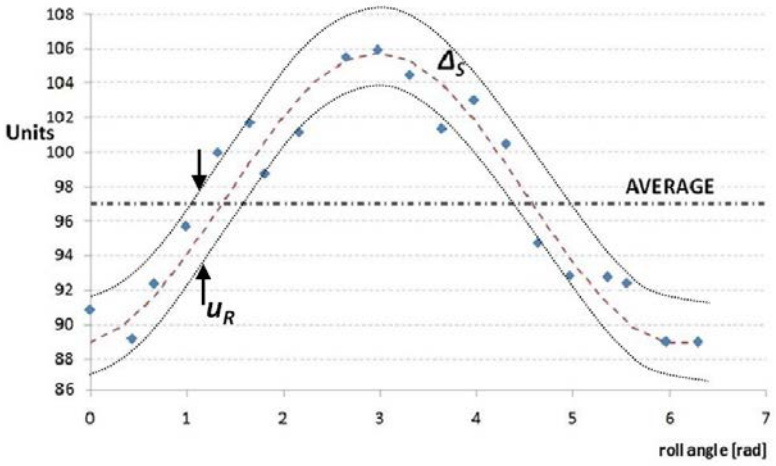

Figure 6.8: Systematic effect ΔS and measurement uncertainty u_R of sextupole field component as a function of the roll angle of the mechanical frame *X-Y* (section 4.3.2).

6.4.1 Measurements results on small-aperture permanent quadrupoles

In Tab. 6.4, the measurement for a permanent magnet of 45-mm length, in continuous rotation mode, is reported. The main metrological characteristics are expressed as units (10^{-4}) of the main field component, for each harmonic, skew (a_n) and normal (b_n). The *1-σ* repeatability u_p is evaluated over 30 turns of the shaft in the same mechanical configuration of the bench. The *1-σ*-uncertainty u_R is calculated as the standard deviation over several measurements in different mechanical configurations by removing Δ_S.
The total uncertainty u_T, computed as the quadratic sum of u_p and u_R, is lower than ± 4 units for all the multipole field components. The highest values is reached for the 16-pole field component (b_8, a_8), because a tangential coil with W_{eff} and R_0 equal to 6.3 and 7.3 mm, respectively, is insensitive to the multipole order having an angular period, or an integer number of periods, corresponding to the coil opening angle $\Delta\theta$:

$$\Delta\theta = \arctan\left(\frac{W_{eff}}{R_0}\right) \tag{6.2}$$

Table 6.4: Main metrological characteristics in units (10^{-4}) of the main field component, for each harmonic, skew (a_n) and normal (b_n), for a permanent magnet of 45-mm length, in continuous rotation mode: 1-σ repeatability u_p, 1-σ uncertainty u_R and overall uncertainty u_T (quadratic sum of u_p and u_R).

Harmonic Order	Average Values [Units]	u_p [Units]	u_R [Units]	u_T [Units]
b_3	-24.21	1.05	1.87	2.14
b_4	2.17	1.35	2.37	2.73
b_5	-9.16	2.29	1.17	2.57
b_6	14.67	0.49	0.99	1.10
b_7	3.37	0.63	3.55	3.61
b_8	-0.10	3.36	1.27	3.59
b_9	0.50	1.90	0.43	1.95
b_{10}	1.02	0.31	0.57	0.65
a_3	-3.63	1.26	0.99	1.60
a_4	-49.14	0.92	0.46	1.03
a_5	-7.53	2.45	1.08	2.68
a_6	-14.46	0.51	0.92	1.05
a_7	-6.19	1.14	3.20	3.40
a_8	-1.56	2.99	2.91	4.17
a_9	0.53	1.74	0.45	1.80
a10	-0.57	0.36	1.46	1.50

In Fig. 6.9, typical results of a harmonic measurement on a PMQ are reported in absolute values of the harmonic content according to the beam optics requirements. The polyvalent system was used to measure the harmonic content of a complete batch of permanent magnets composing the first drift tube of the Linac4. The results have been compared with those obtained at the manufacturer's, by finding the results compatibles [5].
In addition, a double check with a completely independent new instrument based on a vibrating stretched wire developed for smaller-aperture magnets [2] has given a difference of about 0.05 % of standard deviation, showing the compatibility between the two systems.

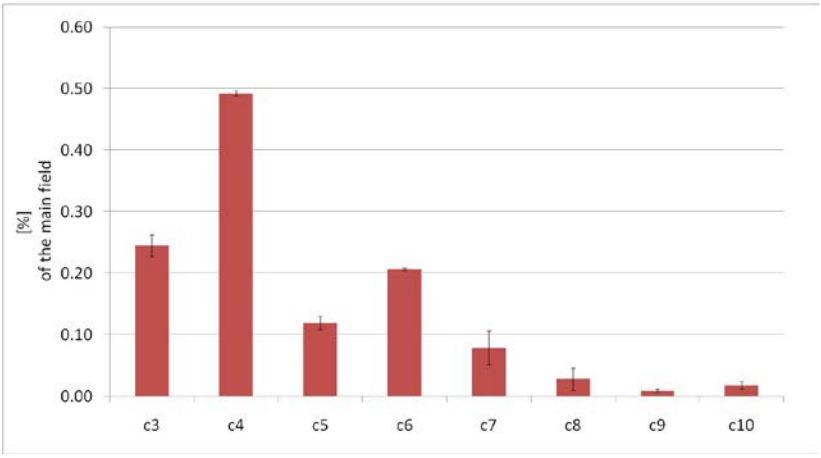

Figure 6.9: Typical result with u_T-bar of a harmonic measurement performed on a permanent magnet.

In Tab. 6.5, the relative difference between the coil-measured and nominal $\int Gdl$ is summarized for all the series magnets of the first drift tube Linac4, along with all other results. After re-matching the optics, the residual 1-σ experimental uncertainty is $\pm$0.13 %, well below the tolerance of $\pm$0.5 %. This tolerance reflects essentially random measurement errors on a magnet-to-magnet basis, virtually identical to the spread between wire measurements at CERN and coil (0.12 %) and at the manufacturer's (0.11 %). The repeatability of the $\int Gdl$ measurement, defined as the standard deviation over at least 3 consecutive taken in the same conditions, is much smaller, about 0.03% for both the instruments [5].

Table 6.5 Field quality summary of the first series of PMQ magnets

Parameter	Tolerance	Average	Standard Deviation
∫Gdl [% of nominal]	0.5	0.00	0.13
$\|c_3\|$ [% of C_2 @ 7.5 mm]	1	0.37	0.16
$\|c_4\|$ [% of C_2 @ 7.5 mm]	1	0.30	0.13
$\|c_5\|$ [% of C_2 @ 7.5 mm]	1	0.17	0.09
$\|c_6\|$ [% of C_2 @ 7.5 mm]	1	0.26	0.11
Field direction (F) [mrad]	1	0.27	1.11
Field direction (D) [mrad]	1	-0.74	1.34
Magnetic center x [mm]	0.1	-0.01	0.04
Magnetic center y [mm]	0.1	-0.01	0.03

6.4.2 Measurements results on fast pulsed quadrupoles

In Tab. 6.6 and Fig. 6.10, the results of a step-by-step measurement on EMQ fast-ramped magnet are reported.

Table 6.6: Main metrological characteristics in units (10^{-4}) of the main field component, for each harmonic, skew (a_n) and normal (b_n), for a fast-pulsed quadrupole up to 600 kA/s: 1-σ repeatability u_p, 1-σ uncertainty u_R, and overall uncertainty u_T (quadratic sum of u_p and u_R).

Harmonic Order	Average Values [Units]	u_p [Units]	u_R [Units]	u_T [Units]
b3	4.32	0.25	1.37	1.39
b4	-4.39	2.10	3.63	4.19
b5	1.38	1.23	1.3	1.79
b6	-1.28	0.42	0.32	0.53
b7	-0.03	0.15	0.28	0.32
b8	-1.23	0.90	0.88	1.26
b9	3.68	0.10	1.30	1.30
b10	11.32	0.47	0.71	0.85
a3	4.09	0.34	1.01	1.07
a4	4.83	2.29	3.46	4.15
a5	-0.64	3.92	1.07	4.06
a6	0.12	0.35	0.44	0.56
a7	0.39	0.19	0.17	0.25
a8	0.13	0.89	0.49	1.02
a9	3.92	0.27	1.16	1.19
a10	-0.04	0.39	1.42	1.47

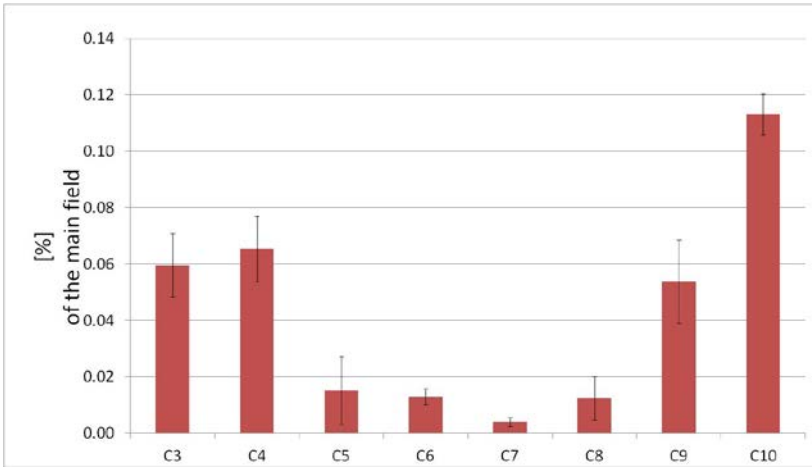

Figure 6.10: Typical result with u_T-bar of a harmonic measurement on a fast-pulsed quadrupole up to 600 kA/s.

In such a case, the accuracy of the measurement depends on the magnet powering history, saturation, and hysteresis effects. However, the proposed system shows high performance also in such critical conditions of aperture dimension and ramp rate. In step-by-step mode, the systematic effects Δ_S are of the same order as for the continuous rotation, but the high voltage signals at the integrator input have reduced the contribution of u_p by one order of magnitude. The high value of the 10^{th} harmonic with respect to the other harmonics is in agreement with the calculated value based on the magnet geometry. For this particular pulsed quadrupole, these measurements confirm those performed with an independent system [11].

The step-by-step measurement procedure depends essentially on the behaviours of the magnet in the time domain (Chapter 4). In other words, it depends on the time constant of the magnet with respect to the current pulse. If the stop integration trigger signal (Fig. 4.7b) is sent before the end of all the dynamic effects, a related systematic error arises in the harmonic field measurements.

The circuital model and the measurement method proposed in Chapter 4 have been used to estimate the time constants of such a magnet.

In the model definition, the main problem is to take into account both the eddy current circuit in the iron yoke lamination and the other circuit created by the fringe field in the plane perpendicular to the magnet axis.

The influence of different eddy current circuits on the time-domain integral measurements was investigated by means of a small coil of 4.5 mm diameter used to scan the field inside the aperture, in different positions with a 5 mm longitudinal step. The observed variation of the eddy current decay is function of the position inside the magnet aperture [2]. The decay includes two contributions: a slower one, tending to disappear when the coil is in the middle of the magnet aperture, and a faster one, present along the magnet length as a whole. For this reason, the model in Fig. 6.11 takes into account 2 parasitic circuits

modeling the eddy current on the pole surface and of the end side, more influent for a short magnet (slower time constant).

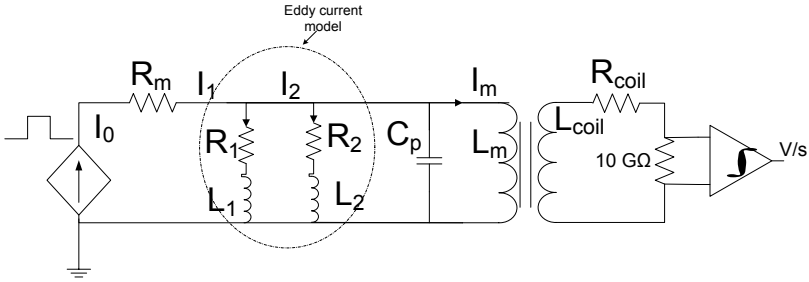

Figure 6.11: complete circuital model of the eddy current and the measurement system.

The circuit reproduces the proposed time-domain measurement scheme [11]. It simulates the flux linked to the pick-up coil used to measure the field inside the magnet aperture. The excitation current waveform (Figure 6.3b) is applied as input to the model. This allows the behavior of the time integral of the voltage at the ends of the transformer secondary winding (Figure 6.11) to be investigated. The resistor of 10 GΩ is the acquisition system resistance.

In Figure 6.12, the time response of the equivalent circuit to the excitation current is shown. The flux both simulated (at the end of the acquisition chain) and acquired (expressed as 6.25) is shown. The circuit is able to replicate the decay effect due to the eddy currents, but the contribution of the mutual coupling of the parasitic circuits with the pick-up coil in the flux measurements is still missing. The difference between measurement and simulation in the time domain still points out a very-small amplitude slow decay during the flattop.

The model verified that the approach to the measurement of the time constant proposed in (4.29) is valid. The results of Fig. 6.13 show that the slowest time constant for this kind of magnet lasts around 200 μs [8].

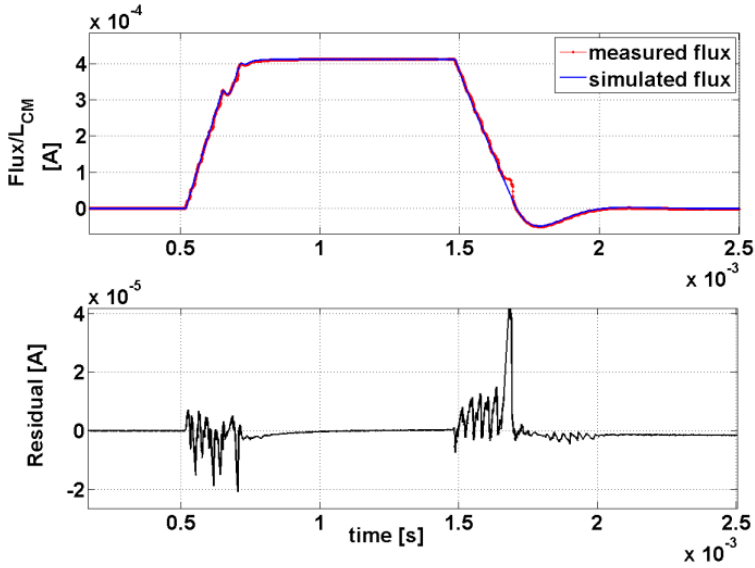

Figure 6.12: measured and modelled flux scaled by the mutual inductance Lm: time domain transients (up), and residual (down).

The measured time lag set a limit in the duration of the field flattop, in other word a particle beam can pass in the field only when all the dynamic effects of the magnetic field are ended. For this reason the quality of the field homogeneity has to be evaluated only after that all the dynamic effect are terminated.

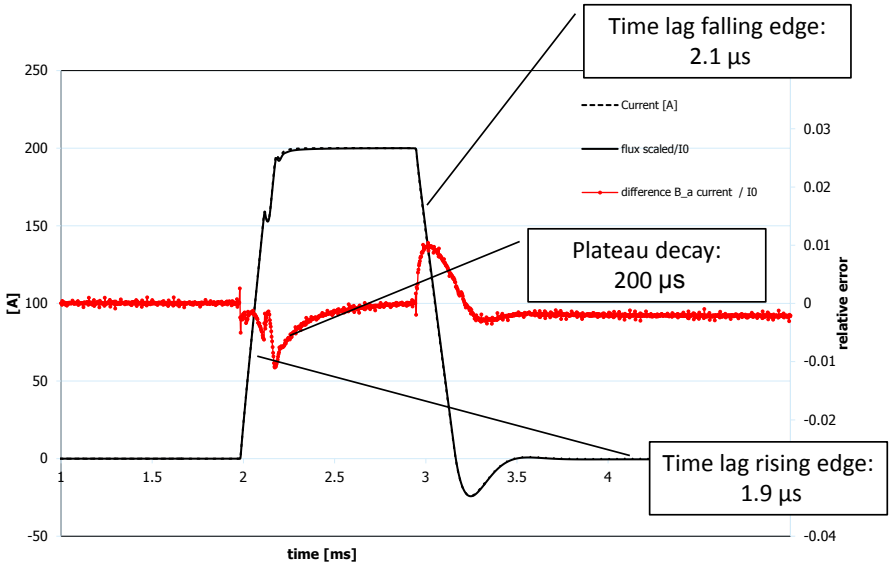

Figure 6.13: Eddy current measurement results of the EMQ fast-pulsed magnet.

6.5 Quality of magnet fiducialization

The fiducialization of the magnetic field axis with respect to the mechanical reference is obtained from (4.14) and (4.15), once the systematic offset between the coil and the mechanical frame is removed.
In Fig. 6.15, the best-fit ellipse of the offset Δs, obtained from the measurement of Δz in (4.14) at different angles when rotating the magnet, is shown. A difference of 2 μm between the two diameters of the ellipse shows that the magnet axis is rotating essentially on a circle. This means that the first-order approximation in (4.14) has a second-order error within ± 2μm, well below the required tolerance.

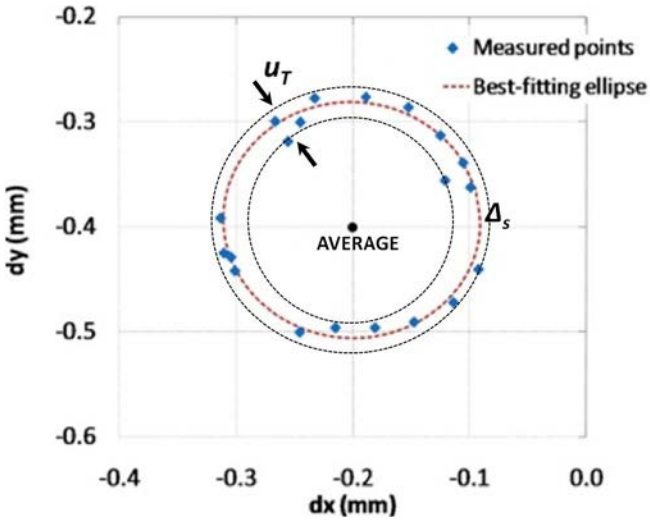

Figure 6.15: Systematic effect Δs and uncertainty u_T of the axis measurements.

In Fig. 6.15, the average (with coordinates ΔX, ΔY) represents the distance between the centre of the mechanical axis and the coil rotation axis. The long-term stability of the fiducialization measurement could be estimated by measuring ΔX and ΔY for different magnets over a long period, because it should remain constant. For the polyvalent system, the stability over three months of the axis fiducialization is better than ±10 μm (Fig. 6.16). The repeatability u_p of the axis measurement was estimated as better than ±3 μm, and the overall uncertainty u_T for such a measurement can be assessed as ±10 μm, ten times lower than the tolerances required by the beam optics.

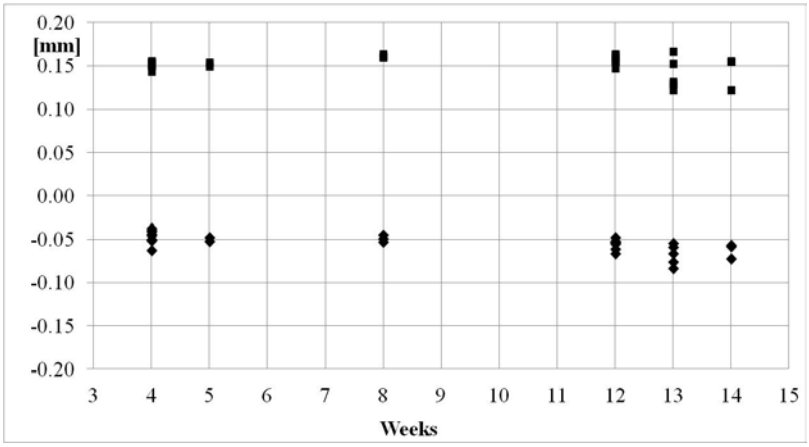

Figure 6.16: the stability of the position of the rotation axis ΔX (■) and ΔY (◆) in the bench coordinate system measured over a time span of three months.

The same procedure can be adopted to assess both systematic and random errors affecting the fiducialization of the field direction. The roll angle is measured according to the procedure resulting from (6.12) and (6.13). From these equations, the systematic angle ζ between the mechanical and the coil frames is estimated. Therefore, the mechanical parts and the zero reference of the angle encoder have to be stable in the long term in order to carry out a reliable measurement. The repeatability evaluated by repeating the measurements by removing and replacing the magnet on the support several times, is better than ±50 μrad.

The flipping method removes all the systematic effects, thus the uncertainty arises from vibrations and mechanical inaccuracy.

The long-term stability of the angle measurements was estimated by measuring the offset ζ during several months and with different magnets under test (Fig. 6.17). A 1-σ long-term stability of ±0.1 mrad is achieved over several months. The 1-σ short-term precision is assessed to ± 0.07 mrad, by measuring several quadrupole in a row, 10 times better than the tolerances required by the beam optics.

The quality of the pin orthogonality measurement (a purely mechanical parameter) was verified by comparing such a measurement with a completely independent mechanical measurement system.

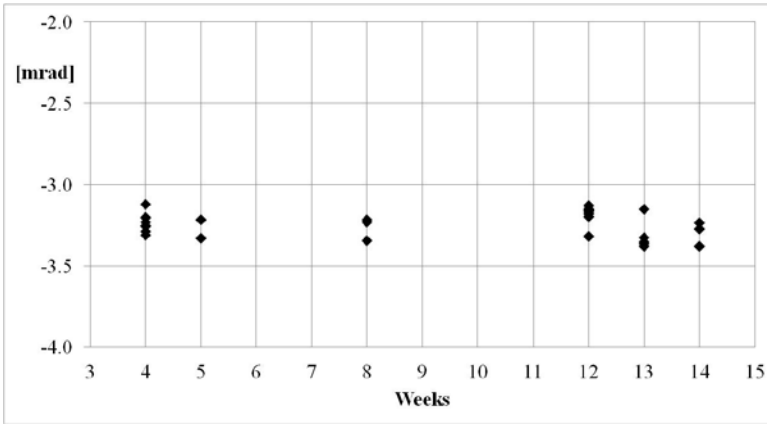

Figure 6.17: Stability of the angular offset between coil and V-support frames over three months.

For all the PMQs the axis is well within the 1 mm nominal tolerance. Also in this case, the systematic offset between the rotating coil axis and the magnet support is recalculated each time and its spread, which is about 0.02 mm, gives an indication of the result uncertainty.

About the field direction fiducialization, each PMQ has two pin holes 90º that allow its installation inside a drift tube, in either focusing or defocusing configuration (corresponding to a positive or negative normal quadrupole). The pins define the *x* and *y* directions of the mechanical reference system of the magnet. In this reference, the field direction is defined as $\alpha = -\frac{1}{2}\tan^{-1}(A_2/B_2)$, where A_2 and B_2 are the skew and normal quadrupole components. In Fig. 6.18, the magnetic field axis, measured with the proposed fiducialization method, is plotted for all the PMQs of the first Linac4 drift tube by pointing out also the circular tolerance.

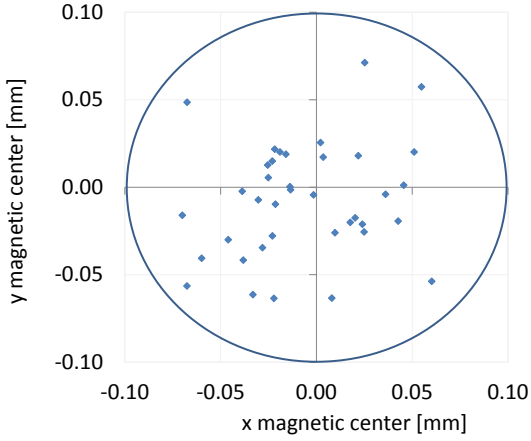

Fig. 6.18: Magnetic centre of all series PMQs w.r.t. the mechanical centre (axis of the external cylindrical surface) The circle represents the tolerance.

The mechanical reference is offset by ζ with respect to the natural reference system of the rotating coil, i.e. with x axis parallel to the coil at the integration start time. The field direction in both focusing and defocusing configurations is plotted in Fig. 6.19. Almost one half of the magnets exceed the nominal tolerance of ±1 mrad by up to almost 3 mrad. Nonetheless, the averages remain within tolerance and the variations can be accepted by beam optics.

The orthogonality error of the pins, measured magnetically, averages about 1.0 mrad with a standard deviation of 0.9 mrad. It was found to be uncorrelated with the field direction error.

The radial fringe field of the strongest PMQ was mapped with a Hall probe to assess the possible deflection of the electron beam used for welding. The level is about 6.2 mT at r of 30.5 mm, i.e. about 1.5 % of the peak field within the aperture. The leaking field has quadrupolar symmetry and decreases as $1/r^2$, meaning that it drops below ambient background level at a $r \geq 55$ mm.

The relative leakage level for the regular Halbach design unit tested was about 3.1%, owing to the magnetized blocks being radially larger. The decay rate for an infinitely long 16-block Halbach quadrupole should be in theory much higher, namely $1/r^{14}$ or higher. The low rate observed may be ascribed to the low longitudinal aspect ratio.

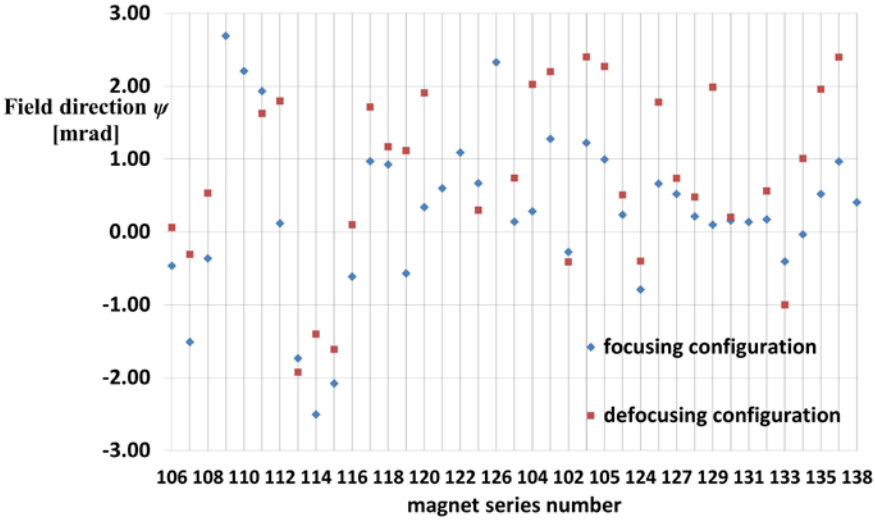

Figure 6.19: Field direction for the two possible configurations of each PMQ. The orthogonality error between the pins is the difference of the two values.

[1] P. Arpaia, A. Masi, G. Spiezia, Digital integrator for fast accurate measurement of magnetic flux by rotating coils, *IEEE Transactions on Instrumentation and Measurements, Vol. 56, No. 2, 2007.*

[2] P. Arpaia, M. Buzio, J. J. G. Perez, G. Golluccio, C. Petrone, L. Walckiers, Experimental validation of multipole magnetic measurements by vibrating wire systems, *Proceeding of Magnet Technnology Conference (MT22), 2011.*

[3] P. Arpaia, M. Buzio, G. Golluccio, L. Walckiers, In situ calibration of rotating sensor coils for magnet testing, *Rev. Sci. Instrum. 83, 013306, 2011*.

[4] M. Buzio, Fabrication and calibration of search Coils, *CERN Accelerator school: specialized course on Magnets, CERN-2010-004, p. 387, 2009*.

[5] M. Buzio, G. Golluccio, A. Lombardi, F. Mateo, Magnetic Qualification of Permanent Magnet Quadrupoles for CERN's Linac4, *IEEE transaction on Superconductivity vol. PP issue: 1, 2011.*

[6] J. Cobb, J. J. Murray, Magnetic field measurement and spectroscopy in multipole fields, *3rd International Conference on Magnet Technology, 1970.*

[7] O. Dunkel, Coil Manufacture, Assembly and Magnetic Calibration Facility for Warm and Cold Magnetic Measurements of LHC Superconducting Magnets, *14th International Magnetic Measurement Workshop (IMMW14), 2005*.

[8] G. Golluccio, Eddy current measurements in fast-cycled linac quadrupole, *16th International Magnetic Measurement Workshop (IMMW16), 2009*.

[9] L. Halbach, Permanent Multipole Magnets with Adjustable Strength, *IEEE Transaction on Nuclear Science v. 30, 1983*.

[10] JCGM, Joint Committee for Guides in Metrology, *International Vocabulary of Metrology 3rd Edition, JCGM 200:2008, 2008*.

[11] R.K. Littlewood, Magnetic properties of the new linac quadrupoles, *CERN PS/SM/77-5, 1977.*

[12] C. Schott, R. S. Popovic, S. Alberti, and M. Q. Tran, High accuracy magnetic field measurements with a Hall probe, *Review of Scientific Instrument, Vol. 70, 2703, 1999.*

[13] N. Smirnov, L. Bottura, M. Calvi, G. Deferne, J. DiMarco, N. Sammut, and S. Sanfilippo, Focusing Strength Measurements of the Main Quadrupoles for the LHC, *IEEE Transactions on Applied Superconductivity vol. 16 no. 2. 2006.*

[14] M. Vretenar *et al.*, Linac4 Technical Design Report, *CERN internal report CERN–AB–2006–084 ABP/RF, 2006.*

[15] M. Vretenar, The Linac4 project at CERN, *Proceeding International Particle Accelerator Conference.(IPAC'11), 2011*.

[16] L. Walckiers, Magnetic measurement with coils and wires, *CERN Accelerator school: specialized course on Magnets, CERN-2010-004, 2009.*

[17] K. Weyand, Magnetometer Calibration Setup Controlled by Nuclear Magnetic Resonance, *IEEE Transactions on Instrumentation and Measurement, vol. 48-2, 1999.*

Chapter 7

Measurement system for magnet monitoring

7.1 Overview

A measurement bench, dedicated to characterize the behaviour of the FMR transducer (Chapter 5) in static and dynamic fields, was set up. In particular, in static fields, the influences on the transducer of the temperature and of the orientation on the YIG filter's linearity were investigated. In dynamic fields, experiments were aimed at evaluating the effect of fast-varying fields on the transducer response, at varying both the ramp rate and the marking levels.

7.2 Metrological characterization of the ferrimagnetic resonance transducer

A preliminary research work was carried out to verify the feasibility and the reliability to use a commercial filter as field sensor [2] in static magnetic field conditions.
In Fig. 7.1, the measurement setup for demonstrating experimentally the suitability of FMR as field marker is illustrated. An microwave Network Analyser E8464B Agilent® is used both as signal generator and resonance detector, working in the range from 1.6 to 9.0 GHz corresponding to about 60 to 320 mT. It measures the transmission coefficient S_{21} of the network for each frequency starting from 1.6 GHz. In this range, the filter YIG [1] (specifically built by Omniyig®) has a Q-factor of about 1,000. The magnetic field is generated by a reference dipole magnet, with a transfer function of 315 mT/A, previously mapped by means of a NMR probe with an absolute uncertainty of $\pm$5 ppm [9]. Two NMR probes, covering the field range under test as a whole, are also installed close to the FMR in order to provide a reference field measurement.

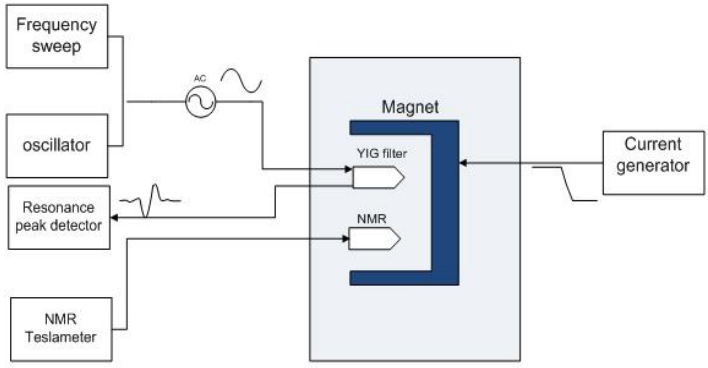

Figure 7.1: Setup of the FMR field marker.

RF interference between NMR and FMR systems is avoided by activating only one at time. In Fig. 7.2, the field map of the magnet along its length as a whole is shown at four different lateral positions.

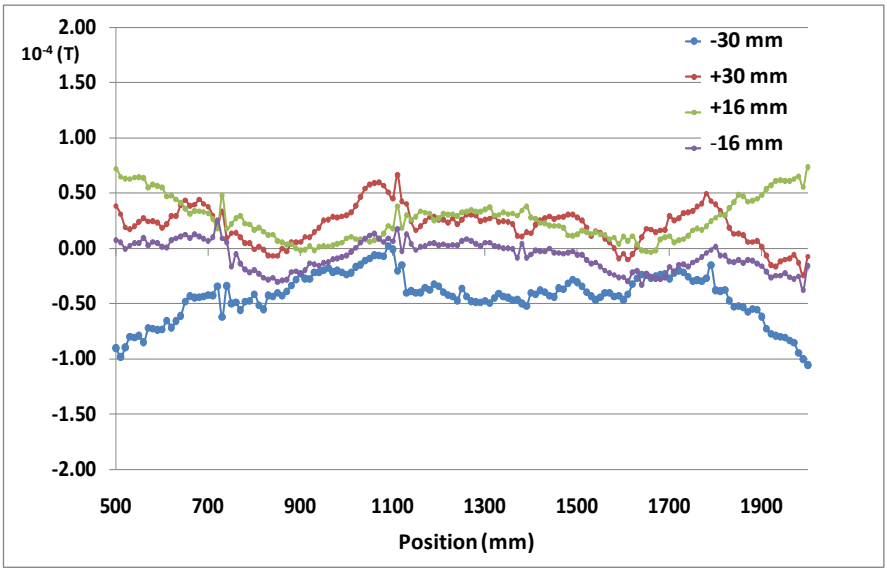

Figure 7.2: Reference magnet field mapping with NMR probe in different horizontal positions with respect to the centre of the magnet (central field 1.0000 T).

The horizontal variation is less than 1·μT /mm (between ±30 mm). In the central region (between 1120 and 1200 mm) where FMR transducer and the NMR probe are placed, the longitudinal field gradient is around 5·μT/mm, by assuring a displacement between the probes of a few of millimetres not influencing the results.

A current generator with high stability and low ripple (10 ppm relative to the nominal value) is used to excite the magnet. It can generate a maximum current of 40 A at 8 V, thus fixing the upper limit of investigation to about 0.135 T.

All the measurements were carried out on a stable hysteresis cycle of the magnet, in order to compare the results obtained over several current cycles. A straightforward stabilization is obtained by 5 pre-cycles of the magnet. The peak frequency measurement is compared to the value obtained with the NMR teslameter PT2025 [9], once the field is stabilized for the static characterization.

The resonance frequency of the YIG filter is evaluated by the peak detection of S_{21} provided directly by the network analyser. The corresponding systematic error is assessed by comparing the resonance curves measured by the network analyser with a parabolic fitting. The high SNR of the transducer guarantees the uncertainty of the resonance peak detection to be less than $\pm$0.005 dB. In other words, the difference between the resonance frequency detected by the network analyser and the one defined by a best fit on the resonance signal is less than 10 kHz, corresponding to 10^{-8} T.

In Figs. 7.3a and 7.3b, the results of the static calibration of the FMR transducer with respect to the NMR are reported as deterministic error and 2-σ relative uncertainty bands, respectively. The calculated gyro-magnetic ratio is 28.084 GHz/T. The theoretical value of 28 GHz/T is degraded by material impurity [10].
An offset of 10·μT in the static calibration agrees with a displacement of 2 mm between the YIG filter and the NMR reference probe, according to the non-homogeneity of the field shown in Fig. 7.2.
The deterministic error trend reveals also a parabolic nonlinearity of about 0.06 mT in the full range of investigation (Fig. 7.3a). This phenomenon depends on the shape of the YIG sphere and on the relative angle between the magnetization field and the principal axis of the YIG crystal.
The relative uncertainty has a maximum of $\pm$40 ppm over the full range (± 2 μT absolute uncertainty in Fig. 7.3b), confirming the suitability of the YIG filter as sensing element of the field marker transducer.

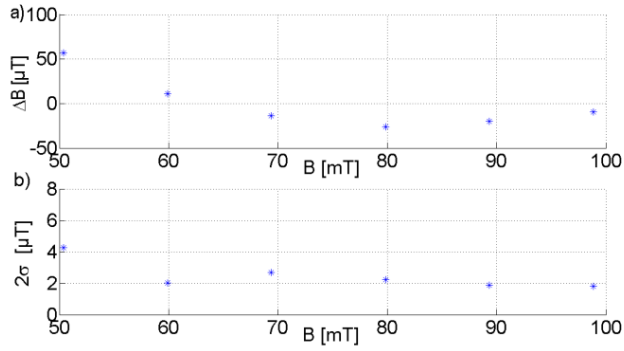

Figure 7.3: a) Deterministic error of the YIG filter, b) 2-σ uncertainty of the transducer.

The FMR transducer (Fig. 7.5) was calibrated in dynamic and static conditions with the setup of Fig. 7.4. The reference measurement for the field is given by an NMR probe, working in a DC field only, supplemented by a fixed coil to provide the field change during ramps. The three probes, including the FMR under test, are stacked as closely as possible in an H-type (see Appendix A) dipole magnet (Fig. 7.5).
The magnet aperture was mapped (Fig. 7.6), according to the grid in Fig. 7.5, to verify the variation in of the field along the *y* and the *x* direction, to correct the magnet non-linearity. The 3-D plot in Fig. 7.6 showed the satisfying magnet homogeneity in the *x* direction (less than 2 μT for the 4 different mapping fields of 53, 73, 94 and 126 mT).
In the direction *y*, the reference magnet presents a non-homogeneity stronger than in the horizontal direction, due to the magnet geometry. By interpolating this curve a systematic correction factor due to the distance (51 mm) between the probes of 60 μT can be estimated. However, the low inductance of this magnet allows the field to be ramped as fast as 3 T/s. Systematic field differences between the positions of the probes were evaluated first by NMR-mapping and then by exchanging the respective locations during the tests.

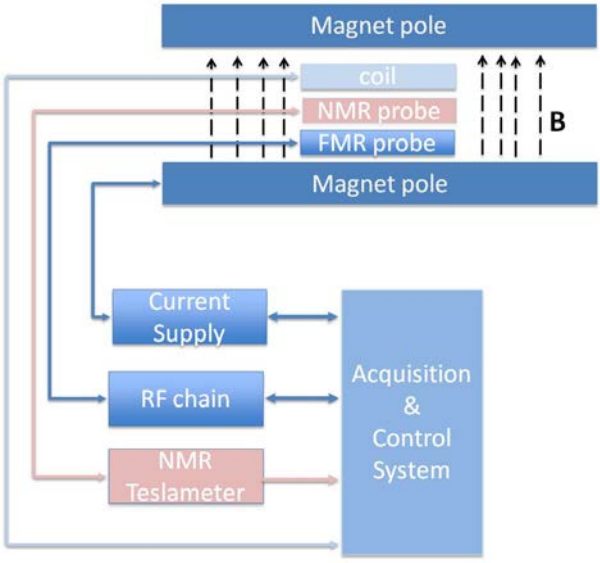

Figure 7.4: Schematic layout of the calibration system

The RF chain is computer-controlled to sweep the input signal in the range from 1 to 3 GHz, corresponding roughly to 50 to 110 mT. The power converter of the magnet is controlled through a WorldFIP bus to generate arbitrarily complex excitation cycles. All the measurements were carried out on a stable hysteresis cycle of the magnet in order to compare the results obtained over several current cycles. A straightforward stabilization was obtained by pre-cycling the magnet for at least five times [3].

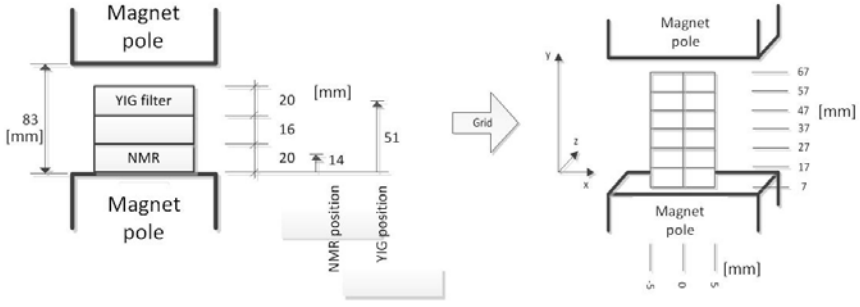

Figure 7.5: Probes configuration for the FMR transducer calibration in the reference magnet.

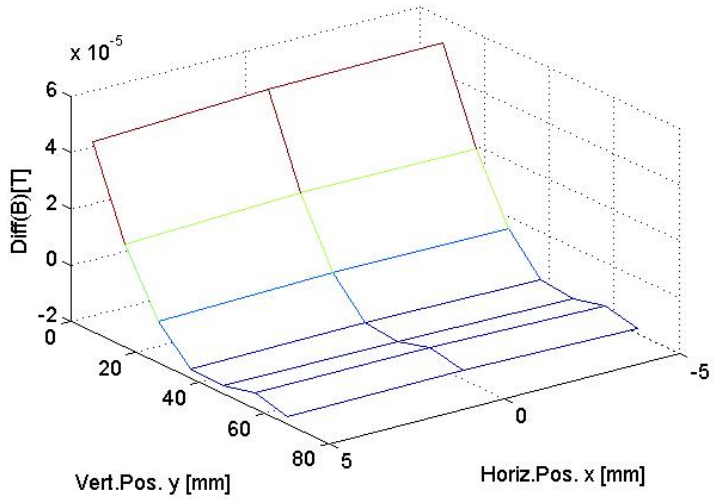

Figure 7.6: field map of the calibration dipole magnet.

7.2.1 Static tests

In Fig. 7.7, the calibration of the transducer as a whole, including the RF chain, repeated in the same excitation as the bare YIG filter by sweeping the filter input with the RF synthesizer, is plotted.

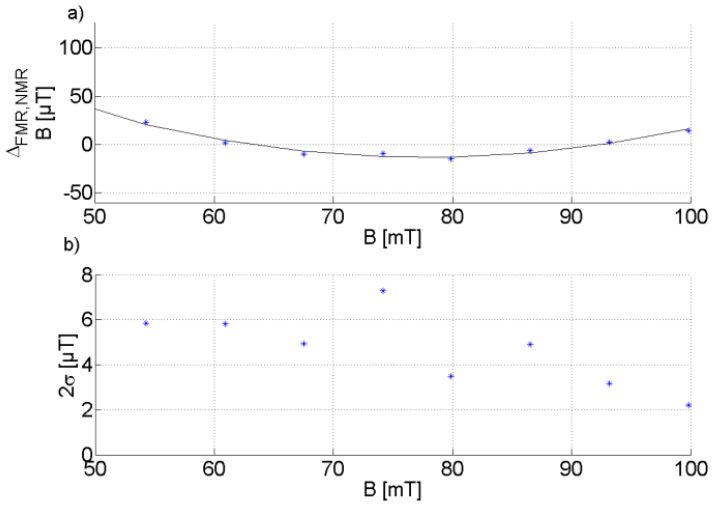

Figure 7.7: Static calibration of the transducer with RF chain: (a) difference ΔB between NMR and FMR transducer with a parabolic fit; and (b) 2σ uncertainty.

The effective gyromagnetic ratio evaluated from a linear regression is found to be 28.09 GHz/T, with a difference less than 2×10^{-4} with respect to the bare YIG filter of Fig. 7.3. The difference of about 0.2 % between this value and the nominal can be attributed to impurities in the YIG filter material [10] and to the imperfect orthogonality of the two semi-circular RF antennae [1].

The linear regression revealed an offset of 0.6 mT, consistent with the field inhomogeneity measured inside the dipole. The non-linearity behaviour of the FMR as field transducer displays a parabolic characteristic (Fig. 7.7a) within ±42 μT, below the specifications and acceptable. The most important result is the very-low 2-σ uncertainty (Figure 7.7): less than ±8 μT in the range of interest, confirming the viability of the transducer for the new monitor system project.

The most critical issue is the temperature dependence of the sensor. The calibration of the transducer was repeated between 22 and 35° C with a reference thermocouple. In the range between 50 and 100 mT, the temperature stability has been found to be between 6 and 2 μT/°C (Fig. 7.8), within the specifications.

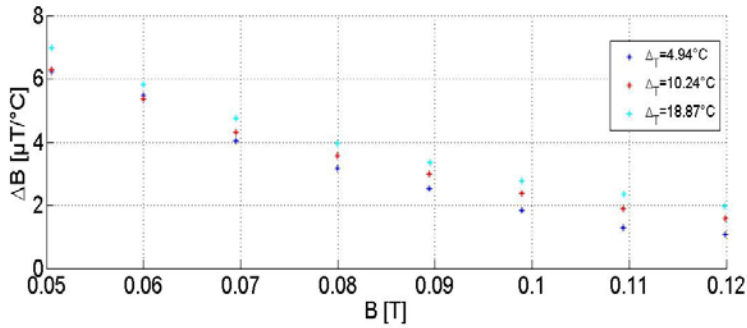

Figure 7.8: Field drift due to temperature variations $\Delta B/\Delta T$ of the FMR transducer as function of the measured field.

However, a larger margin should be achieved through better thermal stabilization inside the magnet gap, as shown in a previous version of the probe installed in the PS reference magnet [4].

The energy of ferromagnetic crystals depends in part on the magnetization direction relative to the crystal axes; this part of the energy is called “anisotropy energy” [8]. In other words, the response of the sensor is completely not linear but, a second order coefficient is function of the angle between the direction of the magnetization and the principal axis of the ferrite crystal. In a polycrystalline specimen, this dependence on the ferrite crystal orientation of the YIF filter linearity is removed because but, on the other hand the resonance in general is broader than in a single crystal, meaning less resolution in field measurement [5]. This effect was studied for the developed probe by rotating the YIG filter in the magnet aperture as shown in Fig. 7.9.

The YIG filter was rotated according to the scheme in Fig. 7.9 around the three axes and the field difference between the NMR and the output of the transducer was measured. The results in Fig. 7.10 confirm [8] and [6].

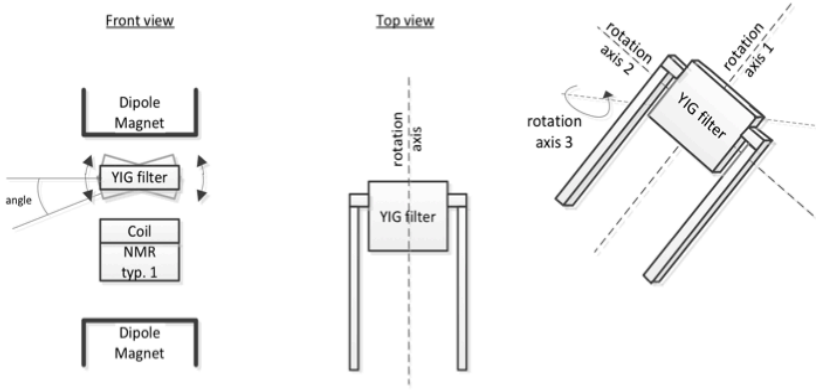

Figure 7.9: mechanical layout for the FMR static characterization as function of the angle between the field direction and the probe.

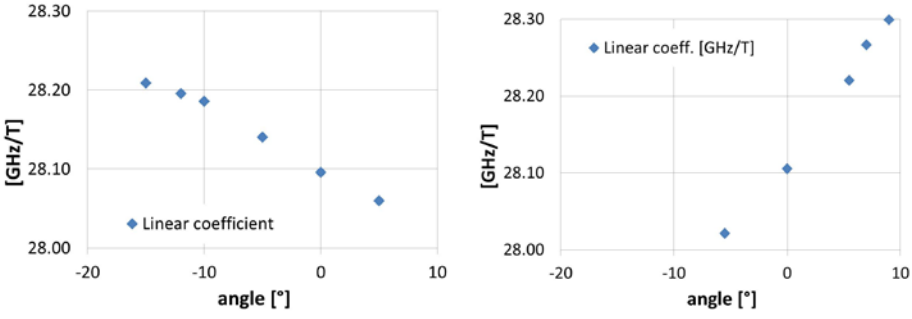

a) b)

Figure 7.10: Variation of the FMR transducer linear coefficient vs angle between the sensor and the magnetic field direction: a) rotation around the axis 2 in Fig. 7.9 and b) rotation around the axis 1 in Fig. 7.9.

Orientation effects are pronounced with single-crystal YIG spheres, but the higher field resolution possible makes their use desirable when the orientation effects can be controlled, such the case of the FMR as field marker, because the installation is fixed. The limits on shift in field direction can be estimated from Kittel's formulas, once the shape of the YIG is well defined. For the probe developed we calculated the linear coefficient changes of 18 MHz/° by rotating around the axis 1 (Fig. 7.10b). By rotating around the axis 2 the effect on the linear coefficient is lower (8 MHz/°), this asymmetry could be caused by the shape of garnet not perfectly spherical as shown in [8]. However, this effect is not relevant for an FMR transducer used as field marker, because in this case the probe is fixed in the magnet and an absolute calibration with respect to the beam is in any case needed [4].

7.2.2 Dynamic tests

For the calibration in a ramping field, the FMR resonance curve was compared with the field value obtained by integrating the output of the reference flux coil. The coil was calibrated using the NMR probe with an uncertainty less than $\pm$10 ppm. In Fig. 7.11, the output signals from the dynamic measurement procedure are shown. The field at the flat bottom is measured with the NMR, then the current start to ramp and the signal generated on the coil is acquired simultaneously with the RF diode output.

$B(t_1)$ is the field measured by the coil when the diode output is minimum. This value is compared with the field corresponding to the frequency set at the YIG filter input. A second NMR measurement (NMR2 in Fig. 7.11) is taken on the cycle flat-top to measure the equivalent surface of the coil and to verify the measurement stability.

By this setup the equivalent surface of the coil was measured to be 0.0862 ± 3e-6 m^2, meaning that the reference field, by this procedure, was known with an uncertainty of ± 40 ppm.

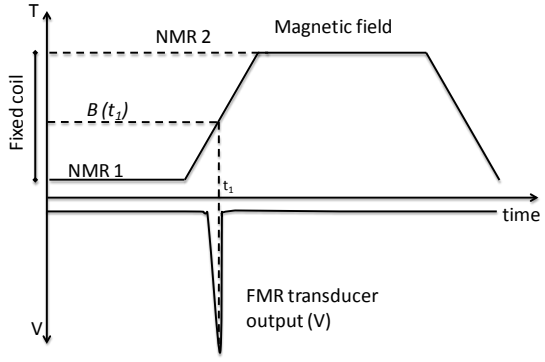

Fig. 7.11: Expected field and FMR transducer output in dynamic tests.

The dynamic calibration has shown the uncertainty to be virtually identical to static test results of Section 7.2.1 of the transducer. However, initial tests using a commercial version of the sensor, made with an aluminium case for better noise immunity and thermal stability, have shown a ramp rate dependence of about 0.4 mT for ramp rates from 0 to 2.5 T/s, resulting in a time constant of 157 μs (the angular coefficient of the red line in Fig. 7.12).

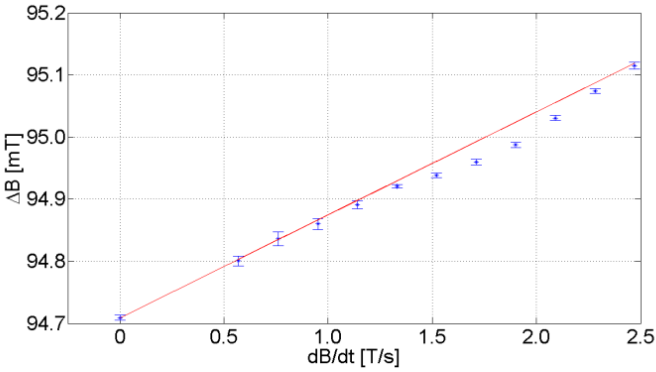

Fig. 7.12: Dynamic calibration results for the original aluminium case YIG filter at B=94.89 mT. The (*) are the experimental data, the straight red line represents the simulated field systematic error, i.e. the lag due to eddy currents.

This effect can be attributed entirely to eddy currents with a time constant around 160 μs, estimated analytically.

Considering the mechanical layout of the aluminium box of the YIG commercial filter (Fig. 7.13), the eddy current induced on this surface can be calculated according to the Ampere's law. A time-varying magnetic induction $\partial B / \partial t$ crossing the surface $A = LW$, generates an *e.m.f.* proportional to:

$$e.m.f = \varepsilon = \frac{\partial B}{\partial t} WL \tag{7.1}$$

this electromotive force will drive a current I_{eddy}:

$$I_{eddy} = \frac{e.m.f}{R_{eddy}} \tag{7.2}$$

The equivalent resistance R_{eddy} seen by that current can be estimated as:

$$R_{eddy} = \rho \frac{l_R}{A_R} \tag{7.3}$$

where ρ is the material resistivity, l_R is the length of the equivalent eddy current, and A_R is the section of the equivalent conductor (Fig. 7.14).

Owing to the physical dimension of the box, I_{eddy} is assumed to circulate on an elliptical path (filling up the entire volume of the aluminium). Thus, l_R and A_R can be calculated as:

$$l_R = 2\pi \sqrt{\frac{1}{2}\left(\frac{W}{2}\right)^2 + \left(\frac{L}{2}\right)^2} \tag{7.4}$$

$$A_R = \frac{1}{2}\left(A_{R1} + A_{R2}\right) = \frac{1}{2}\left(\frac{W}{2}\right) + \left(\frac{L}{2}\right) \tag{7.5}$$

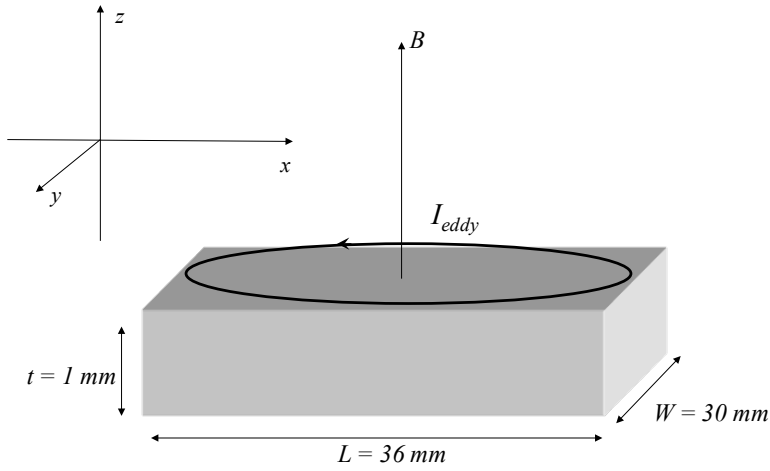

Fig. 7.13: mechanical layout of the YIG commercial filter aluminium box.

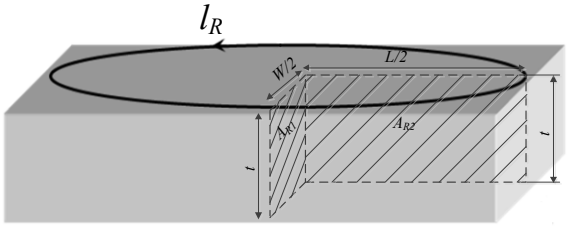

Fig. 7.14: path of the eddy currents on the aluminium case.

The effect of a current circulating on the surface is the generation of a magnetic field H_{eddy} opposed in sign to the main field crossing the surface. The field H_{eddy} and the relative magnetic induction B_{eddy} can be approximated as the field generated by a two-coils solenoid (corresponding in actual conditions to two eddy current circuits for each side of the YIG filter box):

$$H_{eddy} = \frac{I_{eddy}}{L+W} * 2 \rightarrow B_{eddy} = \mu \frac{I_{eddy}}{l_R} * 2 \tag{7.6}$$

The time constant of the eddy currents corresponds to the time constant of the equivalent RL circuit:

$$\tau_{eddy} = \frac{L_{eddy}}{R_{eddy}} \tag{7.7}$$

where the self-inductance of the eddy current circuit can be calculated as the ratio between the flux generated by I_{eddy} flowing through the surface A_R:

$$\Phi_{eddy} = B_{eddy} A_{eddy} = L_{eddy} I_{eddy} \tag{7.8}$$

By considering the geometric parameters of the YIG box in Figs. 7.13 - 7.14 and the resistivity of the aluminium, the resistance R_{eddy} results to be of 167 μΩ, while the self-inductance L_{eddy} = 26 nH. The resulting calculated time constant (τ_{eddy}) of 155 μs is comparable the 157 μs measured, confirming that the delay is due to the eddy current on the aluminium. The effect of those parasitic effects is to delay the field seen by the YIG sensor with respect to the reference field, and this effect is linear with the ramp rate (Fig. 7.12).
Conversely, a new YIG sensor, customized for the marker application with a plastic Noryl casing coated with 8 μm each of copper and silver, shows no measurable ramp rate dependence (Fig. 7.15).

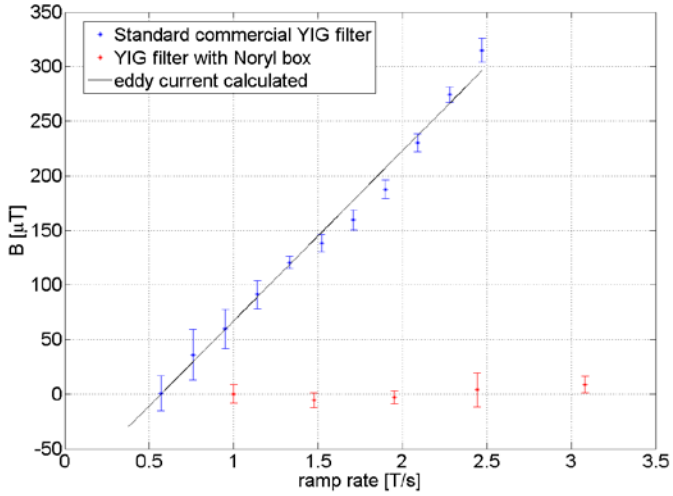

Fig. 7.14: Comparison between the standard commercial unit of YIG filter and the customized version for the field marker as function of the ramp rate.

The transducer with the customized YIG filter has been found to be fully adequate to be used as a high-precision field marker for the real-time field measurement systems of the PS, as well as other injectors at CERN. Its long-term reproducibility is going to be tested in parallel with the existing system and the on field validation will be shown in the next sections, in parallel with an automated peak detection electronic system. The FMR transducer with the customized YIG filter has been tested in the calibration system of Fig. 7.4 at different ramp rates (from 0.5 to 3.1 T/s) and different marker levels (from 0.06 to 0.22 T). As shown in Fig. 7.15 the 3σ precision of the system remains within ± 5 and ± 30 μT. The worst value of ± 30 μT is obtained at highest ramp rate that anyway is inside the specification of the new monitor system. Considering the special application of the field marker in the PS reference magnet, having a ramp rate maximum of 2.3 T/s, the precision of the marker is well inside the tolerances of ± 30 μT, this make the FMR transducer fully adequate to the new challenging requirements of the Proton Synchrotron accelerator.

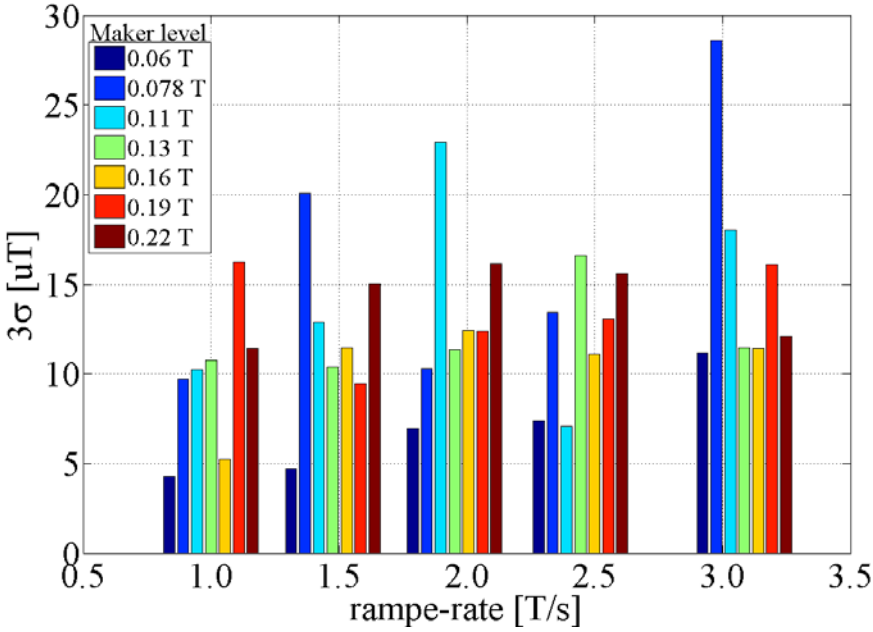

Fig. 7.15: 3-σ precision of the FMR transducer as function of the ramp rate at different marker levels.

7.3 On-field validation

The FMR transducer was tested in the reference magnet of the PS accelerator at CERN to verify its requirements matching for the new monitor system. The on-field validation was carried out during the machine operation, by comparing the trigger instant of the FMR with the field measured by the existing monitor system. During the machine operation, the reference magnet is cycled with different current cycles, according to the experiment of the CERN accelerator complex requiring a particle beam.

The marker level was set to generate the resonance pulse before the cycle reaches the injection plateau as required from the machine operators, corresponding to a field level of 0.06 T.

In Fig. 7.16, the setup of the tests in the reference magnet is shown. All the probes are installed in the defocusing half of the reference magnet. The tool being used for the measurements is a relatively simple PC-based acquisition system. It includes two National Instruments M-series cards, allowing the simultaneous measurement of up to two digital channels at 10 MHz along with up to 16 analog channels at an aggregated sampling rate of 1.2 MS/s. The digital inputs are used to acquire the TTL triggers from two peaking strips (F and D) and to timestamp them with resolution of 0.1 μs (i.e. ~0.002 G). The analog inputs are used to acquire the coils (F and D), the current signals (DCCT outputs) and the FMR transducer output at 200 kHz (i.e. 0.2 G resolution). The field

linked to the coil when the magnet is ramped is calibrated with a peaking strip generating a voltage pulse when the field cross the value of 0.0049 T at each current cycle. Then, starting from this value the voltage on the coil is integrated and multiplied by the coil area to get the field vs the time (Fig. 7.17).

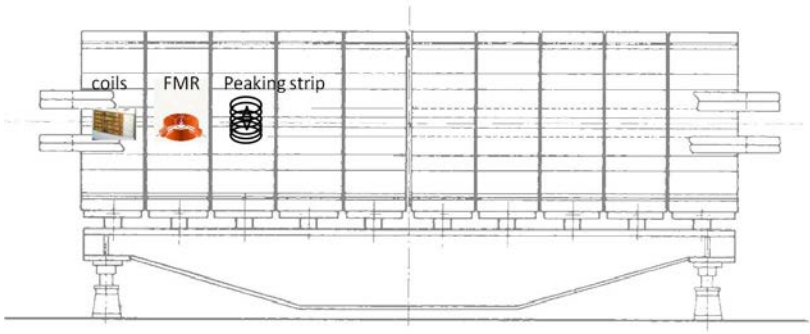

Fig. 7.16: setup for the on field validation of the FMR transducer

The field value B_{FMR} corresponding to the RF frequency set on the FMR transducer of 2 GHz, equal to 0.06 T, is crossed two times for each cycle. It was compared with the value $B(t_1)$ (Fig. 7.11).

The 3-σ of the difference between B_{FMR} and $B(t_1)$, reported in Fig. 7.18, over 1-month measurements, corresponds to the stability of the system. Compared to the value obtained in the calibration dipole in Fig. 7.15, the uncertainty of the transducer is degraded by a factor 2. The possible causes of this discrepancy are: (i) the two probes are installed in two different positions in the reference magnet, and thus the variations of the magnetic field are different; (ii) the field fluctuation at two different field levels (the peaking strip trigger at 4.9 mT while the FMR at 60 mT) are not systematic (fluctuations of the magnet hysteresis); (iii) the noise in the acquisition of the coil signal used as field reference; and/or (iv) the precision of the peaking strip.

Another possible issue could be the magnetic force acting on the magnet's poles and the relative movement of all the sensors installed in the magnet with respect to the magnetic field. A first measurement campaign [5] highlighted a vertical displacement of the upper pole equal to 0.16 mm for current cycle up to 5400 A (maximum current).

Those sources of uncertainty in the reference measurement system of the PS accelerator make difficult to verify on the field the quality of the FMR transducer. A final test with the transducer installed in the new monitor system of the PS and a further crosscheck with the beam position monitor have to be performed.

Anyhow the 3-σ uncertainty of ± 60 μT is still within the tolerances required by application making the FMR the optimal solution as field marker in a complex reference magnet as the one of the PS, as well as other injectors at CERN.

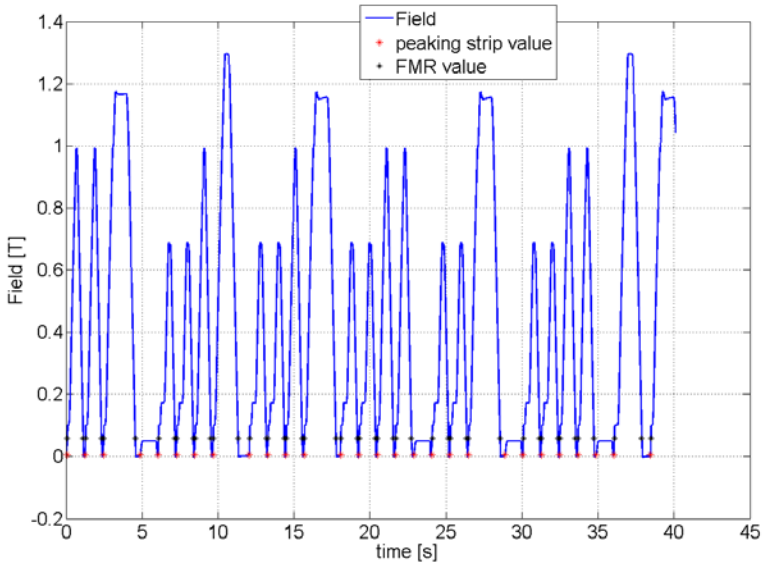

Fig. 7.17: field measured in the reference magnet of the PS (blue line), in red the peaking strip trigger instant and in black the FMR trigger value.

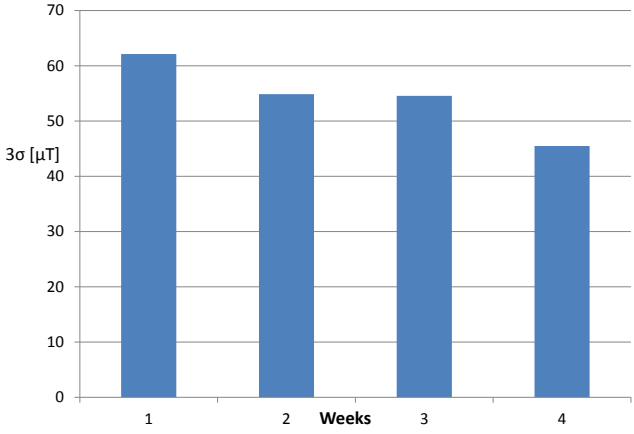

Fig. 7.18: FMR marker 3-σ reproducibility over 1 month tests in the PS reference magnet. The 3-σ is calculated over 30 different current cycles (different injection and extraction level) of the Proton Synchrotron accelerator.

REFERENCES

[1] M. Aigle, G. Hechtfischer, W. Hohenester, R. Jünemann, C. Evers, a systematic way to YIG-filter-design, *37th European Microwave Conference, 2007*.

[2] P. Arpaia, M. Buzio; F. Caspers, G. Golluccio, C. Petrone, Static Metrological Characterization of a Ferrimagnetic Resonance Transducer for Real-Time Magnetic Field Markers in Particle Accelerators, *IEEE International Instrumentation and Measurement Technology Conference, 2011*.

[3] P. Arpaia, M. Buzio; F. Caspers, G. Golluccio, D. Oberson, Metrological Performance of a Ferrimagnetic Resonance Marker for the Field Control of the CERN Proton Synchrotron, *IEEE transaction on Superconductivity vol. PP issue: 1, 2011.*

[4] M. Benedikt, F. Caspers, M. Lindroos, Application of Magnetic Markers for Precise Measurement of Magnetic Fields in Ramped Accelerators, *Particle Accelerators: 63, 1999.*

[5] F.K.Beckmann, H.Dotsch, P.Roschmann, and W.Schilz, Remote Temperature Sensing in Organic Tissue by Ferrimagnetic Resonance Frequency Measurements, *11th European Microwave Conference, 1981.*

[6] C. Carpenter, H. Kenneth; M. K. daSilva, Phaselocked yttrium iron garnet magnetometer for remote measurement of small field changes in a fluctuating background, *Review of scientific instrument Vol. 53, 1982.*

[7] G. Franzini, O. Coiro, D. Pellegrini, M. Serio, A. Stella, M. Pezzetta, M. Pullia, Final Design And Features Of The B-Train System Of Cnao, *Proceeding of 1st International Particle Accelerator Conference (IPAC), 2010.*

[8] C. Kittel, on the Theory of Ferromagnetic Resonance Absorption, *Physical Review, Vol. 73, n. 2, 1948.*

[9] the Metrolab PT2026 user manual, 2003.

[10] N. Vukadinovic, J.Ben Youssef, H. Le Gall, Influence of magnetic parameters on microwave absorption of domain mode ferromagnetic resonance, *Journal of Magnetism and Magnetic Materials, Vol. 150, 1995.*

Conclusions

In particle accelerator development the quality and the control of the magnetic field applied to the particles a critical issue and becomes more influent in synchrotron. The construction of magnets to precise tolerances and the checking of theirs manufacture by even more precise measurements is one of the keys to build of a reliable accelerator. In particular for synchrotron, the characteristics of the magnetic field have often to be monitored with high precision during the operation of the accelerator to avoid particle trajectory variations.

The future upgrades of the LHC injector chain, to improve the luminosity of the LHC has required a large research and development effort to develop new measurement systems for testing the magnets of the upcoming accelerators (Linac4) and to improve the quality of actual field monitor system of the accelerators composing the injection chain of the LHC.

This thesis has reported the results obtained in the improvement and development of magnetic measurement systems for on both aspects: the magnet prototypes for design validation and series production characterization, and the monitoring and measurement during their operation in the machine.

About the series production testing, in particular a polyvalent measurement system to characterize the magnetic properties of small-aperture permanent and fast-pulsed iron-dominated quadrupole magnets was proposed. The system is able to measure the magnet axis, field strength and direction, and multipole harmonic field content in two main configurations: continuous rotation for permanent magnets and high-resolution step-by-step mode for fast-pulsed electromagnets. The quality of the method relies mainly on the quality of the calibration of the rotating coil.

For this reason, a method to calibrate directly in the magnet under test (in situ) the coil sensitivity parameters, namely the coil equivalent area and rotation radius, has been proposed. It was applied to the coils developed for testing the quadrupoles of the accelerator Linac4 at CERN. The uncertainty introduced by the in-situ calibration on the parameters of the coils is 0.3 %, in spite of the small aperture and the little clearance between the coil and the magnet bore. In addition, the sensitivity to higher multipole terms is correctly estimated. The tolerance typically required for the focusing strength of the Linac4 magnets is about 1 %, thus the new procedure was verified to be useful in the series measurements of magnets for the latest generation of linear accelerators.

The main advantage with respect to the traditional calibration is that the systematic measurement errors arising from the calibration of the averages of the coil radius and width are removed, by calibrating a specific longitudinal portion of the coil.

The in situ calibration only requires the knowledge of the quadrupole strength, based on the single stretched wire, and the displacement between the magnet and the coil rotation axes. The method in addition provides a calibration of the sensitivity to the first higher order multipoles. Multipoles above the dodecapole, i.e. the first allowed harmonic, are normally irrelevant for linear accelerator magnets.

The proposed system, after the coil transducer calibration, is able to measure the field strength with an uncertainty of ±0.1 % and the multipole component between ±200 ppm

(i.e. 2 units) of the main field component. The system attains a precision of ±70 μrad for the field direction and ±10 μm for the magnet axis position. In other words, the fiducialization of the magnetic parameters, thanks to a proper measuring procedure of mechanical rotation of the magnet under test, can be attained with high precision.
In addition, the same system can be applied to measure permanent quadrupole as well as fast-pulsed iron-dominated magnets, thanks to the flexibility of the electronic, mechanics and software. In conclusion, an "all-in-one" solution is provided for different measurement parameters and different kind of magnets that can be translated in time and money saving.
For the magnet monitoring during the machine operation, the upgrade of the new measurement system for the PS required the study and the characterization of a new magnetic field transducer, able to mark the field with high precision in a given time instant. Due to the complexity of the magnets used in the PS accelerator, the field marker has to be able to work in the critical conditions of high field ramp rates (higher than 2.3 T/s) and high inhomogeneity (about 2 %/cm). In this thesis, the metrological characterization in static and dynamic field of a FerriMagnetic Resonance transducer, based on an opportunely adapted commercially available YIG (Yttrium Iron Garnet) filter, has been presented.
The calibration in a static field of a transducer, based on a YIG filter opportunely adjusted to remove eddy current effect and reduce the temperature drift, has shown $\pm$40 ppm uncertainty up to 0.13 T.
Concerning the dynamic calibration, the 3-σ uncertainty of $\pm$20 μT in a pure dipole field ramped up to 3 T/s, for field levels up to 0.13T demonstrated that the transducer fully satisfies the new monitor system requirements. Tests in its final destination, the combined function reference magnet of the Proton Synchrotron accelerator, showed a higher uncertainty of about $\pm$50 μT with respect to the calibration results. However, at this stage it is not possible to say whether this is due to a degradation of the FMR performance in a gradient field, or rather to the poor reproducibility of the actual monitor system used as reference measure. This can be assessed when the FMR transducer, will be installed in the new monitor system, to compare the measurement result with the beam position.
The quality of the actual field reference measurement system and the fluctuation of the magnetic field of the PS do not help to discriminate the source of such deterioration. However, even in the worst-case, the uncertainty of the transducer still remains in the tolerance required.
The transducer it is found to be fully adequate to be used as a high-precision field marker for the new real-time field measurement systems of the PS, as well as other injectors at CERN.

Appendix A

Details about magnets for accelerators

Once the field geometry is fixed according to the eq. 1.10, the next step is how to generate multipole field. For a given set of electric charge and currents, by integrating the Maxwell equations is possible to find the magnetic and the electric field generated by those sources. For more complex currents distribution a numerical simulation is mandatory, in the following simplified geometries will be analyzed to understand how to put the current lines to generate a multipole of a specified order. By applying the Ampere law to an infinitely long wire in the free space ($\mu = \mu_0$), the magnetic field $\vec{B}$, to satisfy the Eq. (1.3a), should create concentric loops around the current distribution (Fig. A.1).

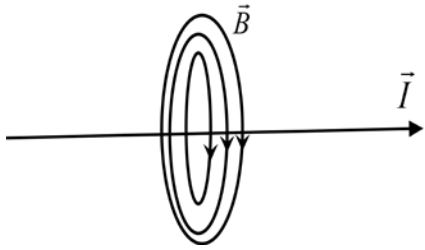

Figure A.1: magnetic field lines generated by a current flowing in an infinite long wire.

By considering circular loops is possible to calculate the field at a radius *r*:

$$B = \frac{I}{2\pi\mu_0 r} \tag{A1}$$

In two dimensions the field generated in a in a arbitrary point (*x, y*) by a current placed at (x_0, y_0) is:

$$B = \frac{I}{2\pi\mu_0} \frac{1}{\left| r\, e^{i\theta} - r_0 e^{i\theta_0} \right|} \tag{A2}$$

Where $\left| r\, e^{i\theta} - r_0 e^{i\theta_0} \right|$ is the vector distance between the source current and the point (*x, y*). The field vector $\vec{B}$ will orthogonal to the vector distance; by applying a rotation of 90° and considering that in two dimensions the components of a vector can be rewritten in its real and imaginary parts, $\vec{B}$ will have the following form [10]:

$$B_y + iB_x = \frac{I}{2\pi\mu_0} \frac{e^{-i\theta_0}}{\left| 1 - \frac{r}{r_0} e^{i(\theta-\theta_0)} \right|} \tag{A3}$$

This expression of the field can be expanded by means of the Taylor series with complex coefficients:

$$B_y + iB_x = -\frac{I}{2\pi\mu_0 r_0} e^{-i\theta_0} \sum_{n=1}^{+\infty} \left(\frac{r}{r_0}\right)^{n-1} e^{i(n-1)(\theta-\theta_0)} \tag{A4}$$

That is valid when r < r_0. The eq. (A.4) corresponds to the 1.10, if we choose R_{ref} equal to r_0 and the $B_{ref} = \frac{I}{2\pi\mu_0 r_0}$, the multipole components of the field are:

$$c_n = (a_n + ib_n) = e^{-in\theta_0} \tag{A.5}$$

This means that the field generated by a single current wire infinitely long can be represented as a sum of the multipoles. To understand exactly how to distribute the currents to generate a given multipole, is better to consider a current flowing on the surface of a cylinder of radius r_0 in given section of the circumference $\delta\theta_0$, the total field is the sum of all the current distributions at all the values θ_0:

$$B_y + iB_x = -\frac{1}{2\pi\mu_0 r_0} \sum_{n=1}^{+\infty} \left(\frac{r}{r_0}\right)^{n-1} e^{i(n-1)\theta} \int_0^{2\pi} e^{-in\theta_0} I(\theta) d\theta_0 \tag{A.6}$$

Eq. (A.6) evidences that the multipole components of the field are related to the Fourier components of the current distributions as function of the angle at a given radius r_0. By assuming a single "tone" of the Fourier components:

$$I(\theta_0) = I_0 \cos(n_0\theta_0 - \phi) \tag{A.7}$$

The eq. A.6 becomes:

$$B_y + iB_x = -\frac{I_0}{2\pi\mu_0 r_0} \left(\frac{r}{r_0}\right)^{n_0-1} e^{i(n_0-1)\theta} \pi e^{-in\phi} \tag{A.8}$$

In other words, comparing eq. A6 and 1.10, each multipole corresponds to a given angle of the current distribution:

$$c_n = -\pi e^{-in\phi} \tag{A.9}$$

Assuming that the $R_{ref} = r_0$ and $B_{ref} = \frac{I_0}{2\pi\mu_0 r_0}$. This mean that by opportunely distributing on a on a cylindrical pattern a sinusoidal current distribution is possible to create in the cylinder the desired multipole. This approach is the basis on which are based the so called coil dominated magnets, that are different from the iron dominated magnet where the multipole are given by the shape of the iron forming the magnet yoke. In the next sections the iron dominated, the coil dominated and the permanent magnets will be described.

A.1 Iron dominated magnets

In iron dominated magnets the field generated is a sum of two contributions: the field from the coil (aluminium, copper or superconducting material also called superferric magnets) and the field from the iron magnetization. Here are described the normal conductive magnets, characterized by the following behaviours [8]:

- The magnetic field is defined mainly by the profile of the pole shape, i.e. the pole profile defines the multipole components in the magnet aperture.
- The maximum field is limited to about 1.5 T.
- The field quality mostly depends on the pole profile that can be shaped with high precision, turning out in high quality fields.
- The conductors placing are not so critical, but to reduce stray fields is important that they are close to the pole.

The hysteresis and dynamic effects in the iron could be an issue during the machine operation and for this reason need to be modelled or measured accurately.

In the following will be described how to derive the profile of the iron to generate the multipole of a given order and later the different yoke configurations actually used in the design of magnets for accelerators.

The analysis starts by considering the magnetic field $\vec{B}$ function of a magnetic scalar potential ϕ that satisfy the local form of the Maxell equation in magnetostatic problems:

$$\vec{B} = -\nabla\phi \tag{A.10}$$

For any function ϕ the curl of a gradient is always zero, meaning that the eq. 1.6 is satisfied by any magnetic field derived from eq. A.10.

By substituting eq. A.10 in 1.5 we find:

$$\nabla^2\phi = 0 \tag{A.11}$$

Where ∇^2 is the Laplacian operator. The scalar potential can be found by resolving this equation with given boundary conditions between the iron and the air gap. In particular on the boundary of a material with infinite permeability (reasonable approximation of a ferromagnetic material) the magnetic field is perpendicular to this surface. A given multipole can be generated by shaping the material in a way to follow the iso-surfaces of magnetic scalar potential for the required multipole. This corresponds to:

$$-\left(\frac{\partial}{\partial x} + i\frac{\partial}{\partial y}\right)\phi = B_y + iB_x = C_n(x+iy)^{n-1} \tag{A.12}$$

By re-writing $x + iy$ in polar coordinates $re^{i\theta}$, a solution to eq. A.12 is:

$$\phi = C_n \frac{r^n}{n} \sin(n\theta - \varphi_n)^{n-1} \tag{A.13}$$

By substituting the eq. (A.13) in eq. (A.10) (writing the gradient in polar coordinates) it can be demonstrated that a scalar potential in eq. (A.13) generates a pure multipole field if the material surface is shaped according to the following parametric curve in θ:

$$r^n \sin(n\theta - \varphi_n) = r_0^n \tag{A.14}$$

Where r_0 is a constant related to the minimum distance between the material surface and the origin of the reference system.

For $(n\theta - \varphi_n) \rightarrow m\pi$ (where m is an integer), r^n goes to infinity, the region between two infinity values is the magnet pole and each n-multipole has $2n$ poles and also the potential ϕ changes sign when moving to one pole to the other defining the north and the south poles.

By summing the scalar potentials for each multipole component is possible to design a surface profile that can generate more than one multipole magnetic component, such kind of magnet are called “combined function” magnets (fig. A.2), that can provide the focusing and the steering of the beam at the same time.

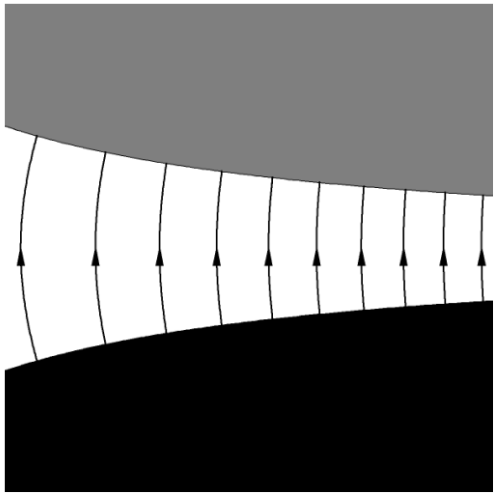

Figure A.2:.pole profile of a combined function magnet.

In iron dominated magnets, the copper coil is wounded around an iron yoke of a given shape confining the field lines. In fig. A.3 are shown the three main shape of the iron yoke for a dipole magnet typically used in the accelerators, looking into their characteristics there is no optimum solution; they all have their advantages and drawbacks. The choice for one or the other option is led by the constraints and requirements such as the function of the magnet, the available space, and the field quality [9].

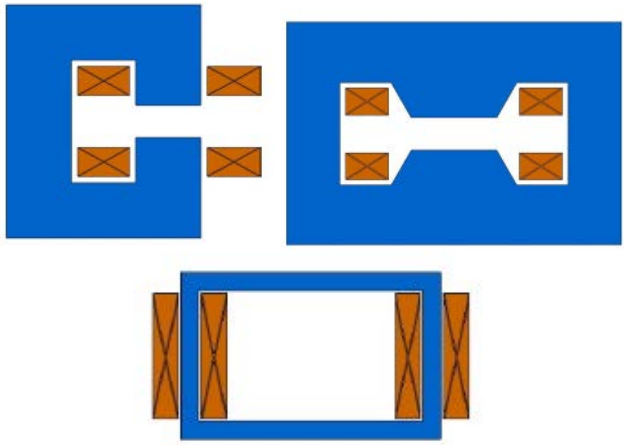

Figure A.3: Classical dipole shapes of the yoke (from the left): a) C-magnet, b) H-magnet, c) O-magnet

The C-shape magnets (Fig. A.3 a) provide a very good accessibility to the beam pipe and are very suitable in the region where adjacent beam line are very close to each other as in the transfer lines. Their volume is higher than the H-magnet with similar performance and they are more affected by attracting magnetic forces when the magnet is pulsed. The field generated with this geometry is affected by multipole errors that change also with the level of the saturation resulting in non-linear behaviours depending on the current excitation level. The H-magnet provides higher mechanical stability and field quality but lower accessibility to the beam pipes. The O-magnets are similar to the H-magnet with a pole height reduced to zero. They have the same characteristic in terms of stability and field quality of an H type but they have a lower efficiency. They are usually used as steering magnets in the accelerators to correct the beam trajectory.

Once the geometry (size, iron shape and material, aperture size) and the field parameters (strength, maximum error in multipole terms) of the magnet are defined, is possible to calculate the excitation currents in the coils required to generate the given field strength. From the Ampere's law, assuming N the number of turns of the excitation coil, the magnetic intensity $\vec{H}$ integrated on a closed path is:

$$\oint \vec{H} d\vec{l} = NI \tag{A.15}$$

By assuming a the constitutive equation $\vec{B} = \mu_0 \mu_r \vec{H}$ for a material with a relative permeability μ_r, and a closed path as shown in fig. A.4, where h is the gap height and λ the path in the iron yoke, ampere turns NI can be calculated as:

$$NI = \frac{Bh}{\mu_{air}} + \frac{B\lambda}{\mu_0 \mu_r} \tag{A.16}$$

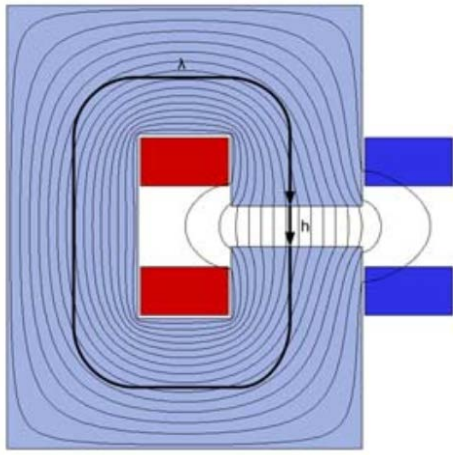

Figure A.4: *integration path in an iron dominated dipole magnet.*

A.2 Coil dominated magnets

The limitation in maximum field of the iron dominated magnets can be overcome with coil dominated magnet using superconducting coils to generate the field required. The technology of superconducting magnets relies on relatively recent developments in materials and designs of conductors and cables. Now days the superconducting technology allows to build magnets for accelerators that can provide field up to 9 T using Nb-Ti composed wires. The iron yoke in superconducting magnets plays only a limited role and it is the positioning of the conductors, which is of paramount importance for the field quality [3].

The coil design in the majority of these magnets is based on some interesting properties of uniformly-distributed, counter-flowing currents in the following geometries [4]:

- Overlapping conductors of circular cross-section (Fig. A.5a): The overlap region forms a current-free aperture in which there is an exactly uniform dipole field.
- Overlapping conductors of elliptical cross-section (Fig. A.5b): this similar arrangement also gives an exactly uniform dipole field in the current-free overlap region.
- Overlapping elliptical conductors set at 90° (Fig. A.5c): this arrangement gives a perfect quadrupole field.

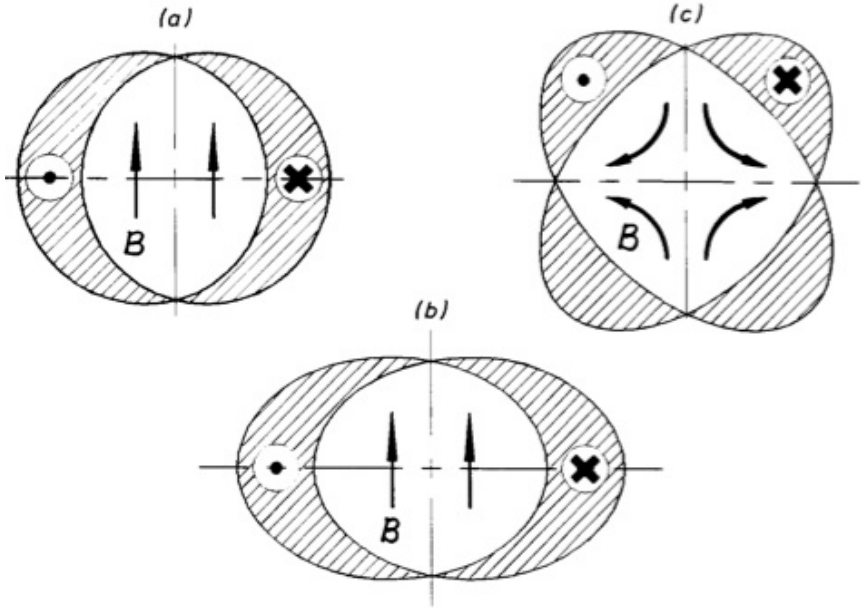

Figure A.5: Ideal current distributions used in superconducting magnets. (a) Dipole, (b) dipole, (c) quadrupole.

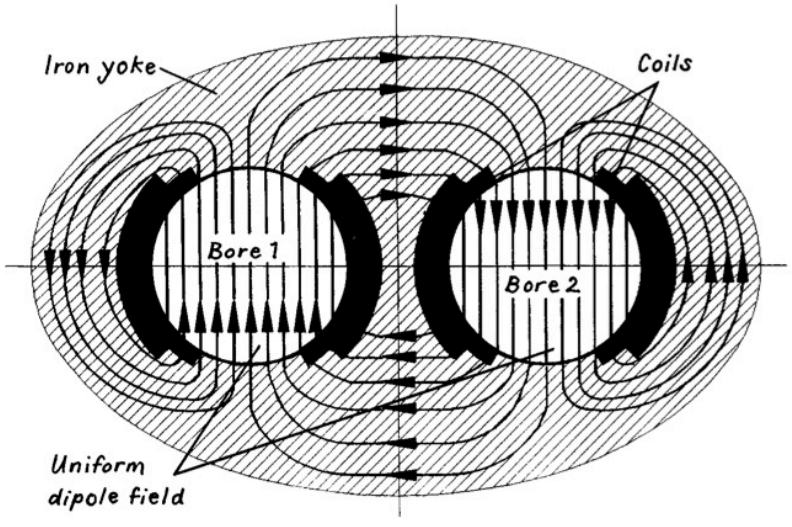

Figure A.6: twin bore magnet.

In reality the ideal current distributions are substituted with conductors in blocks and layers [Russenckuch, 2010]. The careful positioning of the current blocks by use of modelling and optimization tools yields the required field. The whole coil assembly with its clamps is mounted inside a cylindrical iron yoke. To the first approximation this yoke does not introduce any new multipoles and by virtue of

the image currents it re-enforces the main component. As cost-saving design a twin-bore solution was designed for accelerators where two beams are circulating. The design made by Blewett [2] (Fig. A.6) is made in a way that the two aperture shares the same flux with a reduction in the ampere turns needed of 40 %.
Probably the best example is the LHC magnets. The LHC dipole is like a split pair of circular coils, stretched along the particle trajectory in such a way that the dipole field is generated only along the beam pipe. The LHC dipoles are based on a compact and cost-saving two-in-one design, where two beam channels with separate coil systems are incorporated within the same magnet [6]. The main parts of an LHC dipole are depicted in Fig. A.7. The superconducting cables of the coils for the LHC magnets are made of NbTi hard superconductor multi-wires, embedded in a copper stabilizer. Such wires are wrapped together to form the so-called Rutherford type cable. The coils are surrounded by the collars, which limit the conductor movements [7]. The iron yoke shields the field so that no magnetic field leaves the magnet. The so-called cold-mass is immersed in a bath of superfluid liquid helium acting as a heat sink. The helium is at atmospheric pressure and is cooled to 1.9 *K* by means of a heat exchanger tube. The cold mass is delimited by the inner wall of the beam pipes on the beam side and by a cylinder on the outside. The iron yoke, the collars, and the cylinder compress the coil by withstanding the Lorentz forces during excitation. The cylinder case improves the structural rigidity and longitudinal support and contains the superfluid helium.

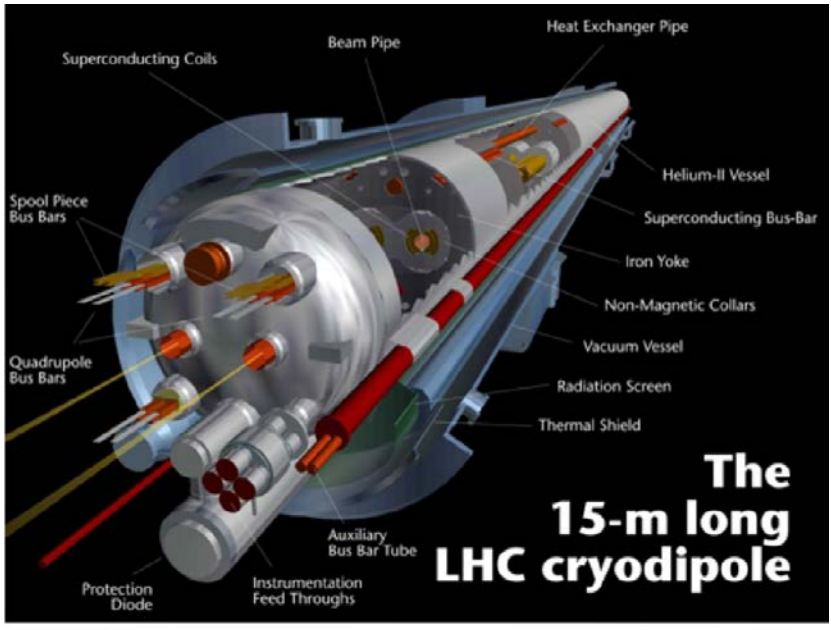

Figure A.7: Cross section of an LCH normal quadrupole

A.3 Permanent magnets

Iron dominated and coil dominated magnets provide high flexibility in adjust the accelerator parameters, however when the flexibility can be reduced another solution that can be adopted to bend and focus the particles beam are permanent magnets. The generic advantages in use permanent magnets are: (i) strong field in small dimensions of the magnet, (ii) no power supply neither cooling systems, (iii) no power consumption. On the other side their field strength cannot be adjusted in the machine so a carefully design of the machine operation is needed and their long-term stability is limited by the temperature dependence of the material used to assembly the magnets. The design is based on the use of oriented Rare Earth Cobalt material (REC) [5]. The powder of cobalt and some earth material is first exposed to a strong magnetic field and subjected to high pressure, to physically rotate the grains until their magnetically preferred axes are parallel to the applied field. This process is needed to align all magnetic moments along the direction of magnetization, commonly called the easy axis. The property that makes REC so valuable is that this magnetization is very strong, and that it can be changed in a substantial way only by applying a strong field in the direction opposite to the one used to magnetize the material. The so-called Halbach cylinder is the most used design to produce strong multipole fields by using REC material. In fig. A.8 are shown the designs of different multipole by using the Halbach geometry. A Halbach cylinder of length L made of segments of REC material opportunely oriented to generate in the aperture a specific multipole [1].

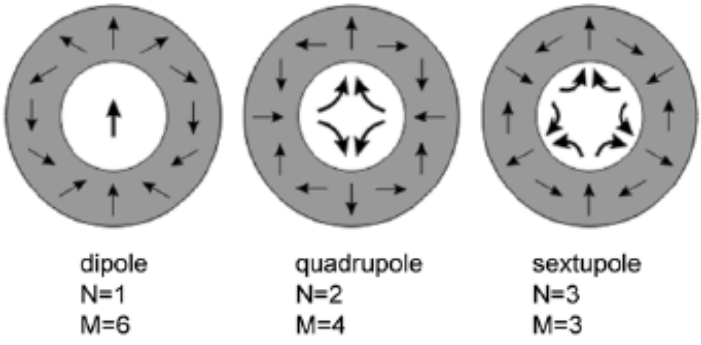

Figure A.8: Sketch of the Halbach cylinder design for permanent accelerator magnets: a) dipole, b) quadrupole, c) sextupole

The field in the aperture can be expressed as follow:

$$\vec{B}(\vec{z}) = \vec{B}_r \sum_{v=0}^{\infty} \left(\frac{\vec{z}}{r_1}\right)^{n-1} \frac{n}{n-1}\left(1-\left(\frac{r_1}{r_2}\right)^{n-1}\right) K_n \qquad \text{(A.17)}$$

Where $\vec{B}_r = B_{rx} + iB_{ry}$ is the vector of the remanent field. The index is $n = vM + N$, where N is the multipole to generate (ex. $N = 1$ for dipole), M is the number of permanent magnet blocks r_1 and r_2 are respectively the inner and the outer radius of the cylinder. K_n is defined as follow:

$$K_n = \cos^n(\varepsilon\pi/M)\frac{\sin(\varepsilon\pi/M)}{n\pi/M} \tag{A.18}$$

where ε is a factor taking in to account the geometry of the permanent element. Because of their special importance for accelerators, we discuss some details of quadrupoles. From eq. A.17 for a quadrupole ($N = 2$) and $\varepsilon = 1$ follows that:

$$\vec{B}(\vec{z}_0) = \vec{B}_r \frac{\vec{z}_0}{r_1} 2\left(1 - \frac{r_1}{r_2}\right)\cos^2\left(\frac{\pi}{M}\right)\frac{\sin\left(\frac{2\pi}{M}\right)}{\frac{2\pi}{M}} \tag{A.19}$$

In order to get a strong quadrupole the best choose is M = 12 or 16 [Halbach, 1980]. The gradients achievable with a 16-piece quadrupole are quite high, particularly when they are compared with those of conventional quadrupoles. For $M = 16$, $r_1/r_2 = 4$, and B_r-=-0.95 T is possible to obtain an aperture field of 1.34 T. In contrast, a high quality conventional quadrupole is very difficult to make with more than 1T at the aperture, and even that is possible only for fairly large aperture magnets. Fig. A.9 shows a schematic cross section of a 16-piece quadrupole, with the of the easy axis direction indicated in each piece. It follows, from the diagram, that pieces with five different orientations of the easy axis relative to the trapezoidal shape are necessary to make a 16-piece quadrupole. With a large number of identical pieces it may be advantageous to measure magnetization direction and magnitude for each piece, and then assemble the quadrupole in such a way that magnetization errors do the least harm to the field quality.

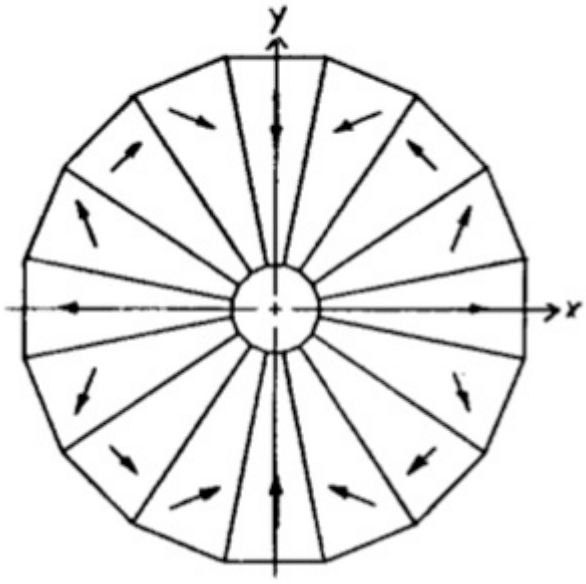

Figure A.9: diagram of a 16-piece permanent quadrupole.

[1] J. Bahrdt, 2009, Permanent magnets including undulators and wigglers, *CERN Accelerator School CAS 2009: Specialised Course on Magnets, 2009*.

[2] J. P. Blewett, 1971, 200 GeV intersecting storage accelerators, *8th International Conference on High-Energy Accelerator, 1971*.

[3] P. Bryant, 1993, The Principles of Circular Accelerators and Storage Rings, *Cambridge University Press, 1993*.

[4], H. Brechna, 1973 Superconducting magnet systems, Springer-Verlag, 1973.

[5] K. Halback, 1980, Design of permanent multipole magnets with oriented rare earth cobalt material, *Nuclear instrument and method vol. 169, 1980.*

[6] L. Rossi, 2004, Superconducting magnets for the LHC main lattice, *IEEE Transactions on Applied Superconductivity, 2004*.

[7] L. Rossi, 2003, The LHC main dipoles and quadrupoles toward series production, *IEEE Transactions on Applied Superconductivity, vol. 13, 2003*.

[8] S. Russenschuck, 2010, Field Computation for Accelerator Magnets: Analytical and Numerical Methods for Electromagnetic Design and Optimization, *John Wiley & Sons, 2010.*

[9] T. Zickler, 2009, Basic design and engineering of normal-conducting, iron-dominated Electromagnets, *CERN Accelerator School CAS 2009: Specialised Course on Magnets, 2009.*

[10] A. Wolski, 2009, Maxwell equations for magnets, *CERN Accelerator School CAS 2009: Specialised Course on Magnets, Bruges, 2009.*

Appendix B

Details about measurement methods

(A.9)

B.1 Stretched wire

. By defining a pure quadrupolar field as [3]:

$$B_y = G \cdot x \qquad B_y = G \cdot y \tag{B.1}$$

The magnetic axis is defined by the point where:

$$B_y = B_y = 0 \tag{B.2}$$

The main field direction is defined by the symmetry planes:

- $B_x=0$ in the horizontal symmetry plane,
- $B_y=0$ in the vertical symmetry plane.

Moving a SSW vertically from position y_1 to position y_2 (Fig. B.1a) gives the measured flux of Eq. (B.3), i.e., a parabolic dependence. The effective length L_{eff} hides the integral over the magnet length:

$$\psi(x_1, x_2) = \int_0^L \int_{y_1}^{y_2} G \cdot y \cdot dy \cdot dl = L_{eff} \frac{G}{2} (y_2^2 - y_1^2) \tag{B.3}$$

A further correction must be applied to take into account the wire sagitta that could reach millimetres for a 10 to 15 m long distance between the stages. This error source is more detrimental for the measurement of the strength of a quadrupole. To obtain accuracy in the result requires therefore time, even with fully automated equipment and procedures, since loops at different tensions are internal to iteration to align the wire coordinate system to the magnet axis. An accurate measurement of the gradient can only take place after a full alignment procedure. This requires the wire has to able to measure the field direction and the yaw/pitch angles [2]. The difficulties encountered when measuring a quadrupole strength are that the wire has a natural deflection in the millimetre range if the wire or magnet length reaches several metres, this is not the case for short magnets. In addition, it is difficult to find CuBe wire that has zero magnetic susceptibility. Unfortunately the industrial standards describing this type of material rarely include the impurity content of non-zero susceptibility. Several batches purchased from the same manufacturer could have appreciably different magnetization and the only way to sort the best batch is to test with a permanent magnet. In conclusion the wire deflection depends on the position in the quadrupole cross-section, in both amplitude and direction. The accuracy is also limited by the high order multipoles present in the magnet that perturb the value of $G \cdot L_{eff}$ obtained from eq. B.3. These perturbations grow with the distance from the magnet axis, and a detailed estimation is needed to either limit the range of the

displacement allowed or to include relevant correction factors in the data analysis. In practice, the estimation of the quadrupole strength is obtained from the last set of data measured once the SSW reference system is fully aligned with the quadrupole axis. The SSW is the only measurement able to provide an accuracy of 10^{-3} in measuring the field gradient in small aperture quadrupoles.

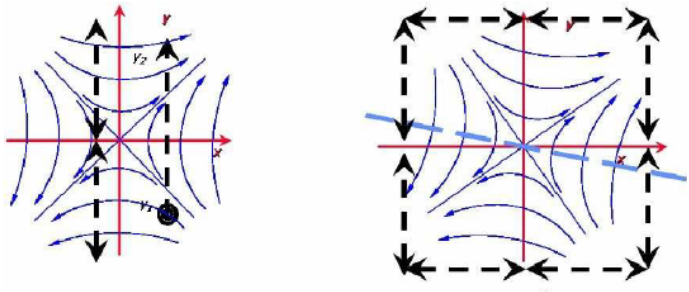

Figure B.1: (a) The single stretched wire displaced vertically in a quadrupole. Two measurements are needed to find the minimum of the parabolic dependency, i.e., the horizontal symmetry plane. (b) The axis and field direction (i.e., tilt of the quadrupole field) are found with eight measurements.

B.2 Vibrating Wire

The vibrating wire technique is based on the the resolution of the differential equation to solve for standing wave solutions:

$$W\frac{\partial x^2}{\partial t^2} = T\frac{\partial x^2}{\partial z^2} - \gamma\frac{\partial x}{\partial T} + I(t)B(z) \tag{B.3}$$

with $x(0,t)= x(L_W, t) =0$ the boundary conditions, W the weight of the wire per unit length, T the wire length, γ the damping coefficient, $I(t) = I_0 e^{j\omega t}$ the current AC in the wire and $B(z)$ the transverse magnetic field. The solution of equation B.3 is a sum of standing waves with a given amplitude x_n measured by the optical sensors:

$$x(z,t) = \sum x_n \sin\left(\frac{\pi n z}{L_w}\right) e^{j\omega t} \tag{B.4}$$

with the coefficient x_n equal to:

$$x_n = \frac{I_0}{W}\frac{1}{\omega^2 - \omega_n^2 - j\omega\gamma} B_n \tag{B.5}$$

$B(z)$ can be reconstructed knowing the series of B_n:

$$B(z) = \sum B_n \sin\left(\frac{\pi n z}{L_w \omega}\right) \tag{B.6}$$

In Fig. B.2 is shown an overview of the vibrating wire system. The wire is tensioned between two supports a lock-in amplifier is used to measure the voltage generated from two optocouplers detecting the wire vibration. The lock-in amplifier is locked on the current generator signal giving the reference for the optical sensor voltage measurement [4]. The coordinate measurement system is used for the second step of the fiducialization process [5].

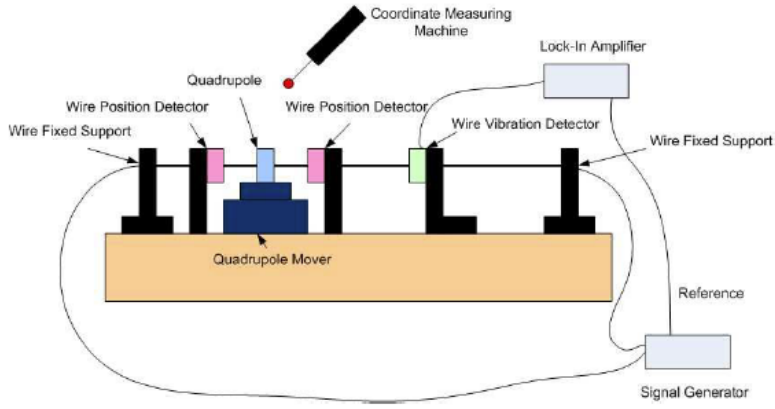

Figure B.2: Overview of the vibrating wire equipment measuring the magnetic axis in a quadrupole. The wire vibration detector and the quadrupole are longitudinally located to have maximum signal with the second harmonic of the natural oscillation frequency.

B.3 Hall Probes

A Hall probe is a semiconductor-based detector which uses the Hall effect to allow the strength of a magnetic field to be measured. The Hall Effect is seen when a conductor is passed through a uniform magnetic field. The natural electron drift of the charge carriers causes the magnetic field to apply a Lorentz force (the force exerted on a charged particle in an electromagnetic field) to these charge carriers. The result is what is seen as a charge separation, with a build up of either positive or negative charges on the bottom or on the top of the plate.
An expression for the sum signal S of a group of m plates with equal sensitivities in a magnetic field with normal and skew multipole components B_k and A_k, respectively, is given by [1]:

$$S = \sum_{k=1}^{\infty} 3\left(\frac{R}{R_{ref}}\right)^{(2k-1)m-1} (-1)^{\frac{(2k-1)m-1}{2}} mB_{m(2k-1)} + \sum_{k=1}^{\infty} (-1)^{mk}\left(\frac{R}{R_{ref}}\right)^{2km} mA_{2km} \tag{B.6}$$

In an ideal case, where all the Hall plates are well aligned and have equal sensitivities, the only multi-poles contributing to the total signal *S* are the normal odd and the skew even multiples of order *m*. In an arrangement of three plates, the sum signal *S* is compensated for the dipole, and only normal multipoles of order 3(2*k*-1) (i.e. B_3, B_9, B_{15},…) and skew harmonics of order 6k (i.e. A_6, A_{12}, A_{18},…) contribute according to:

$$S = \sum_{k=1}^{\infty} 3\left(\frac{R}{R_{ref}}\right)^{3(2k-1)-1} B_{3(2k-1)} + \sum_{k=1}^{\infty} (-1)^{k} 3\left(\frac{R}{R_{ref}}\right)^{6k-1} A_{6k} \tag{B.7}$$

In the case of a pure sextupole field, this yields:

$$S = 3\left(\frac{R}{R_{ref}}\right)^{2} B_3 \tag{B.8}$$

The sum signal of a decapole arrangement with five plates (*m* = 5) is:

$$S = \sum_{k=1}^{\infty} 5\left(\frac{R}{R_{ref}}\right)^{5(2k-1)-1} (-1)^{\frac{(2k-1)5-1}{2}} B_{5(2k-1)} + \sum_{k=1}^{\infty} (-1)^{k} 5\left(\frac{R}{R_{ref}}\right)^{10k} A_{10k} \tag{3.18}$$

In the case of a pure decapole field, this yields:

$$S = \sum_{k=1}^{\infty} 5\left(\frac{R}{R_{ref}}\right)^{4} B_5 \tag{3.19}$$

[1] Breschi et al., Fast measurement of field harmonics through a set of Hall probes, *CERN Internal Note LHC-MTA-IN-2000-103, 2000*.

[2] J. Di Marco et al, Field alignment of quadrupole magnets for the LHC interaction regions, *IEEE Trans. Appl. Supercond., vol. 10-1, 2000*.

[3] L. Walckiers, Magnetic Measurement with coils and wires, *CERN Accelerator School: specialized course on magnets, 2009*.

[4] Z. Wolf, A Vibrating Wire System For Quadrupole Fiducialization, SLAC internal note*, LCLS-TN-05-11, 2005*.

[5] A Jain, Results from vibrating wire R.D. for alignment of multipoles in NSLS-II, *Proc. of 16th International Magnet Measurement Workshop, 2009.*